Definitive treatment for early-stage breast cancer with FLASH proton therapy

Dosimetric feasibility and optimization with intensity-modulated ridge filtered beams and toxicity-model endpoints

A. Maasland

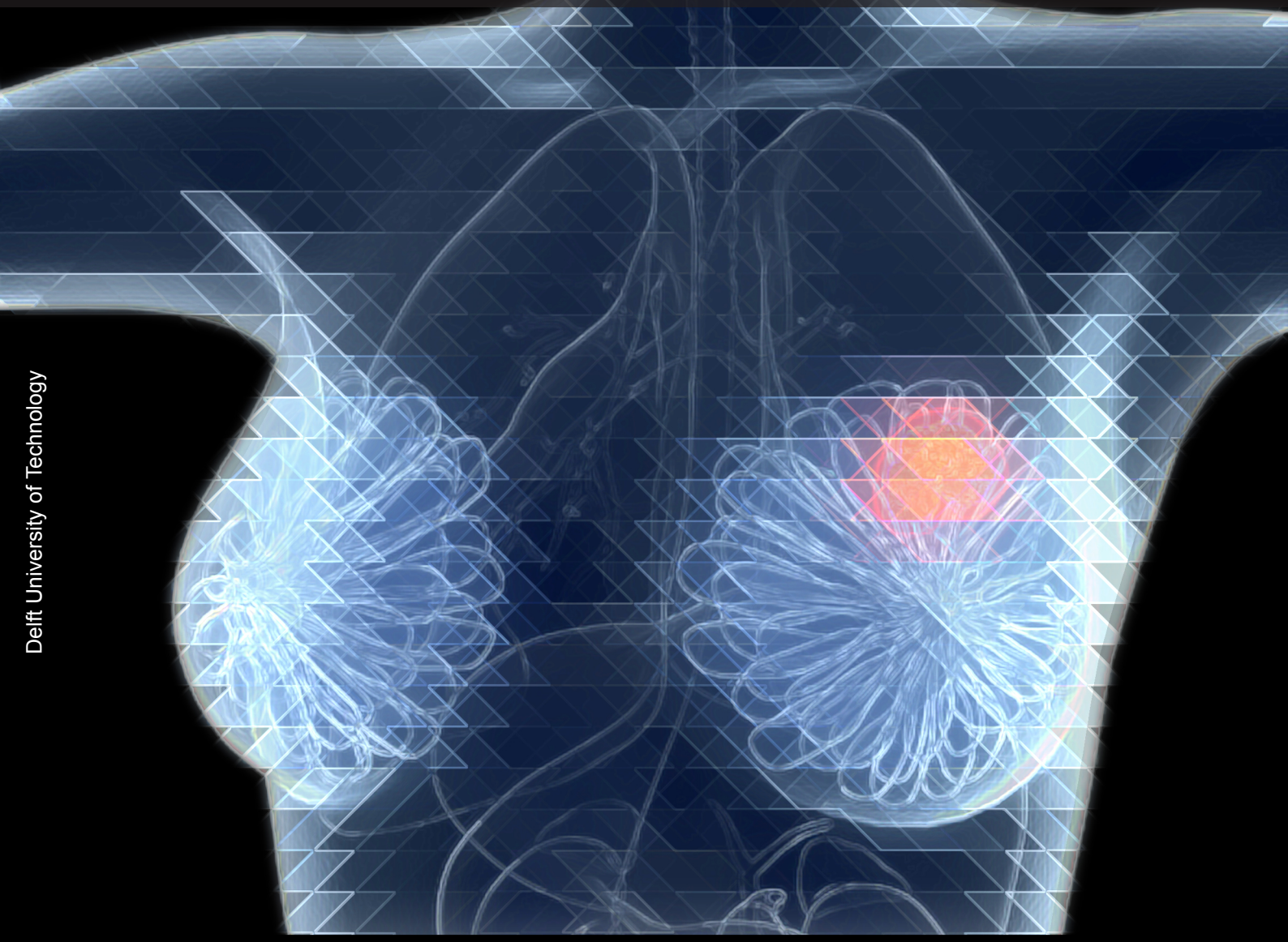

Delft University of Technology

TU Delft

Definitive treatment for early-stage breast cancer with FLASH proton therapy

Dosimetric feasibility and optimization with intensity-modulated ridge filtered beams and toxicity-model endpoints

by

A. Maasland

to obtain the degree of Master of Science
at the Delft University of Technology,
to be defended publicly on Thursday November 24, 2022 at 9:00 AM.

Student number:	4476255	
Project duration:	March, 2022 – November, 2022	
Thesis committee:	Dr. S. J. M. (Steven) Habraken,	Erasmus MC and HollandPTC,
	Dr. ir. D. (Danny) Lathouwers,	TU Delft,
	Prof. dr. M. S. (Mischa) Hoogeman,	TU Delft, Erasmus MC, and HollandPTC.

An electronic version of this thesis is available at http://repository.tudelft.nl/.

Cover Image: Graphic visualization of a tumor in a female breast - made by ANK Design

TU Delft

Erasmus MC
University Medical Center Rotterdam

HollandPTC
Proton Therapy Centre

Abstract

The aim of this thesis is to study the dosimetric feasibility of FLASH proton therapy for early-stage breast cancer patients. The biological effect of FLASH is seen under ultra-high dose-rates conditions and is beneficial in the damage to healthy tissue. The FLASH effect could enable the clinical feasibility of definitive radiotherapy for low-risk early-stage breast cancer patients. Some of these patients can not receive surgery for medical reasons and definitive conventional radiotherapy carries a high risk of toxicities. FLASH proton therapy could be a viable option for these patients. The biological FLASH effect enables to reduce the risk of toxicities by sparing healthy tissue and proton therapy enables to deliver dose to the cancer cells effectively.

This thesis proposes a pencil beam scanning (PBS) ridge filter simulation set-up to achieve ultra-high dose-rates. The ridge filter generates spread-out Bragg peak (SOBP) beams that cover a broader depth of the tumor, avoiding the time-consuming energy switching of conventional PBS. An optimization is performed with intensity-modulated ridge filtered beams. SOBP beams with a width of 3 cm are implemented in the in-house treatment planning software Erasmus-iCycle to generate ridge filter treatment plans for two patients.

In this study, the dosimetric feasibility is determined by comparing the ridge filter treatment plans to conventional intensity-modulated proton therapy (IMPT) treatment plans. The clinical acceptability of the treatment plans is assessed by dose uniformity and dose coverage. Furthermore, toxicity-model endpoints for fat necrosis and fibrosis are used to evaluate the treatment plans. The generated ridge filter treatment plans outperform the generated IMPT treatment plans for a FLASH enhancement ratio between 1.19-1.39 for one of the patients. The other patient required a FER in the order of magnitude of 2.0.

The results of the study suggest that it is feasible to generate ridge filter treatment plans with the proposed set-up. However, the dosimetric feasibility comes with limitations in the tumor characteristics (size and position) and needs further investigation. More knowledge is needed of the optimal ridge filter, the optimization of SOBP beams, and the FLASH effect before clinically acceptable FLASH-compatible ridge filter treatment plans can be achieved.

Contents

Nomenclature

Abbreviations

Abbreviation	Definition
APBI	Accelerated partial breast irradiation
BED	Biologically effective dose
CI	Conformality index
CT	Computed tomography
CTV	Clinical target volume
Erasmus MC	Erasmus medical center
EUD	Equivalent uniform dose
FER	FLASH enhancement ratio
GTV	Gross tumor volume
HI	Homogeneity index
HollandPTC	Holland proton therapy center
IMPT	Intensity-modulated proton therapy
MFO	Multi-field optimization
NTCP	Normal tissue complication probability
PBS	Pencil beam scanning
PTV	Planning target volume
SBPF	Single beam per fraction
SFO	Single-field optimization
SOBP	Spread-out Bragg peak
TU Delft	Delft University of Technology
UHDR	Ultra-high dose-rate
WBI	Whole breast irradiation

Symbols

Symbol	Definition	Unit
α/β	Radiosensitivity of tissue	[Gy]
D	Dose	[Gy]
D_{eq}	Equivalent single fraction dose	[Gy]
D_{FLASH}	Dose delivered with FLASH treatment	[Gy]
D_{IMPT}	Dose delivered with IMPT treatment	[Gy]
D_{max}	Maximal dose received by healthy tissue volume	[Gy]
D_{pr}	Prescribed dose	[Gy]
D_2	Dose level received by respectively 2% of the PTV	[Gy]
D_{98}	Dose level received by respectively 98% of the PTV	[Gy]
h	Repair factor in between fractions	[-]
m	Slope of dose-response curve	[-]
n	Parameter for the volume effect of irradiated tissue	[-]
N	Number of fractions	
v	Relative sub-volume of healthy breast tissue	[cc]
V_{PTV}	Volume of PTV	[cc]
$V_{95\%}$	Volume of breast receiving 95% of the prescribed dose	[cc]

1 Introduction

Cancer is the world's second leading cause of death according to the World Health Organization [61]. The most common treatments for cancer patients are surgery, radiotherapy, chemotherapy, immunotherapy, and hormone therapy. Radiotherapy is one of the most widely applied treatment modalities, often combined with surgery or chemotherapy [33].

In radiotherapy, high doses of radiation are delivered to patients to kill cancer cells and shrink tumors. The radiation induces DNA damage to human cells. Radiotherapy aims to irradiate cancer cells so that cancer cells with severely damaged DNA can no longer repair and divide themselves and eventually die. However, during the irradiation of cancer cells, it is almost inevitable to also irradiate the surrounding organs, thereby causing damage to healthy tissue cells. Fortunately, healthy tissue cells are less sensitive to radiation compared to tumor tissue and are often able to repair themselves. The dose delivered to organs at risk during radiotherapy is limited to reduce radiation-induced toxicities.

Recently, radiotherapy with ultra-high dose-rates (UHDR) has demonstrated a differential impact on the damage observed between healthy and tumor tissue. This phenomenon, called the FLASH effect, has shown promising results in saving healthy tissue while maintaining tumor control.

FLASH as a differential effect in radiotherapy was first discovered by Favaudon et al. [16] in 2014. This study demonstrated a reduction in damaged healthy lung tissue in irradiated mice with UHDR electron beams compared to conventional dose-rates. The FLASH effect attracted scientific interest, and the number of studies related to FLASH radiotherapy has increased since. Besides electron therapy, studies have investigated the FLASH effect in other radiation modalities, such as photon and proton therapy. Especially the latter has been highlighted in recent FLASH studies due to its high potential in combination with FLASH [1, 5, 12, 13, 58].

In this thesis, we will investigate the feasibility of FLASH in current proton treatment planning for early-stage breast cancer patients. For a complete understanding of the topic, some elementary knowledge of the FLASH effect, proton therapy, and breast cancer treatment is required. These details will be covered in this chapter. Also, the aim and purpose of this thesis are proposed.

1.1. FLASH effect

FLASH is a biological effect that is seen under ultra-high dose-rates conditions. Conventional radiotherapy irradiates with dose-rate $\leq$ 0.03 Gy/s [16] while the FLASH effect is observed at dose-rates exceeding 40 - 100 Gy/s (UHDR) [5, 57]. In comparison to conventional radiation therapy, beam delivery with UHDR has shown a significant reduction in healthy tissue toxicity while preserving efficacy in killing tumor tissue in multiple animal studies [12, 13, 15, 30, 51, 53, 63].

A mechanism that might play a role in the differential FLASH effect is oxygen depletion. UHDR pulses might cause radiation-induced chemical reactions that occur faster than blood cells can reoxy-

genate [5]. In general, healthy tissue is more oxygenated than tumor tissue, possibly making it more resistant to radiation. However, recent studies have shown that the role of oxygen depletion might not fully describe the FLASH effect [8, 28]. Other hypotheses include the kinetics of radicals and an intrinsic differentiation in oxygen delivery between tumor and healthy tissue microenvironments [14]. Until now, no conclusive evidence has been found on the precise mechanisms behind the FLASH effect. Nonetheless, the results of in vivo animal studies are promising, and research on the possibility of bringing it to the clinic has been initiated. In 2019, the first patient was treated with FLASH therapy using electrons [6] and another clinical trial of FLASH radiotherapy for the treatment of symptomatic bone metastases (FAST-01) is ongoing (NCT04592887).

1.2. Proton therapy

The physical and radiobiological features of charged particles, such as protons, enable dose delivery up to the edge of the tumor. In contrast, photon beams irradiate through the whole intersection of the patient. This difference is illustrated with dose-depth curves of the different radiotherapy modalities, shown in fig. 1.1. The photon dose distribution curve deposits a relatively high dose over the whole depth, while the proton curve deposits most of its dose in a peak at an energy-specific depth. The characteristic peak in the dose distribution curve of protons and carbon ions is called the Bragg peak. The Bragg peak range depends on the proton beam energy and the material the beam transverses.

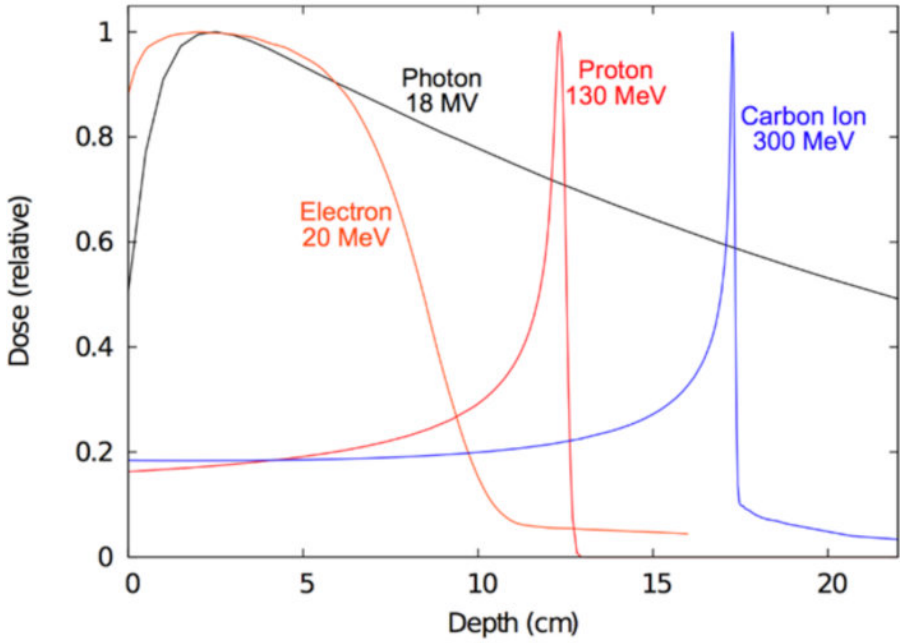

Figure 1.1: Dose distribution in water as a function of depth shown for electron (orange), photon (black), proton (red), and carbon ion (blue) beams [29].

A variation in energy adjusts the range of the Bragg peak and thereby the depth where the majority of the dose is deposited. This superior physical property makes proton therapy well-suited for deep-seated targets. Moreover, almost no dose is deposited beyond the Bragg peak, thereby saving healthy tissue distal (beyond) the target. In order to achieve the same dose in the tumor, less dose has to be delivered elsewhere, making proton therapy more effective. In fig. 1.2, the difference in dose distribution between photon and proton therapy is visualized with examples of treatment plans for a lung tumor. However, it can be seen from both the Bragg peak curve in fig. 1.1 as the example in fig. 1.2 that with proton therapy there is still some dose deposition proximal (before) to the tumor. Introducing the FLASH effect in proton treatment could result in a significant improvement, saving both healthy tissue proximal (due to FLASH) and distal (due to proton physics) to the tumor while preserving tumor control.

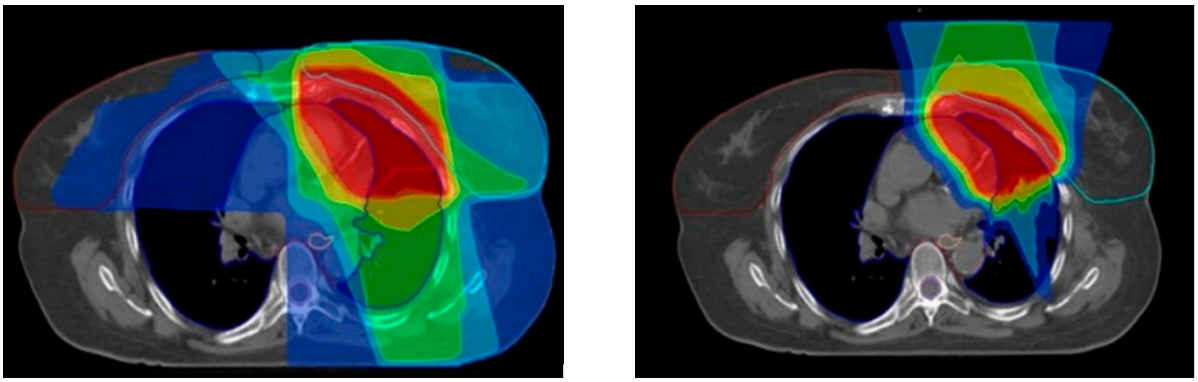

(a) (b)

Figure 1.2: Example of the dose distribution with photon (a) and proton (b) beams in radiotherapy [31].

1.2.1. Pencil beam scanning

The latest advanced proton therapy technology irradiates targets using pencil beam scanning (PBS). A schematic view of this delivery method is shown in fig. 1.3. A narrow proton beam (typical width of 3 cm [43]) is used to fully irradiate the tumor, spot by spot, layer by layer [63]. Between the layers, the proton beam's energy is changed to adjust the depth of the Bragg peak. Starting with the maximum energy at the distal edge, the energy is lowered layer by layer until the full depth of the tumor is covered. Dipole magnets steer the proton beam within each layer to enable the scanning spot by spot.

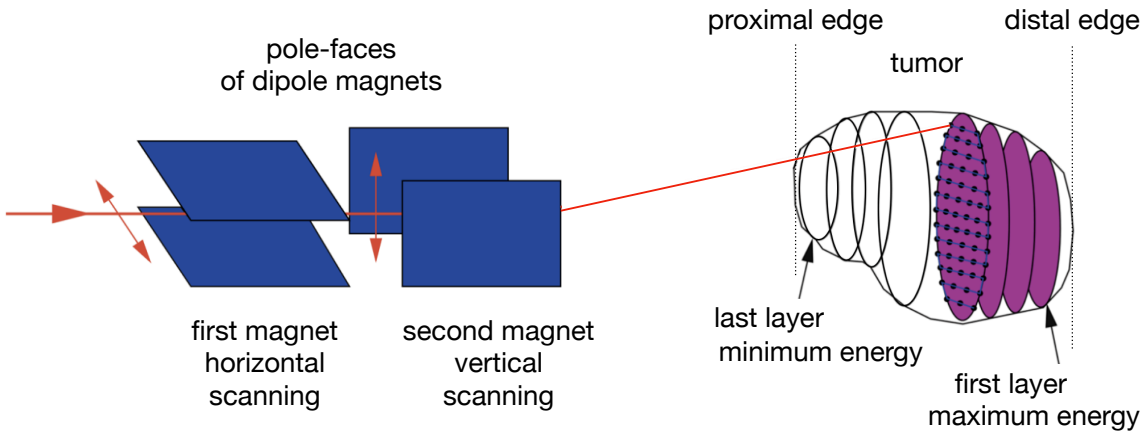

Figure 1.3: Schematic view of pencil beam scanning. Edited image from Krämer and Durante [32].

Besides PBS, several methods exist to modify the proton beam to irradiate the target, such as passive scattering. Passive scattering uses scattering foils to broaden the size of the incident beam. The incident beam is then divided over a broader beam, and thereby the dose is deposited over a larger volume, pulling down the dose-rate. As a result, the intensity of the beam is not large enough to irradiate the target with FLASH-compatible dose-rates.

Nevertheless, achieving ultra-high dose-rates with conventional PBS systems presents its own challenges. PBS requires switching of the beam energy during treatment, usually taking 0.1-1.0 s [1] due to the mechanical displacement of moderator material. With UHDR treatment times $\leq$ 0.1 s, the spot scanning speed must be in the order of milliseconds to stay within this time constraint. To reduce the time of energy degrading, Patriarca et al. [46] proposed the use of a ridge filter, which allows a time saving by a factor of 5-10. A ridge filter functions as an energy modulator by forming a spread-out Bragg peak, which will be explained in section 1.2.2.

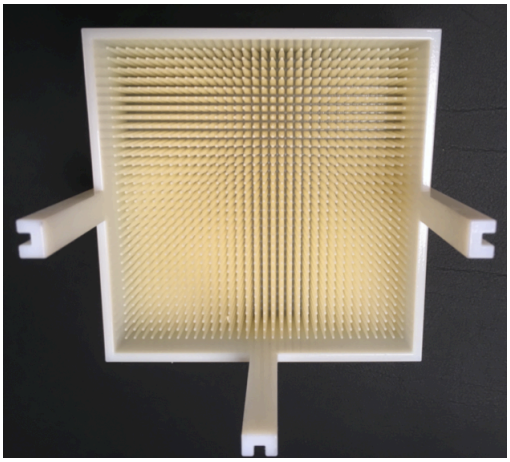

Figure 1.4: Ridge filter produced by GSI [25].

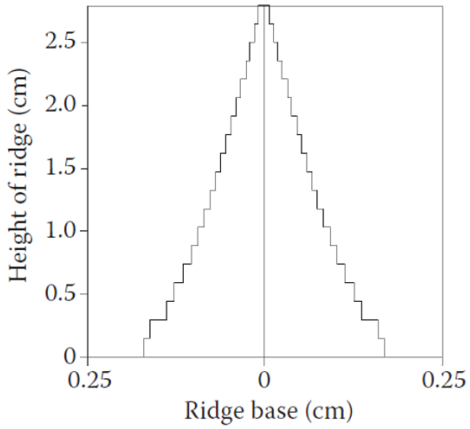

Figure 1.5: Typical cross-section of a pin in a ridge filter [43].

1.2.2. Spread-out Bragg Peak

A typical ridge filter consists of multiple pyramid-shaped pins, as shown in fig. 1.4. Figure 1.5 shows the cross-section of these pins. The principle of the ridge filter is that when a mono-energetic proton beam propagates through, it exits the filter with a spread-out energy distribution.

Protons passing through without interacting with the ridge filter have their Bragg peaks at the range of the initial energy, while protons hitting the ridge filter are slowed down so that their Bragg peaks end up earlier in the target. This generates a broad and continuous energy spectrum.

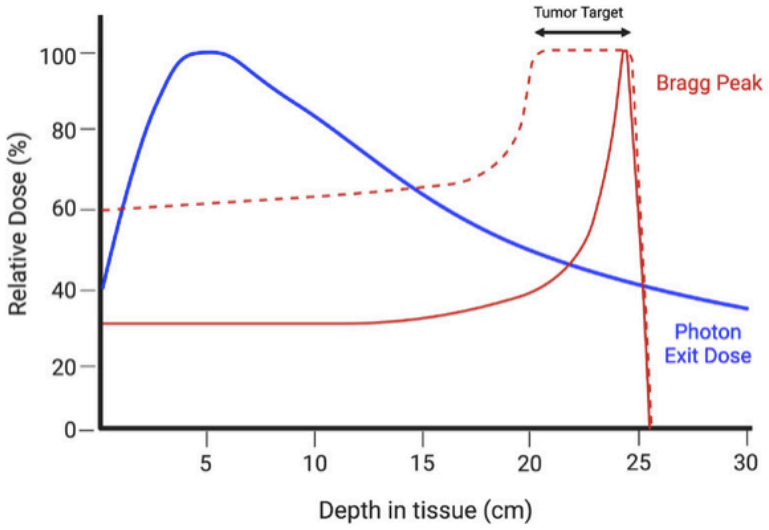

Figure 1.6: Dose-depth curves for photon (blue), proton (red), and spread-out Bragg peak (SOBP) (striped red) beams [40].

The pullback of the peaks is determined by the thickness of the ridge filter steps, while the weight of the shifted Bragg peaks is determined by the width of the ridge filter steps. In this way, an initial proton beam will give a spread-out dose distribution in the patient. The dose distribution looks like a spread-out of a Bragg peak curve and is therefore named a spread-out Bragg peak (SOBP). Figure 1.6 shows the typical relative dose distributions for a photon beam (blue), a mono-energetic proton beam (red), and a mono-energetic proton beam passing through a ridge filter (striped red). The spread-out Bragg peak enables dose delivery to a broader depth of tumor tissue with just one initial energy. The use of SOBP beams avoids the time-consuming process of switching the beam energy in between energy layers, which is required in conventional PBS (fig. 1.3).

1.2.3. Treatment delivery

Fractionation

In radiotherapy, including proton therapy, the dose is often delivered in multiple fractions. This is done because healthy cells are less sensitive to radiation than tumor cells, and fractionation increases the differential in damage between healthy and tumor cells. The fractionation sensitivity of tissue cells is expressed in the α/β ratio. Generally, the α/β ratio of healthy tissue is around 3 Gy and the tumor tissue $\alpha/\beta = 10$ Gy. The result of this fractionation difference is that healthy cells are more capable of repairing from irradiation than tumor cells.

Beam angles

A single proton beam can deliver a uniform dose distribution to the tumor by varying the energy in between layers, as shown in fig. 1.3. Even though, in proton therapy often several beam angles are used to further optimize the dose distribution [43]. Dose delivery from multiple angles often improves precision and increases the dose coverage. The dose to the organs at risk can be limited while the tumor is irradiated multiple times from different angles. The proton system in HollandPTC (fig. 1.7) can rotate completely around the patient and irradiate from 360°.

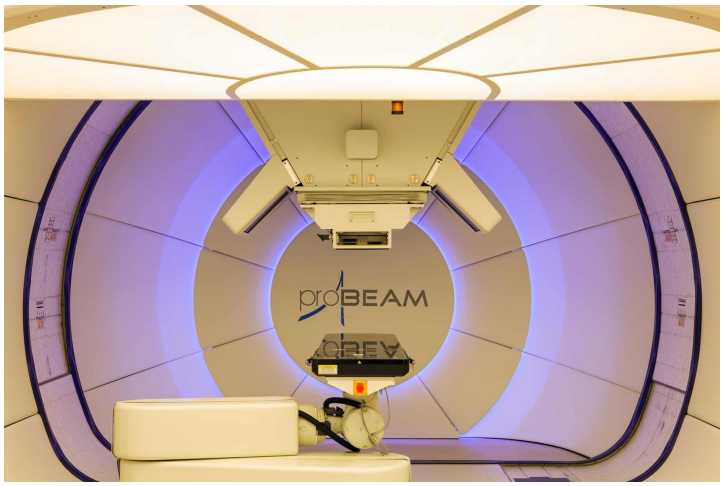

Figure 1.7: HollandPTC proton therapy system.

Treatment optimization

The main delivery approaches for PBS use single-field optimization (SFO) or multi-field optimization (MFO), also referred to as intensity-modulated proton therapy (IMPT). With SFO, the dose distributions of each beam angle are individually optimized, while with IMPT, the dose distributions of multiple beams are optimized together. The most common application of SFO is a single-field uniform dose (SFUD), where one or more homogeneous dose distributions are delivered to the target to make a composite plan. With IMPT, each individual beam will deliver an inhomogeneous dose to the target. The combination of dose distributions from multiple beam angles together form a homogeneous dose that matches the shape of the target.

1.3. Early-stage breast cancer

The investigation of FLASH with spread-out Bragg peak beams can be started in early-stage breast cancer. More specifically, low-risk early-stage breast cancer patients who can not receive surgery due to medical reasons. This study proposes definitive radiotherapy with FLASH proton therapy for this patient group. In breast cancer patients treated with radiotherapy, there is a need to decrease the level of toxicity [23, 62]. The healthy tissue sparing effect of FLASH proximal to the target could contribute to decreasing the toxicities.

1.3.1. Current treatment

In the current standard of care, patients with early-stage breast cancer undergo breast-conserving surgery to remove the tumor. Depending on the presence of tumor cells in lymph nodes and the likelihood of metastases, the patient can be treated with adjuvant radiotherapy and/or chemotherapy. The standard of care for post-operative radiotherapy is whole breast irradiation (WBI), which is beneficial in reducing the risk of local recurrence and breast cancer mortality [20].

Fractionation

For many years, the whole breast irradiation dose schedule was a dose of 50 Gy delivered in 25 fractions of 2 Gy. Usually, these fractions are given daily during working days over a period of 5 weeks. In the case of breast cancer, the α/β ratios of tumor tissue range from 3.0 to 4.8 Gy [2, 24, 47, 52, 60], meaning that healthy cells and tumor cells have a similar degree of repair after irradiation and no benefit of conventional fractionation (2 Gy per fraction) is present. The biological rationale to opt for higher doses per fraction has been investigated in clinical trials studying the effect of hypofractionation for breast cancer, using fraction doses $>$ 2 Gy. It was found that hypofractionation yields improved results in tumor control, acute toxicity, and late toxicity compared to conventional fractionation schemes [3, 52, 60]. These results and the convenience for both patients and radiotherapy facilities to reduce the number of treatment days resulted in the global implementation of hypofractionation schedules. The standard post-operative whole-breast treatment schedule in HollandPTC, a center for proton therapy located in Delft, for early-stage breast cancer is now 40.05 Gy in 15 fractions of 2.67 Gy.

1.3.2. Partial breast irradiation

Hypofractionation has also been implemented in partial breast irradiation. In this treatment, a relatively high dose is delivered only to the area surrounding the tumor bed (margin of 10-20 mm) since most local recurrences are expected to occur in the tumor bed region. Due to the volume reduction, the number of fractions could be reduced even further, resulting in accelerated partial breast irradiation (APBI). The increased dose results in an increased local recurrence rate in high-risk patients. Therefore, APBI is only used in selected patients with early-stage breast cancer and low-risk characteristics, such as relatively small tumor volumes. A common treatment schedule for hypofractionated APBI is 10 fractions of 3.85 Gy. Over the last few years, the COVID-19 pandemic has pushed even more on reducing the number of treatment days. In HollandPTC, this resulted in the standard fractionation schedule for partial breast of 5 fractions of 5.2 Gy, delivered every working day for one week.

1.3.3. Definitive radiotherapy

The favorable results in the efficacy and safety of APBI have stimulated research in pre-operative radiotherapy. With pre-operative APBI, the size of the tumor lesion can be reduced, which enables to undergo breast-conserving surgery for a larger patient group [24, 41, 44]. Some studies even suggest the possibility of a definitive radiotherapy treatment with curative intent [9, 35, 54, 62]. This treatment could benefit low-risk patients who cannot receive surgery due to medical risk factors, e.g., age.

Compared to post-operative radiotherapy, where the tumor bed is already removed, a definitive treatment requires a substantial increase in dose to kill all tumor cells. This increase in dose carries toxicity risks, given that the organs at risk with breast cancer radiotherapy are dose-limiting [52].

1.3.4. Treatment toxicities

The main radiation side-effects found in breast cancer patients treated with hypofractionated radiotherapy are necrosis in surrounding fat tissue, and fibrosis [22]. Fat necrosis is an inflammatory process that causes the death of cells. Most cases of fat necrosis occur after surgery or radiotherapy. With conventional dose schedules, fat necrosis is not a common complication. However, with the increased doses given in hypofractionated schedules, this has been observed [35, 56, 60]. Breast fibrosis is one of the most concerning toxicities of radiotherapy for healthy breast tissue surrounding the tumor. It is associated with poor cosmetic outcomes, and severe fibrosis can even lead to functional impairment [4]. Both toxicities are related to the dose given to healthy breast tissue. The healthy tissue sparing effect of FLASH in proton therapy could offer a suitable treatment by reducing these radiation toxicities in the breast tissue (due to FLASH) and possibly sparing organs at risk distal to the target, such as the heart and lungs (due to proton therapy).

1.4. Research goal

The purpose of this study is to investigate the feasibility of FLASH proton therapy with spread-out Bragg peak beams for definitive treatment for low-risk early-stage breast cancer patients who cannot receive surgery due to medical reasons. The aim is to determine the magnitude of the FLASH effect required to generate clinically acceptable plans with the proposed ridge filter beam set-up.

Treatment plans are generated using the in-house developed multi-criteria optimizer iCycle of Erasmus Medical Center (Erasmus MC) for IMPT plans [7]. Spread-out Bragg peak beams are simulated from a ridge filter set-up and implemented in iCycle. Different magnitudes of the FLASH effect are applied to the generated ridge filter treatment plans and evaluated using constraints from conventional proton therapy and dosimetric parameters for both fibrosis and fat necrosis. The evaluation results are compared to IMPT treatment plans in order to determine the magnitude of FLASH for which the ridge filter treatment plans give improved or similar results.

The thesis project started with a systematic review of the literature about the biological, technological, and clinical aspects of FLASH proton therapy, which can be found in appendix A. After the required theory in this chapter, the next chapter will elaborate on the methodology of generating a treatment plan with ridge filter generated spread-out Bragg peak beams. The results of the treatment plans for breast cancer patients will be shown in chapter 3 and discussed in chapter 4. Ending with the conclusions in chapter 5.

This thesis is performed at Delft University of Technology (TU Delft) and Erasmus Medical Center (Erasmus MC) in collaboration with Holland Proton Therapy Center (HollandPTC).

2

Methodology

In this chapter, the methods used in the thesis are described. First, the details of patient data are discussed. This is followed by the methodology of generating the treatment plans, including the implementation of ridge filter beams in the in-house treatment planning system from Erasmus MC. Moreover, the choice of dose fractionation schedules is explained. A metric is given to apply the FLASH effect to the ridge filter treatment plans. Finally, evaluation metrics are stated to analyze the generated treatment plans on clinical acceptability and toxicity-model endpoints.

2.1. Patients and CT scans

The patient data available are anonymized CT (computed tomography) data of breast cancer patients eligible for accelerated partial breast irradiation (APBI). No tumor tissue is visible on the CT because this data is post-operative. To delineate the tumor bed, surgical markers that are placed during surgery at the edges of the tumor are used. In this way, the post-operative CT data is used as if the clinical target volume (CTV) contained the tumor bed (gross tumor volume, GTV), see fig. 2.1. The included patients followed the 2017 ASTRO selection guidelines [10] for APBI, a Tis or T1 tumor $\leq$ 2.5 cm, and patients aged $\geq$ 50 years.

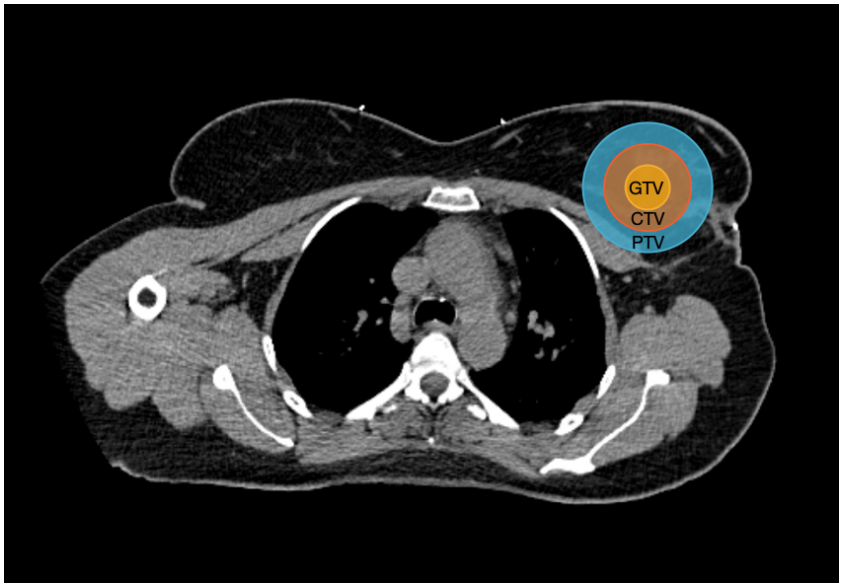

Figure 2.1: Visualization of the target volume concepts in radiotherapy: gross tumor volume (GTV), clinical target volume (CTV), and planning target volume (PTV). GTV is defined as the visible tumor in images and in this study defined by the surgical markers, CTV includes a margin for invisible tumor cells, and PTV includes a margin for uncertainties as delineation of patient set-up and organ movements.

2.2. Treatment planning

FLASH-compatible ridge treatment plans are generated by implementing spread-out Bragg peak (SOBP) beams in the existing Erasmus-iCycle IMPT optimization. The FLASH effect is applied in the ridge filter treatment plans and compared to conventional IMPT treatment plans to assess the clinical acceptability. For all treatment plans, dose-fractionation schedules are suggested to ensure tumor control while limiting toxicity.

2.2.1. Erasmus-iCycle

The treatment plans are created using Erasmus-iCycle [7]. This in-house developed treatment planning software is a multi-criterial beam-profile optimizer using a wishlist. In the wishlist, planning constraints and prioritized objectives are specified. The constraints are fixed while the objectives are strived to be achieved and optimized one by one in order of priority. When a current objective is achieved, the next objective will be optimized, and so on. The optimization is an iterative process and results in Pareto-optimal plans, meaning that it is impossible to improve one objective without deteriorating another. The wishlist is defined by the user and can be used to automatically generate treatment plans for a population of patients with the same tumor site [7].

Wishlist

General wishlists are created for patients with left- and right-sided breast cancer. Since Erasmus MC currently does not treat partial breast patients with definitive radiotherapy, a new wishlist was created based on the ICRU recommendations [26, 27] and in collaboration with a medical physicist.

The constraints and objectives of the wishlists can be found in appendix B. There are seven constraints and objectives, mainly defined for the minimum and maximum dose in the target volume and the maximum dose in the healthy breast tissue. All the constraints and objectives are defined relative to the prescribed dose, so a different dose-fractionation schedule only requires adjusting the prescribed dose and the number of fractions. Also, the number of beams and beam angles could be adjusted in the wishlist.

2.2.2. Spread-out Bragg peak beams

SOBP beams are implemented in Erasmus-iCycle, which has been performed in the master thesis project of Meijer [39]. Meijer developed a ridge filter model to generate FLASH-compatible proton beams for treatment planning in Erasmus-iCycle. The proposed ridge filter model uses PBS with a ridge filter and a compensator to degrade the energy, visualized in fig. 2.2. The ridge filter set-up is implemented in a simulation of the HollandPTC beamline to simulate the SOBP beams exiting the ridge filter. Subsequently, code is written to enable optimizing treatment plans with SOBP beams instead of pristine Bragg peak beams. This section will provide a summary of the implementation performed by Meijer [39].

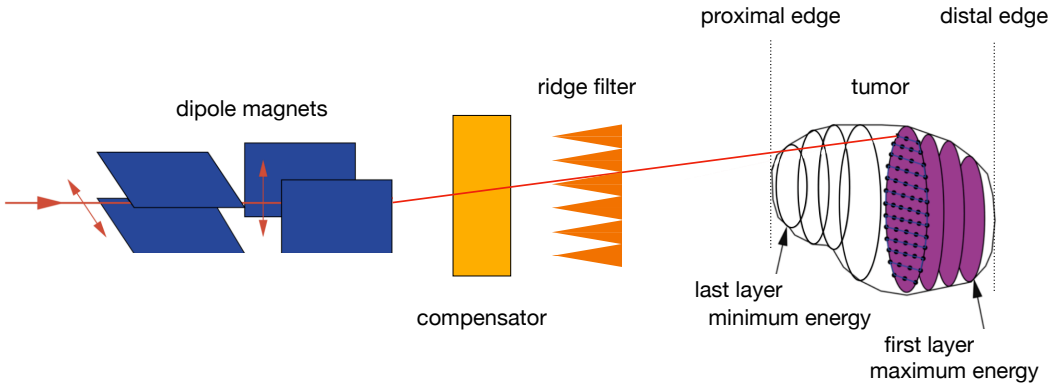

Figure 2.2: Schematic overview of pencil beam scanning with ridge filter and compensator set-up. Edited image from Krämer and Durante [32].

Set-up
The set-up presumes a maximal initial proton beam energy to realize the highest achievable dose-rate. For the HollandPTC beamline, this maximum is 244 MeV. This is the initial energy of the beam, visualized as the red line in fig. 2.2. The dipole magnets steer the proton beam to the lateral positions of the tumor. Next, the proton beam transverses through the compensator. The compensator is placed to slow down the proton beam to the energies belonging to the required energy layer (depth of the tumor). Besides this variation in energy, there is a static compensator (range shifter) present that shifts the proton beam range by 57 mm. The slowed-down proton beam then propagates through the ridge filter and exits with a spread-out Bragg peak. In this way, the tumor can be irradiated with SOBP beams instead of pristine Bragg peaks, as with conventional PBS. The ridge filter and compensator are placed as near to the patient as possible to limit additional scattering. The next section describes how this set-up is simulated to acquire a database with SOBP beams that can be implemented in iCycle.

Ridge filter data
The SOBP database is generated by Monte Carlo simulations of the HollandPTC R&D (research and development) beamline. First, the beam characteristics of the proton beam are implemented in the simulation and the conventional proton beam set-up is simulated for energy levels from 70 to the maximal beam energy of 244 MeV. The pristine Bragg peak dose-depth curves found in the simulation are compared and validated to those found in real measurements performed by Varian, manufacturer of the proton therapy system used in HollandPTC. Second, a ridge filter is placed in the simulation setup. This ridge filter is a 3D file of an existing ridge filter, produced by GSI and designed to give a spread-out Bragg peak of 3 cm for a beam energy of 154 MeV. A visualization of the 3D file of the ridge filter is shown in fig. 2.3. From the simulation set-up with the ridge filter, the energy spectra of the SOBP are retrieved and compared to measurements executed in the master thesis of Ibrahimi [25].

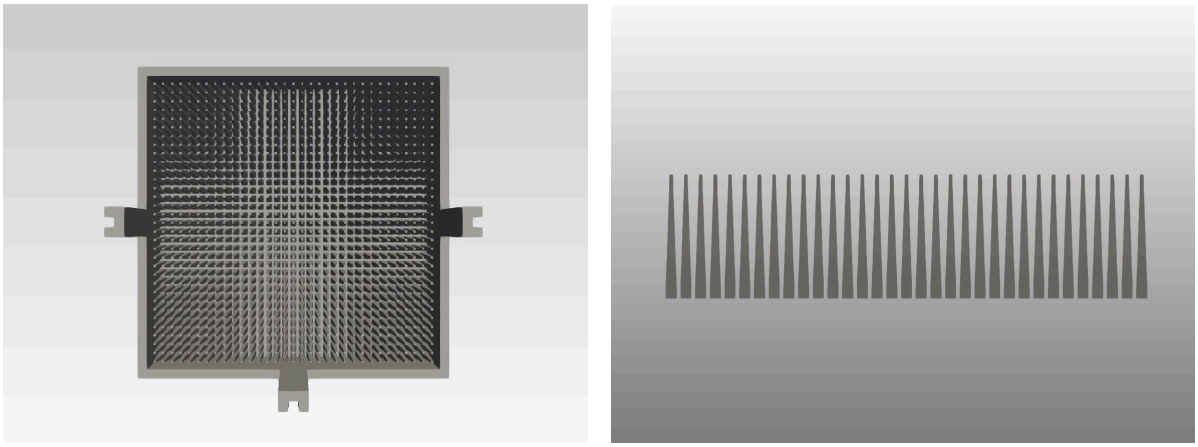

(a) Top view. **(b)** Cross section view.

Figure 2.3: 3D model of the ridge filter used to create the SOBP database in the thesis of Meijer [39].

Since the iCycle proton optimization algorithm is based on pristine Bragg peak pencil beams, it is convenient to rewrite the simulated SOBP energy spectra as a weighted sum of pristine Bragg peaks of HollandPTC beamline pencil beam energies. A non-negative linear least squares optimization is performed to approximate the combination of pencil beam energies to build up each SOBP energy spectrum. In this optimization, the spacing between the pencil beams of one SOBP is restricted by a range difference of approximately 3 mm. For energies under 200 MeV, this is approximately 3 MeV and for energies above 200 MeV this is an energy difference of approximately 2 MeV. The result is a database where each SOBP energy level from the Monte Carlo simulation is built up of a weighted sum of 8 - 10 pristine Bragg peaks with energies from the HollandPTC beamline. This database only contains nominal SOBP energies between 110 - 244 MeV, because the energy spectra below the 110 MeV could not be approximated with the energies from the HollandPTC beamline (70 - 244 MeV) [39].

To sum up, the final SOBP database contains for every SOBP energy level 8 - 10 energies and 8 - 10 accompanying weights. Figure 2.4 shows the SOBP dose-depth curve for 154.04 MeV from the database, built up out of nine weighted pristine Bragg peak beams of pencil beams within the HollandPTC beamline.

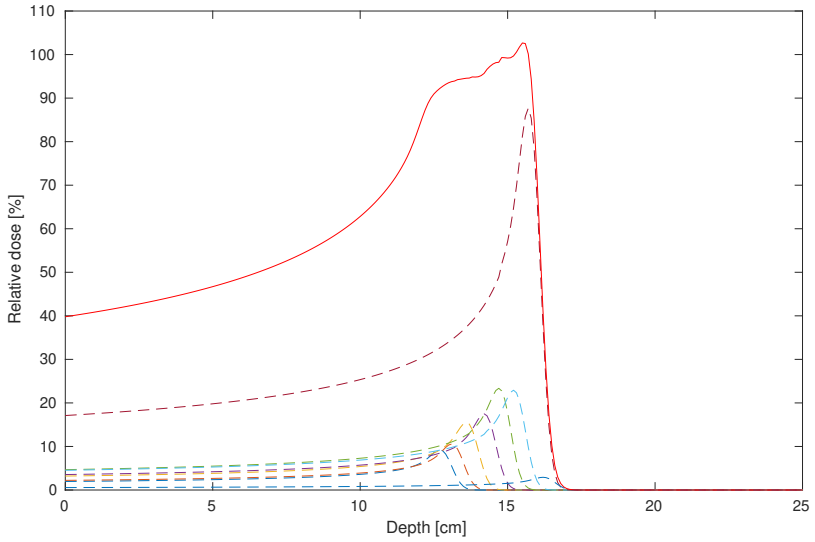

Figure 2.4: Example of an SOBP relative dose-depth curve (red) in water from the SOBP database with energy 154.04 MeV, built up out of nine weighted pristine Bragg peak beams (striped).

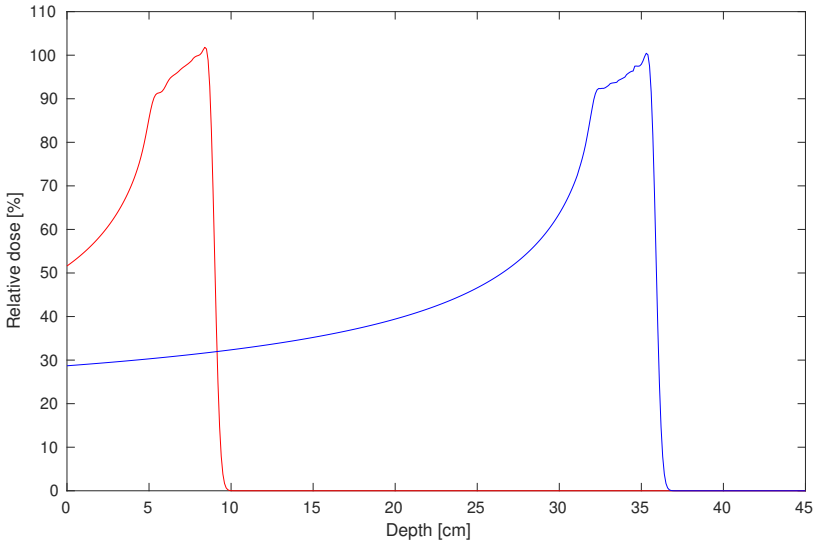

Figure 2.5: Dose-depth curves in water of SOBPs from the database. The minimal (110.42 MeV) and maximal (244.00 MeV) SOBP energies are shown in respectively red and blue.

Patient exclusion

The final SOBP database limits the group of patients eligible for this study. As can be seen in fig. 2.5, the range of the SOBP database in water is approximately 7.0 - 35.5 cm in water (looking at the 95% relative dose). However, the depth of the proton beam depends on the material it transverses. Compared to water, the SOBP will end up slightly deeper in the patient since breast tissue is primarily made up of fat tissue, which has a slightly lower density than water ($\sim$0.9 g/cm^3 [38] versus 1.0 g/cm^3). Moreover, the static range compensator of 57 mm of the set-up decreases the range by 5.7 cm. With the limited range of the used SOBP database, it is expected that it will not be feasible to generate treatment plans for tumors located outside the range of roughly 2.5 - 30 cm. Therefore, these patients will be excluded from this study.

2.2.3. Implementation in iCycle

The Erasmus-iCycle code for IMPT treatment plans is adjusted for the implementation of SOBP beams. Proton treatment optimization starts with the challenge of pencil beam reduction. If all the possible pencil beams laying within the target volume would be used, this would result in far too many pencil beams. Aside from the time-invasive optimization, actual treatments would be too time-consuming. It is therefore desired to reduce the number of pencil beams while striving for clinically acceptable dose distributions. In this thesis, the initial pencil beam selection is defined on a regular grid with relative energy spacing, which will be explained in the following paragraphs. The implementation of the SOBP is included later in the optimization, after the initial pristine Bragg peak pencil beam selection.

Regular grid

In the IMPT code, two methods of pencil beam selection are implemented by Water van de et al. [59]: resampling and regular grid. With resampling, the multi-criterial optimization is repeated. Starting with a random sample of candidate spots laying in the target volume, spots with small contributions are excluded during each iteration and a new sample of random spots is added. However, FLASH-compatible SOBP beams have a restriction in the localization of spots. Because switching beam energy during treatment is too time-consuming for UHDR, as discussed in section 1.2.1, only one energy can be used for every lateral position. Where the Bragg peak depths in an IMPT treatment plan can be randomly placed, SOBP beams require the pristine Bragg peak beams belonging to one SOBP to be placed in the same lateral position. It is therefore chosen to select candidate pencil beams with the regular grid optimization method, where the optimizer is restricted to only use spots laying on a specified grid, shown in fig. 2.6. In this study, a regular grid with a lateral spacing of 5 mm is used.

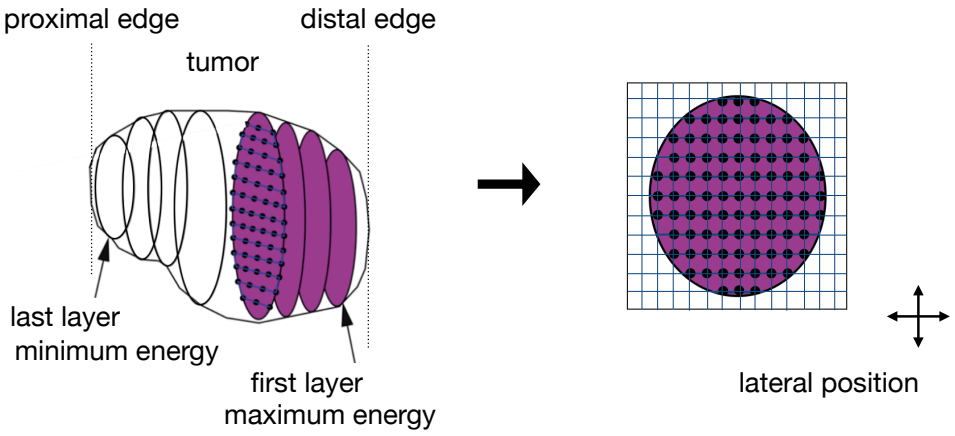

Figure 2.6: Visualization of pencil beam spot selection with a regular grid for the lateral spot position.

Energy layers

Where the regular grid covers the lateral position of the pencil beam spots, the distal spacing is determined by the energy layers, see fig. 2.6. The HollandPTC beamline could provide an energy layer approximately every 0.1 cm. Thus for a tumor size of 3 cm, 30 energy layers would be suitable. However, in clinical IMPT a much larger energy spread is used, partly because of the irradiation time and partly due to the minimal weight per pencil beam. Besides, that many energy layers might not even be needed to have a clinically acceptable dose distribution. To reduce the number of energy layers in the optimization in this study, relative energy spacing is used. First, the maximum beam energy is determined by the depth of the distal edge of the tumor. The pencil beam energy belonging to this depth is used as a starting point. Subsequently, the depth of the energy layer next in line is compared to the width of the current Bragg peak. If the depth of the current energy layer minus the width of the Bragg peak is lower than the depth of the next considered pencil beam, the overlap between the two Bragg peak curves is too close and the considered pencil beam will be skipped, fig. 2.7a. The comparison continues until the next energy layer has a depth lower than the current depth minus the Bragg peak width, fig. 2.7b. That energy layer will be the starting point for the next comparison. This process is repeated until the proximal edge of the tumor is reached and the minimum energy layer is found. In the optimization in this study, a relative energy spacing of 1 is used at 80% relative dose, meaning that the energy spacing must be at least 1 Bragg peak distance at 80% relative dose.

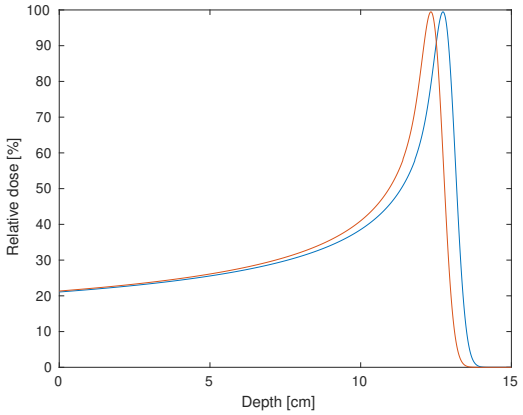

(a) Bragg peaks for pencil beam energies 135.84 MeV (blue) and 133.42 MeV (red).

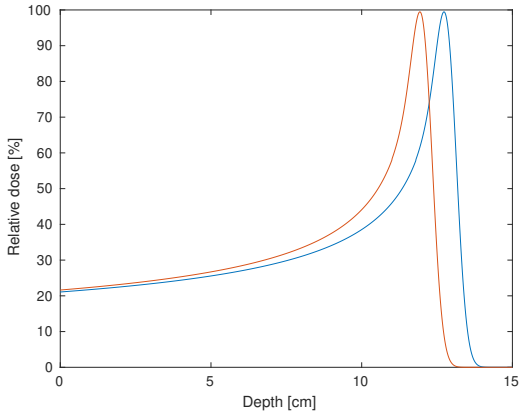

(b) Bragg peaks for pencil beam energies 135.84 MeV (blue) and 130.98 MeV (red).

Optimization

The optimization starts with a selection of candidate pencil beams on a regular grid with relative energy spacing, based on the patient CT and chosen beam direction. This results in a list of potential pencil beams with specified energy and lateral position (x and y positions on the regular grid).

Subsequently, the candidate pencil beams with energies below 110 MeV are removed from the list (described in section 2.2.2). The remaining pencil beams are replaced by the SOBP beams from the same energy from the database, consisting of 8 - 10 weighted pencil beams. This gives an extended list of pencil beams with specified energy, lateral positions, and weights. The pencil beams belonging to one SOBP beam have the same lateral position and relative weights.

Next, the dose deposition matrix for the extended list of pencil beams is calculated. This dose deposition matrix describes the dosimetric impact of one pencil beam for one monitor unit (MU) on a voxel in the patient. The monitor unit values could be interpreted as the minimum irradiation time per pencil beam.

The dose-deposition matrix is the input for the multi-criteria optimization together with the objectives and constraints of the wishlist. The result is a matrix that contains the optimized monitor unit values for each pencil beam, which together with the dose deposition matrix, gives the dose delivered to each voxel in the patient.

After the multi-criteria optimization, the SOBP beams with low monitor unit values are removed. By removing pencil beams with low monitor values, only pencil beams that have a significant contribution to the dose remain. This is done through an iterative process.

In the final step of the optimization in iCycle, double lateral positions are indexed and the SOBP beams with the lowest weight are removed as only one energy can be chosen for every lateral position. With the remaining SOBP beams and their unique lateral positions, the final dose calculation is performed.

2.2.4. Dose-fractionation schedules

Fractionation

The α/β ratio for breast cancer ranges in literature from 3.0 to 4.8 Gy [2, 24, 47, 52, 60]. Based on this literature and discussions with radiotherapist-oncologist in HollandPTC, an α/β ratio of 3 Gy is used in this study. With this α/β ratio, healthy cells and tumor cells have the same degree of repair after irradiation so there is no biological benefit of fractionation.

For FLASH proton therapy, there is a benefit of fractionation since it enables dose delivery from different beam angles. Changing beam angles during one fraction of treatment requires shifting the gantry and couch. With FLASH dose delivery this would be too time-consuming such that the average dose-rate will be compromised far below the FLASH dose-rate threshold of 40 Gy/s. Therefore, FLASH-compatible irradiation with multiple beam angles does require multiple fractions. Additionally, FLASH proton therapy is clinically limited to hypofractionated treatments due to its fraction dose threshold of 7 Gy [37].

It is unclear to what extent the FLASH effect remains when healthy tissue is irradiated more than once during one fraction. This can be overcome by single beam per fraction (SBPF) delivery. SBPF is a treatment approach with one or more fractions, where in each fraction a uniform dose from one beam angle (SFUD) is delivered to the target to ensure tumor control. Habraken et al. [21] investigated the trade-off between the FLASH effect and the loss of fractionation in FLASH-enhanced SBPF versus all beams each fraction. They found that for a FLASH enhancement ratio (FER) ranging from 1.3 to 1.1 the FLASH effect outweighs the loss of fractionation in proton therapy of lung lesions. In this thesis, the ridge filter treatment plans are designed using the SBPF approach. Thus the number of fractions of a ridge filter treatment plan is equal to the number of selected beam angles.

Dose level

The biological effect of dose-fractionation schedules is expressed in the biologically effective dose (BED), eq. (2.1). The equation for BED is derived from the Linear Quadratic (LQ) model[1]. Fractionated treatments with equal BED will result in an equal biological effect and are called iso-effective. Moreover, the BED of consecutive fractionated treatments can be summed to calculate the biological effect of the overall treatment.

$$\text{BED} = D \cdot \left(1 + \frac{D}{N \cdot \alpha/\beta}\right) \tag{2.1}$$

With D the total dose delivered in N fractions and α/β the radiosensitivity of the tumor tissue.

As mentioned in section 1.3.1, the current treatment schedule for postoperative radiotherapy in Erasmus MC is 15 fractions of 2.67 Gy for whole breast irradiation and 5 fractions of 5.2 Gy for partial breast irradiation, giving a BED of relatively 75.70 Gy and 71.07 Gy. However, the dose delivered during postoperative radiotherapy is intended to reduce local recurrence of tumor cells and is delivered after the tumor is removed, while with definitive radiotherapy the number and density of tumor cells are significantly higher. Therefore definitive radiotherapy requires a different dose-fractionation schedule than postoperative radiotherapy.

[1] The cell survival is expressed in the surviving fraction $SF_d = e^{-(\alpha d + \beta d^2)}$ with d the dose per fraction. For fractionated treatment with $N(= D/d)$ fractions, the cell survival is expressed by:

$$SF_{Nd} = (SF_d)^N = e^{-N(\alpha d + \beta d^2)} = e^{-(\alpha D + \beta D^2/N)} = e^{-\alpha \cdot \text{BED}}$$

Definitive radiotherapy for early-stage breast cancer has been investigated in multiple studies. Recent phase I and II trials use hypofractionation schemes of 5 fractions of 10 Gy [35] and even single fraction doses up to 25 Gy [54], having biological effective doses in a range of 168.00 - 233.33 Gy. Most of these clinical trials are still ongoing, however, the study of Horton et al. [24] is one of the trials that published the first results. Single fraction doses of 15, 18, and 21 Gy were delivered with photon therapy to three patient cohorts and at a median follow-up of 23 months, no local occurrences or dose-limiting toxicities were noted. The cosmetic outcomes were good and long-term toxicities were low. These results have led to an increase in the initiation of clinical trials for preoperative early-stage breast cancer patients, mostly investigating single fraction IMRT with a dose of 21 Gy: NCT03520894, NCT01727011, NCT02482376, and NCT02212860 [62].

In this study, iso-effective dose-fractionation schedules of a single fraction dose schedule of 21 are used. So all fractionation schedules will have the same BED as the BED of 1 fraction of 21 Gy (168.00 Gy). This dose level is chosen because it has shown sufficient efficacy in tumor tissue in literature [9, 24, 44] with good cosmetic outcomes, no local occurrences, and a low number of chronic toxicities. As the aim of this study is to generate clinically acceptable plans it is important to assure tumor control such that the possible benefits of the FLASH effect for healthy tissue can be investigated.

Schedules
The iso-effective dose schedules of 21 Gy in a single fraction are determined and listed in the second column of table 2.1. The maximum number of 5 fractions is chosen because the FLASH effect comes with a fraction dose threshold of 7 Gy [37]. Therefore, the benefit of FLASH on healthy tissue is not expected to play a role if the dose per fraction is nearby the 7 Gy, which is the case for more than 5 fractions with a BED of 168 Gy.

Table 2.1: Dose-fractionation schedules of the ridge filter and IMPT treatment plans.

Number of beam angles	Ridge filter	IMPT
1	1 x 21.00 Gy	1 x 21.00 Gy
2	2 x 14.45 Gy	1 x 21.00 Gy
3	3 x 11.55 Gy	1 x 21.00 Gy
4	4 x 9.83 Gy	1 x 21.00 Gy
5	5 x 8.65 Gy	1 x 21.00 Gy

The IMPT treatment plans in this study are all single fractions of 21 Gy. Because IMPT is planned as a multi-field optimization, multiple beam angles can be delivered during one fraction. To be able to compare the fractionated ridge filter treatment plans with the single fraction IMPT plan, the ridge filter treatment plans will be recalculated to the equivalent single fraction dose D_{eq}. This can be done by summing the BED of each individual fraction and determining the dose for the case of 1 fraction by solving eq. (2.2). With the dose-fractionation schedules in table 2.1, the equivalent single dose distribution should have a dose level of 21 Gy.

$$\text{BED}_{\text{sum}} = \text{BED}_{\text{fraction1}} + \text{BED}_{\text{fraction2}} + ... = D_{eq} \cdot \left(1 + \frac{D_{eq}}{N \cdot \alpha/\beta}\right) \tag{2.2}$$

In this research, beam angle optimization is not considered, so the same beam angles are chosen in a range of 0 - 50° for all plans. This is done manually based on the results for the homogeneity indices. The beam angles are defined for left-sided breast cancer and have a minus sign for right-sided breast cancer, as shown in fig. 2.8.

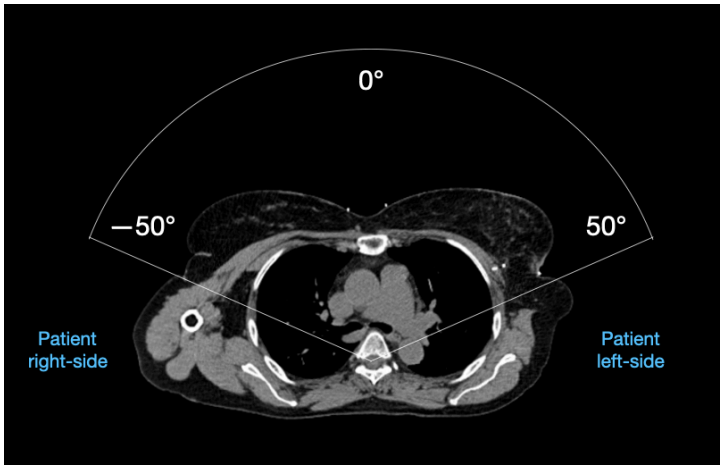

Figure 2.8: Axial plane of a CT scan of a torso with visualized beam directions. For left-sided breast cancer, the beam angle range is between 0° and 50° and for right-sided, the beam angle range is between 0° and -50°.

2.2.5. FLASH effect

A measure to express the FLASH effect is the FLASH enhancement ratio (FER) metric, eq. (2.3). This is the ratio of dose resulting in the same biological effect delivered with a conventional dose-rate (IMPT in this study) versus an ultra-high dose rate (FLASH proton therapy). To simulate the FLASH effect in our ridge filter treatment plans, the dose in all healthy tissue voxels will be reduced by the FER. Since FLASH is considered a fraction dose effect [37], the FER will be applied to each fraction dose. Besides, the FLASH effect comes with a fraction dose threshold of 7 Gy. This means that the differential reduction is only seen if the healthy tissue receives more than 7 Gy. Therefore, the FER is applied to the physical fraction doses of all healthy tissue voxels receiving $>$ 7 Gy.

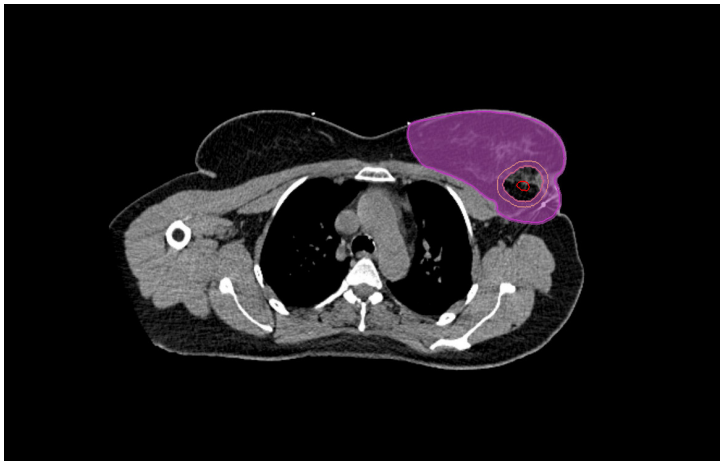

Figure 2.9: Visualization of the voxels where the FER is applied in pink, all voxels in the breast excluding the CTV. From the inside to the outside the red, orange, yellow, and pink delineations represent respectively the GTV, the CTV, the PTV, and mamma ipsilateral (the breast, either left or right, where the tumor is located).

This study focuses on the toxicities to healthy breast tissue where all breast tissue voxels excluding the clinical target volume are considered healthy tissue voxels, as shown in fig. 2.9. The exact magnitude of the FLASH effect remains unknown, so in this study FERs from 1.0 (no FLASH effect) to 2.0 (100% damage reduction) are considered in steps of 0.1.

$$\text{FER} = \left.\frac{D_{\text{FLASH}}}{D_{\text{IMPT}}}\right|_{\text{Same biological effect}} \tag{2.3}$$

2.3. Analysis

The generated IMPT and ridge filter plans are all assessed on metrics for the clinical acceptability of plans (dose uniformity and coverage) and toxicity-model endpoints (fibrosis and fat necrosis). It is expected that ridge filter treatment plans will underperform compared to the IMPT treatment plans since ridge filter beams have limitations in spot selection. However, the FLASH effect might compensate for this. Therefore, different values for the FER will be applied to the ridge filter plans and analyzed by the metrics explained in this section to determine the magnitude of FER for which the ridge filter treatment plans benefit the IMPT treatment plans.

2.3.1. Dose uniformity & coverage

Homogeneity

A common evaluation metric for the dose uniformity of a treatment plan is the homogeneity index (HI) of the planning target volume (PTV), eq. (2.4). $D_{2\%}$ and $D_{98\%}$ represent the near maximum and near minimum absorbed dose in the PTV. The HI describes the uniformity of a dose plan. In an optimal homogeneous plan all voxels in the PTV receive the prescribed dose D_{pr}, giving a negligible difference between $D_{2\%}$ and $D_{98\%}$ and therefore HI will go to 0. The ICRU [27] recommendations prescribe 107% and 95% of the prescribed dose for the near maximum and near minimum dose, so a homogeneity index of 0.12.

$$\text{HI} = \frac{D_{2\%} - D_{98\%}}{D_{\text{pr}}} \tag{2.4}$$

In this study, all treatment plans are scaled such that 98% of the PTV receives 95% of the prescribed dose. When comparing plans with the same prescription dose, the $D_{98\%}$ will have the same value, so eq. (2.5) will be used as the evaluation metric for the homogeneity.

$$\text{HI} = \frac{D_{2\%}}{D_{\text{pr}}} \tag{2.5}$$

Recalculating the values for eq. (2.4) results in a maximum HI of 1.07 (107%) for eq. (2.5) of a clinically acceptable dose plan.

Conformity

To express the dose coverage of a treatment plan, the conformity index is used, eq. (2.6).

$$\text{CI} = \frac{V_{95\%}}{V_{\text{PTV}}} \tag{2.6}$$

$V_{95\%}$ is the volume of the breast that receives 95% of the prescribed dose in cc (cm^3) and V_{PTV} is the planning target volume in cc. A conformity index of 1 corresponds to an ideal coverage, as the volume receiving 95% of D_{pr} is equal to the PTV. A conformity index greater than one indicates that the irradiated volume exceeds the target volume and covers part of the healthy tissue. With FLASH, it is expected that the volume receiving dose will be decreased so the CI will decrease. Because of the decreased dose in healthy tissue, the risk of developing fibrosis and fat necrosis will be reduced.

2.3.2. Fibrosis

To estimate the risk of breast fibrosis, multiple normal tissue complication probability (NTCP) models have been proposed. In this thesis, the model of Avanzo et al. [2] is used. This NTCP Lyman model [36] uses the biologically equivalent uniform dose (BEUD) where the equivalent uniform dose (EUD) is the dose that is assumed to produce the same toxicity probability as the inhomogeneous dose distribution when delivered uniformly.

$$\text{EUD} \equiv \left(\sum_i v_i (D_i)^{\frac{1}{n}} \right)^n \tag{2.7}$$

In eq. (2.7) v_i is the relative sub-volume of the healthy breast tissue irradiated with dose D_i. The volume effect of the irradiated tissue is described by parameter n. Equation (2.7) is actually a generalized average where the volume effect is added. With $n = 1$, the EUD is equal to the average dose, the

weighted sum of the relative volumes v_i receiving dose D_i. However, if the volume effect n is decreased, eq. (2.7) will tend more toward the maximum dose, indicating an organ at risk where complication occurs already when a small volume receives too much dose.

In order to investigate the biological effect of fractionated uniform dose delivery, the EUD is corrected for the α/β ratio, the number of fractions N in which the dose is delivered, and the repair factor h in between fractions to determine the BEUD:

$$\text{BEUD} \equiv \text{EUD}\left(1 + \frac{\text{EUD}}{N \cdot \alpha/\beta}[1+h]\right) \tag{2.8}$$

For conventional fractionation schedules (fractions given once a day) it is assumed that complete repair of healthy tissue cells occurs overnight, with a repair factor $h = 0$. If for example, two fractions are given on the same day, there is less time for healthy tissue to recover from sublethal damage so the biological effect of the fractioned schedule will be higher, indicated with $h > 0$.

The BEUD indicates the biological effect of the dose distribution if it would be delivered uniformly. To determine the risk of fibrosis to the healthy breast tissue, the BEUD of the ipsilateral breast without the tissue in the CTV is calculated. The ipsilateral breast is the breast (left or right) where the tumor is located. The BEUD is then compared to BEUD_{50}, eq. (2.9), the BEUD where there is 50% risk on developing fibrosis, with m the slope of the dose-response curve. This results in X, a measure of the damage in the breast tissue. The normal tissue control probability is then the integration of the area under the gaussian distribution to the level X, eq. (2.10).

$$X = \frac{\text{BEUD} - \text{BEUD}_{50}}{m \cdot \text{BEUD}_{50}} \tag{2.9}$$

$$\text{NTCP} = \frac{1}{\sqrt{2\pi}} \int_0^X e^{-\left(\frac{2}{2}\right)} \mathrm{d}x \tag{2.10}$$

In the analysis of the treatment plans, the risk of ipsilateral breast fibrosis is determined with a fixed α/β ratio and complete repair because the dose is delivered in not more than one fraction a day. The parameters used from the model of Avanzo are: BEUD_{50} =107.2 Gy, n =0.06 and m =0.22 for an α/β =3.0 Gy and h =0 [2]. In fig. 2.10 the curve of the NTCP with a BEUD of 107.2 Gy is shown.

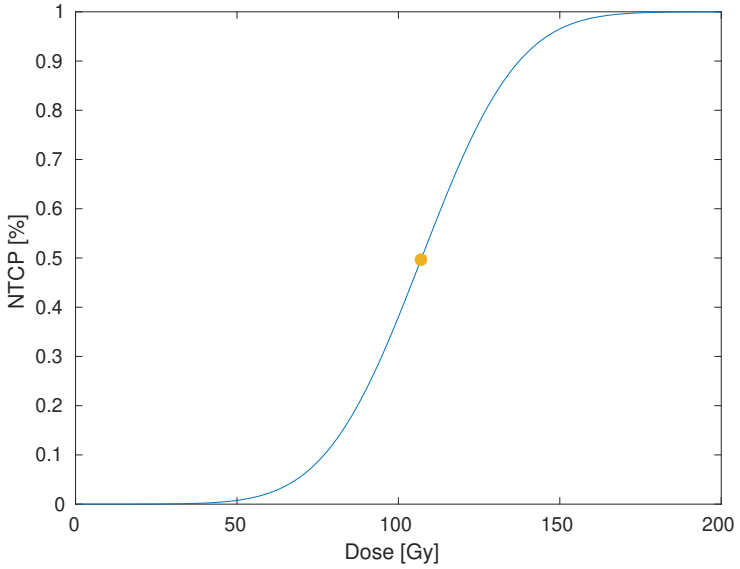

Figure 2.10: Normal tissue control probability of developing fibrosis curve. The marker indicates the value of BEUD_{50} =107.2 Gy where the risk of developing fibrosis is 50%.

2.3.3. Fat necrosis

Fat necrosis as a side-effect of hypofractionated radiotherapy has been observed in partial-breast irradiation studies with electron, and photon beams [48, 55, 56]. The study of Vicini et al. [56] treated patients using photon beams with accelerated partial-breast irradiation (APBI). The patients with a tumor size $\leq$ 3 cm were treated post-operative after surgery with a dose of 34-38.5 Gy in 10 fractions given twice daily. Toxicity results were scored based on the radiation therapy oncology group toxicity grade [11]. In 8% of the patients, fat necrosis was reported, equally divided into grade I (painless) and grade II (painful) symptoms. Veronesi et al. [55] used intraoperative electron therapy to deliver a dose of 21 Gy. Of the 590 treated breast cancer patients with tumor sizes $\leq$2.5 cm in diameter, fat necrosis was reported in 15 patients (2.5%). It was noted that the complication occurred mainly in patients aged above 70 years with relatively more fat tissue in the breast. Both studies stated that no conclusions on dose constraints could be drawn due to the low incidence of fat necrosis.

A recent report from Rahimi et al. [48] studying the development of fat necrosis after PBI does conclude on dosimetric and physiologic parameters. This dose-escalation phase I trial included 75 patients with tumor size $\leq$ 3 cm. The patients were divided into five cohorts, each with different dose schedules varying between 30 - 40 Gy in five fractions. Dosimetric parameters, fractionation, the maximal dose, and the ipsilateral breast volume were considered for the evaluation. The results were graded with grade I and grade 2, respectively painless and painful fat necrosis. Of the 75 patients, 11 developed fat necrosis, of which five grade 1 and six grade 2. The results were translated into dosimetric recommendations, which will be used in this thesis to include the risk of fat necrosis in our evaluation of FLASH treatment plans, table 2.2. As these recommendations are based on dose schedules with five fractions and all the treatment plans in this study are recalculated to a single fraction, the recommendations are translated to a single fraction using eq. (2.1). The volume factors $V_{X\text{Gy}}$ in table 2.2 represent the volumes of the healthy breast tissue in cm^3 receiving $\geq X$ dose.

Table 2.2: Dose constraint recommendations for partial breast irradiation to prevent painful necrosis in patients with breast volume greater than 1000 cm^3 [48], recalculated to a single fraction with an α/β ratio of 3 Gy.

Factor	Constraints
Maximal dose D_{max}	23.14 Gy
V18.34 Gy	95 cm^3
V19.53 Gy	85 cm^3
V20.66 Gy	50 cm^3
V21.79 Gy	20 cm^3
V22.92 Gy	1 cm^3
Planning target volume	$\leq$ 100 cm^3

Unfortunately, the constraint recommendations of Rahimi et al. [48] are not yet expressed in a normal tissue control probability curve for healthy breast tissue. Therefore, no analytical number can be given to the risk of developing fat necrosis. It is assumed that no painful fat necrosis will develop with treatment plans that meet the dose constraints.

3

Results

In this chapter, first the characteristics of the patients are stated followed by the results of the IMPT and ridge filter treatment plans for one patient. Results from the second patient can be found in appendix C.

3.1. Patient data

The study included two patients eligible for APBI and where the tumor is located in the range of 2.5 - 30 cm. In table 3.1 the volumes of the GTV, PTV and mamma ipsilateral (the breast, either left or right, where the tumor is located) are given. Moreover, the distance of the proximal and distal edge from the skin, measured from a beam angle of 45° are listed.

Table 3.1: Characteristics of the tumor of the patients.

	Tumor	**Volume GTV (cc)**	**Volume PTV (cc)**	**Volume mamma ipsilateraal (cc)**	**Proximal edge PTV (cm)**	**Distal edge PTV (cm)**
Patient 1	Left-sided	3.02	74.78	1309.34	9.5	3.3
Patient 2	Right-sided	12.16	111.78	1475.53	9.2	3.8

3.2. IMPT treatment plans

An example of a generated IMPT treatment plan is shown in fig. 3.1. The treatment plan prescribed a dose of 21 Gy to the PTV (delineated in red). The yellow delineation represents the GTV. The uniformity of this plan is expressed in the HI = 1.032 and the coverage of the PTV is 1.0151.

The results of the optimization of IMPT treatment plans are presented in table 3.2, including the treatment planning times and the number of energy layers and lateral positions in the final plan. In fig. 3.2, the dose distributions of the selected energy layers in water for the single fraction IMPT treatment plan are shown.

Table 3.2: Optimization results of the treatment planning times, number of selected energy layers, and the number of lateral positions for the IMPT treatment plans.

Treatments plans	**Beam angles (°)**	**Treatment planning time (HH:MM)**	**Number of energy layers**	**Number of lateral positions**
1 fraction	30	01:02	17	227
2 fractions	25, 45	03:10	31	282
3 fractions	25, 30, 45	05:40	40	287
4 fractions	25, 30, 40, 45	10:48	53	289
5 fractions	20, 25, 30, 40, 45	14:58	58	294

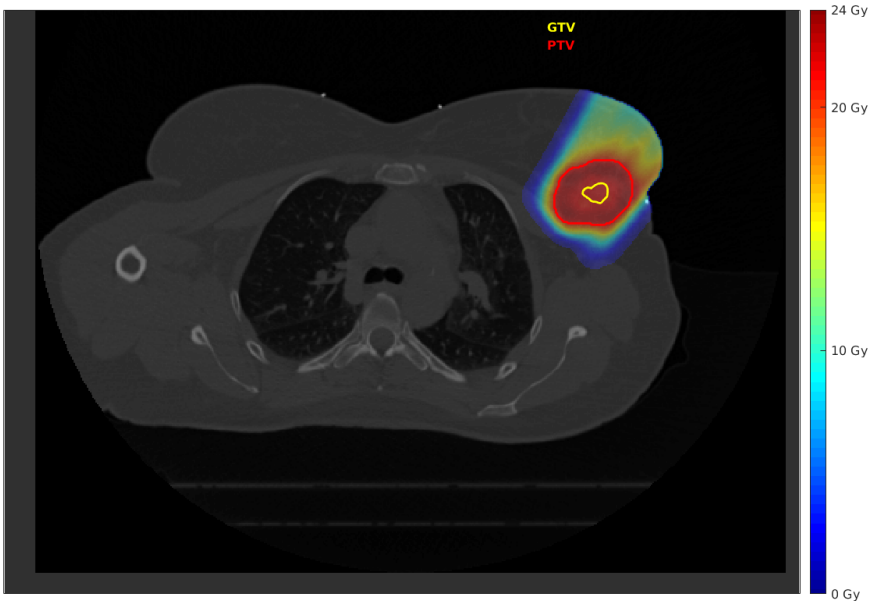

Figure 3.1: Dose distribution of a single fraction IMPT plan with a prescribed dose of 21 Gy and three beam angles, 25°, 30°, 45°.

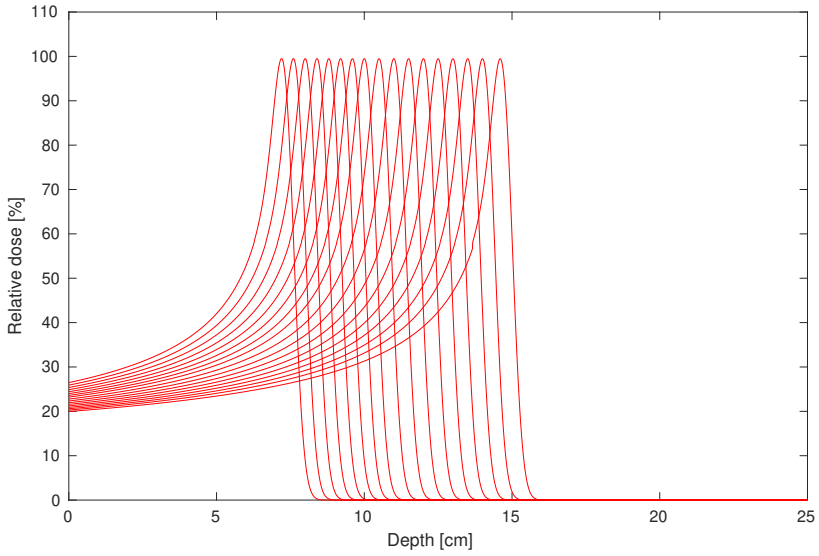

Figure 3.2: Relative dose distribution in water of the selected energy layers for a single fraction IMPT treatment plan with a beam angle of 30°.

3.3. Ridge filter treatment plans

An example of a generated ridge filter treatment plan is shown in fig. 3.3. This treatment plan is the iso-effective single-fraction dose distribution of three separate SFUD plans. In fig. 3.4 the dose distribution of the individual plans is given. These treatment plans are prescribed on 11.55 Gy such that the three fractions together have an iso-effective single-fraction dose of 21 Gy, comparable to the IMPT treatment plan in fig. 3.1. The HI of the individual fraction doses are 1.129, 1.119, and 1.179 for respectively the beam angles 25°, 30°, and 45°. The conformality index of the overall ridge filter plan is 1.5605, indicating an overdose.

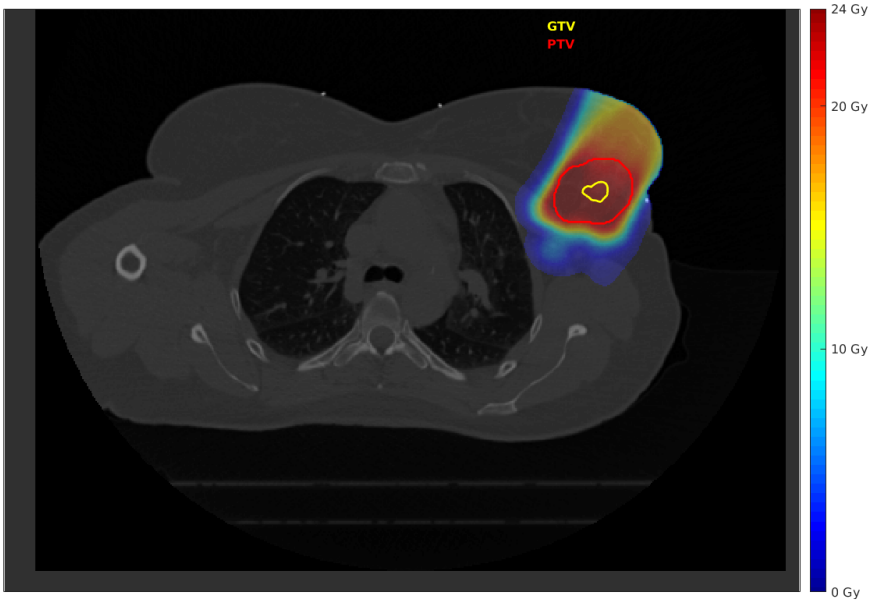

Figure 3.3: Dose distribution of a ridge filter plan consisting of three single-field uniform dose fractions with three different angles, 25°, 30°, 45°, and each fraction a prescribed dose of 11.55 Gy.

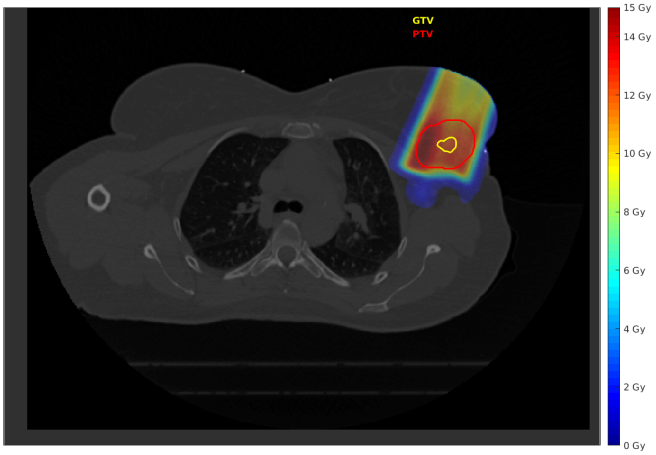

(a) Beam angle 25°.

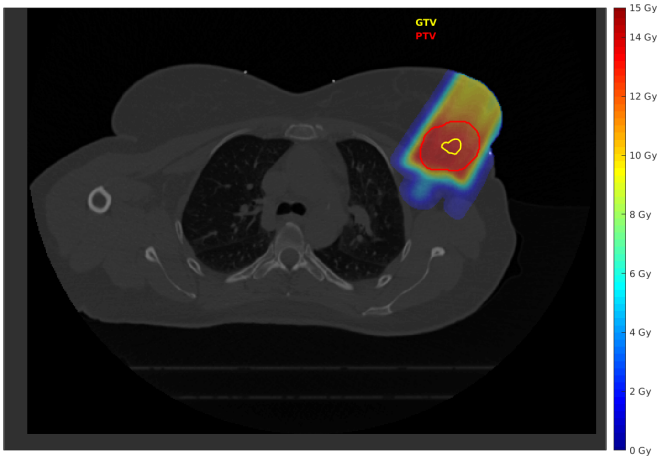

(b) Beam angle 30°.

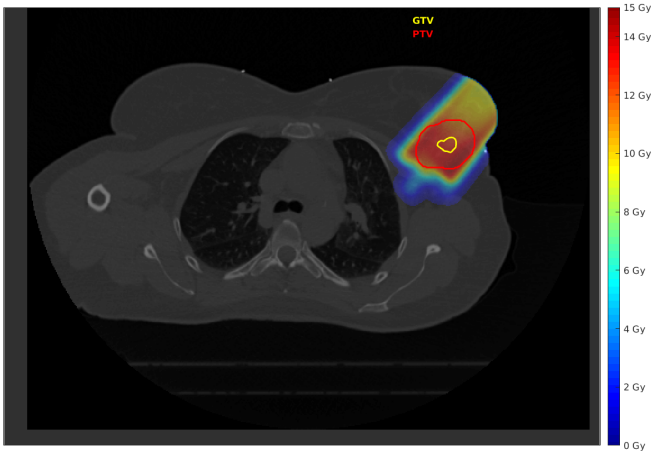

(c) Beam angle 45°.

Figure 3.4: Dose distribution of three SFUD fractions, each having a prescribed dose of 11.55 Gy.

3.3.1. Implementation in iCycle

The main difference between the IMPT and ridge filter treatment plans is the freedom of spot selection. Where IMPT has the freedom to position pristine Bragg peaks across the entire target volume, ridge filter treatment plans require the pristine Bragg peaks belonging to one SOBP to be positioned at the same lateral position. Besides, only one SOBP can be selected for every lateral position. Figure 3.5 shows this difference in positioning of the pristine Bragg peaks for generated treatment plans of both IMPT and ridge filter. It can be seen that the Bragg peak spots of the ridge filter plans are all positioned in series on a specified regular grid.

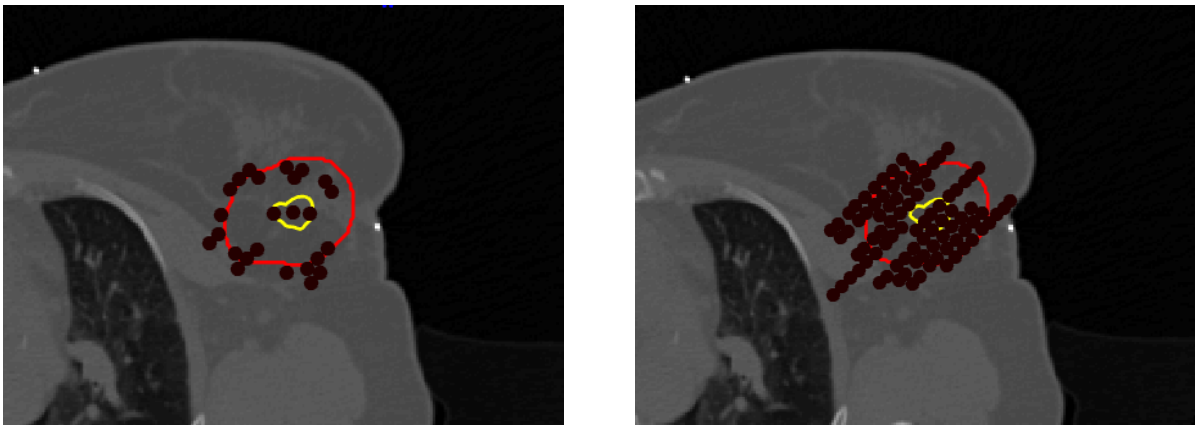

(a) (b)

Figure 3.5: Example of the pristine Bragg peak locations (black dots) in an IMPT (a) and ridge filter (b) treatment plan with single beam angle 45°. The yellow and red circles are delineations of respectively the GTV and PTV.

The optimization results of the ridge filter treatment plans are stated in table 3.3. In fig. 3.6 the depth range for one treatment plan is shown, by plotting the SOBP beams belonging to the selected energy layers.

Table 3.3: Optimization results of the treatment planning times, number of selected energy layers, and the number of lateral positions for the beam angles of the five fractions ridge filter treatment plan.

Beam angle (°)	Treatment planning time (HH:MM)	Number of energy layers	Number of lateral positions
20	2:09	8	76
25	2:25	8	77
30	3:17	9	74
40	2:09	9	65
45	2:07	9	69

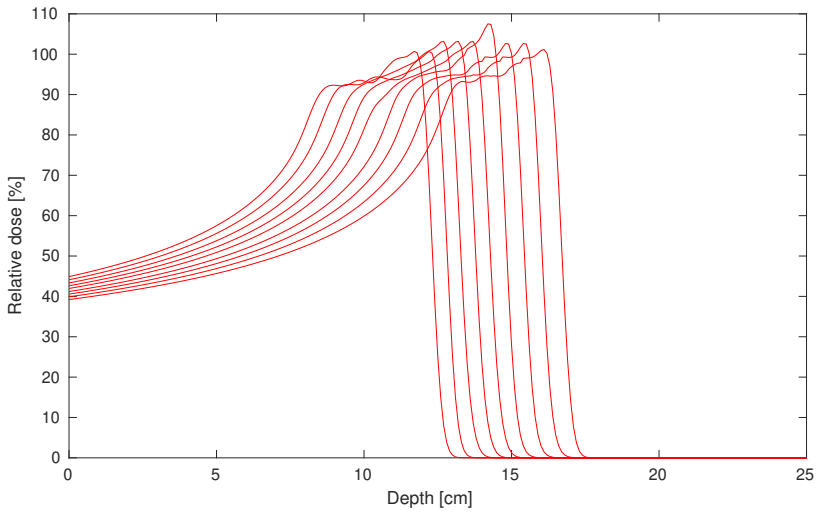

Figure 3.6: Relative dose distribution in water of the SOBP beams of the selected energy layers for a single fraction ridge filter treatment plan with a beam angle of 30°.

3.3.2. SBPF

The ridge filter treatment plans are generated as single beam per fraction delivery, where each fraction a uniform dose is delivered. In table 3.4 the homogeneity indices for ridge filter treatment plans with a prescribed dose of 8.65 Gy (five fraction schedule) are given. The final SBPF ridge filter treatment plans are generated with the five beam angles with favorable homogeneity indices (closest to 1.07), varying between 15 and 50 degrees for each patient. This is repeated for the treatment plans with 1, 2, 3, and 4 beam angles. For this patient, this resulted in the beam angles listed in table 3.5. To compare the IMPT and ridge filter treatment plans, the IMPT treatment plans are planned with the same beam angles as the equivalent ridge filter treatment plans, as listed in table 3.2.

Table 3.4: HI for different beam angles for SFUD ridge filter treatment plans with single fraction doses of 8.65 Gy.

Beam angle (°)	Homogeneity index
15	1.8113
20	1.1922
25	1.1199
30	1.1125
35	1.6724
40	1.1625
45	1.1855
50	1.9755

Table 3.5: Selected beam angles for the SBPF fractionated ridge filter plans

Number of fractions	Selected beam angles (°)
1	30°
2	25°, 45°
3	25°, 30°, 45°
4	25°, 30°, 40°, 45°
5	20°, 25°, 30°, 40°, 45°

3.3.3. FLASH effect

The FLASH effect is applied by reducing the dose in the healthy breast tissue by the FLASH enhancement ratio. The dose distribution with applied FLASH effect by increasing FER is shown in fig. 3.7. It can be seen that the dose in the voxels outside the CTV is reduced while the dose in the CTV remains the same. Moreover, the dose of voxels below the threshold of 7 Gy is not changed.

3.4. Analysis

The generated IMPT and ridge filter treatment plans are all assessed on the homogeneity and conformity index for clinical acceptability. Moreover, toxicity-model endpoints for fibrosis and fat necrosis are taken into account. This section will show the evaluation results for five different treatment plans varying the number of beam angles: 1, 2, 3, 4, and 5. To conclude the analysis, the results of the IMPT and ridge filter treatment plans are summarized and the FERs for which the ridge filter treatment plans outperform the IMPT plans are listed.

3.4.1. Uniformity

Figure 3.8 gives the results of the homogeneity indices of the five generated ridge filter treatment plans, which are compared to the results for the IMPT treatment plans, table 3.6. It can be seen that the HI curves decrease by an increase in FER. The HI indicates the ratio of the near minimum dose in the PTV and the prescribed dose in the PTV. As the FER is applied to all voxels except for the CTV cells, within the PTV the FER is only applied to the voxels laying in a ring around the CTV. The near-minimum dose of the PTV is expected at the edge of the PTV, probably most likely outside the CTV. It is therefore expected that the near-minimum dose and thereby the HI follows the linear regression of the FER. With a FER of 1.1130, all treatment plans satisfy the clinical recommendation for the homogeneity index and from a FER of 1.1697, the ridge filter treatment plans benefit the IMPT plans in uniformity. The ridge filter treatment plan with 5 fractions shows the most homogeneous treatment plan.

Table 3.6: Homogeneity indices for the five IMPT treatment plans with single fraction doses of 21 Gy.

Number of beam angles	Homogeneity index
1	1.0066
2	1.0337
3	1.0320
4	1.0307
5	1.0268

3.4.2. Coverage

Figure 3.9 gives the results of the conformity indices of the five generated ridge filter treatment plans, which are compared to the results for the IMPT treatment plans, table 3.7. It can be seen that the CI reaches a certain threshold of approximately CI = 0.5. This limitation is the volume ratio of the CTV and PTV. For a certain FER, there are no voxels outside the PTV receiving a dose level $\geq$ 95% of the prescribed dose. The dose level of the voxels in the CTV does not change so the conformality index will just be the volume of the CTV divided by the PTV. With a FER of 1.1153, all treatment plans benefit the IMPT plans in conformity. The ridge filter treatment plan with 2 fractions shows the highest coverage in the dose distribution.

Table 3.7: Conformity indices for the five IMPT treatment plans with single fraction doses of 21 Gy.

Number of beam angles	Conformity index
1	1.0374
2	1.0117
3	1.0151
4	1.0158
5	1.0138

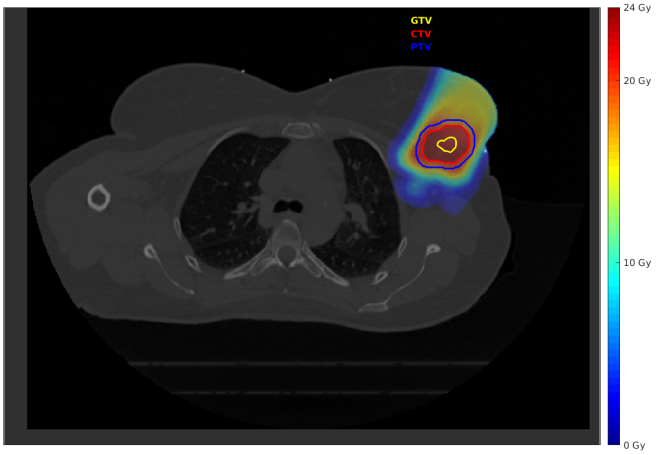

(a) FER=1.2.

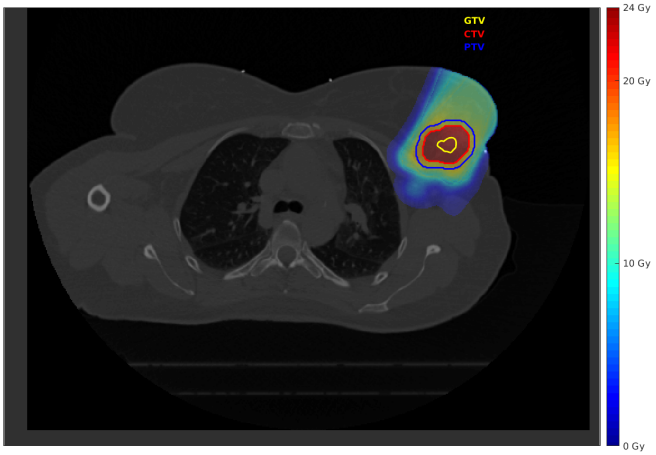

(b) FER=1.5.

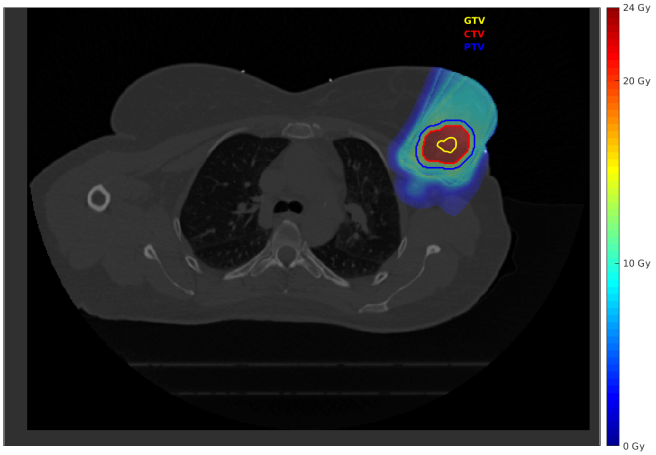

(c) FER=2.0.

Figure 3.7: Dose distribution of three fraction ridge filter treatment plan from fig. 3.3 for different values for FER applied to the healthy tissue.

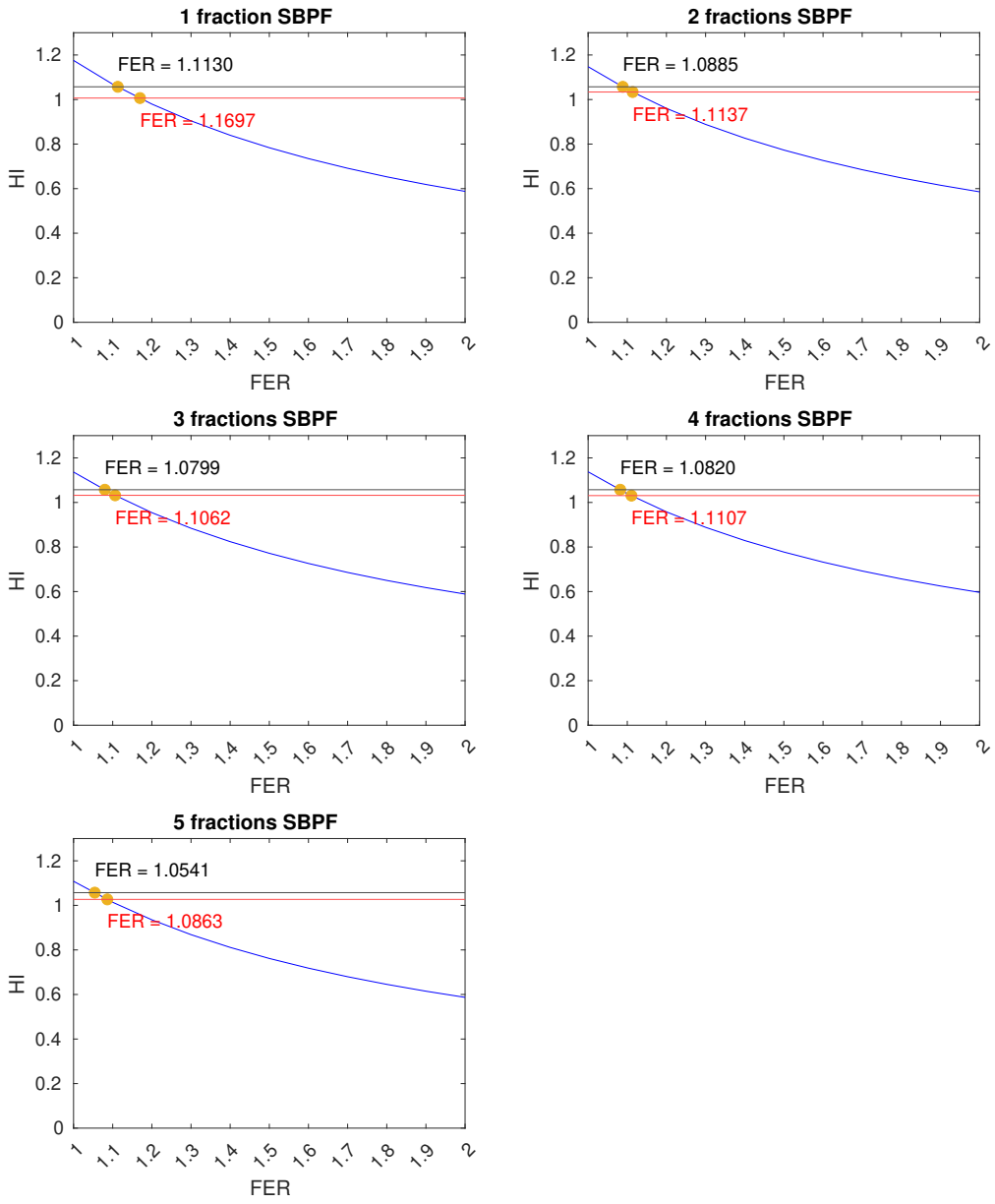

Figure 3.8: Homogeneity indices of the five ridge filter treatment plans for different magnitudes of the FLASH enhancement ratio. The black line represents the clinical recommendation of HI = 1.07 and the red line represents the HI of the IMPT plans, which can be found in table 3.6

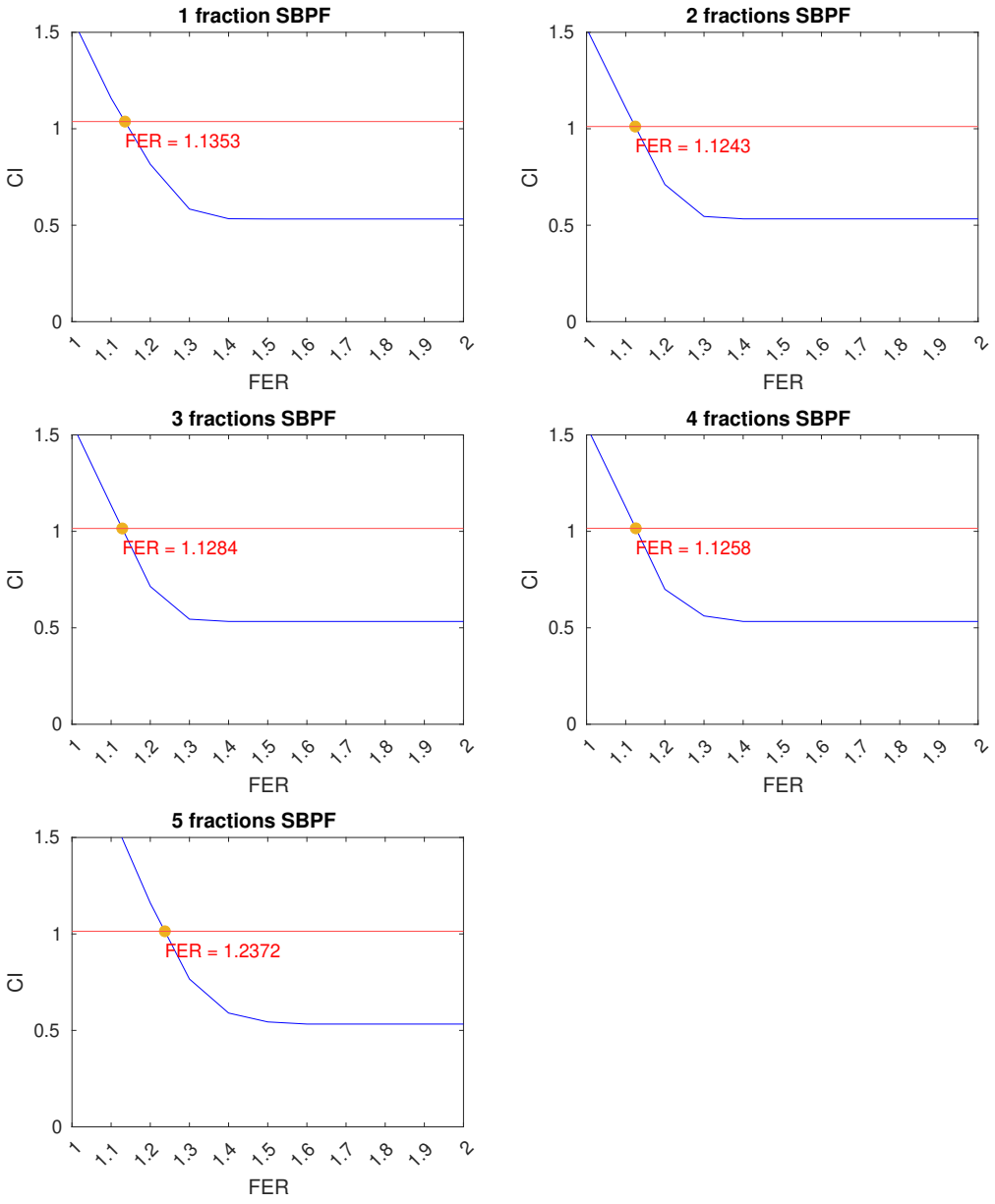

Figure 3.9: Conformality indices of five ridge filter treatment plans for different magnitudes of the FER. The red line represents the CI of the IMPT plans, which can be found in table 3.7

3.4.3. Fibrosis

The risk of fibrosis is expressed through the normal tissue control probability and the results are shown in fig. 3.10. It can be seen that the FER has a substantial impact on the risk of fibrosis. With a FER of 1.2730, all treatment plans benefit the IMPT plans in the risk of developing painful fibrosis. The ridge filter treatment plan with 2 fractions shows the most favorable values for NTCP.

Table 3.8: Normal tissue control probabilities for the five IMPT treatment plans with single fraction doses of 21 Gy.

Number of beam angles	NTCP
1	0.6013
2	0.6056
3	0.6098
4	0.6137
5	0.6089

3.4.4. Fat necrosis

The first metric on fat necrosis is the maximum dose in the healthy tissue, results can be found in fig. 3.11. The results for the 1 - 4 fractions are quite similar while the maximal dose of the 5 fractions treatment plan is substantially higher. With a FER of 1.3474, all treatment plans satisfy the recommendations from Rahimi et al. [48], and from a FER of 1.3924, the ridge filter treatment plans benefit the IMPT plans. The ridge filter treatment plan with 3 fractions shows the lowest maximal dose curve.

Table 3.9: Maximal dose for the five IMPT treatment plans with single fraction doses of 21 Gy.

Number of beam angles	D_{max}
1	21.9236
2	22.4361
3	22.4008
4	22.4488
5	22.4163

The other recommendations of Rahimi et al. [48] prescribe limitations on the volumes receiving 18.94, 19.56, 20.66, 21.79, and 22.92 Gy. In fig. 3.12, the dose-volume curves for the healthy breast tissue are shown. It can be seen that for a FER of 1.4, all ridge filter treatment plans benefit the IMPT treatment plans. Moreover, it can be seen that the smallest discrepancy of the ridge filter plan curves with the constraint curves is often near the maximum dose.

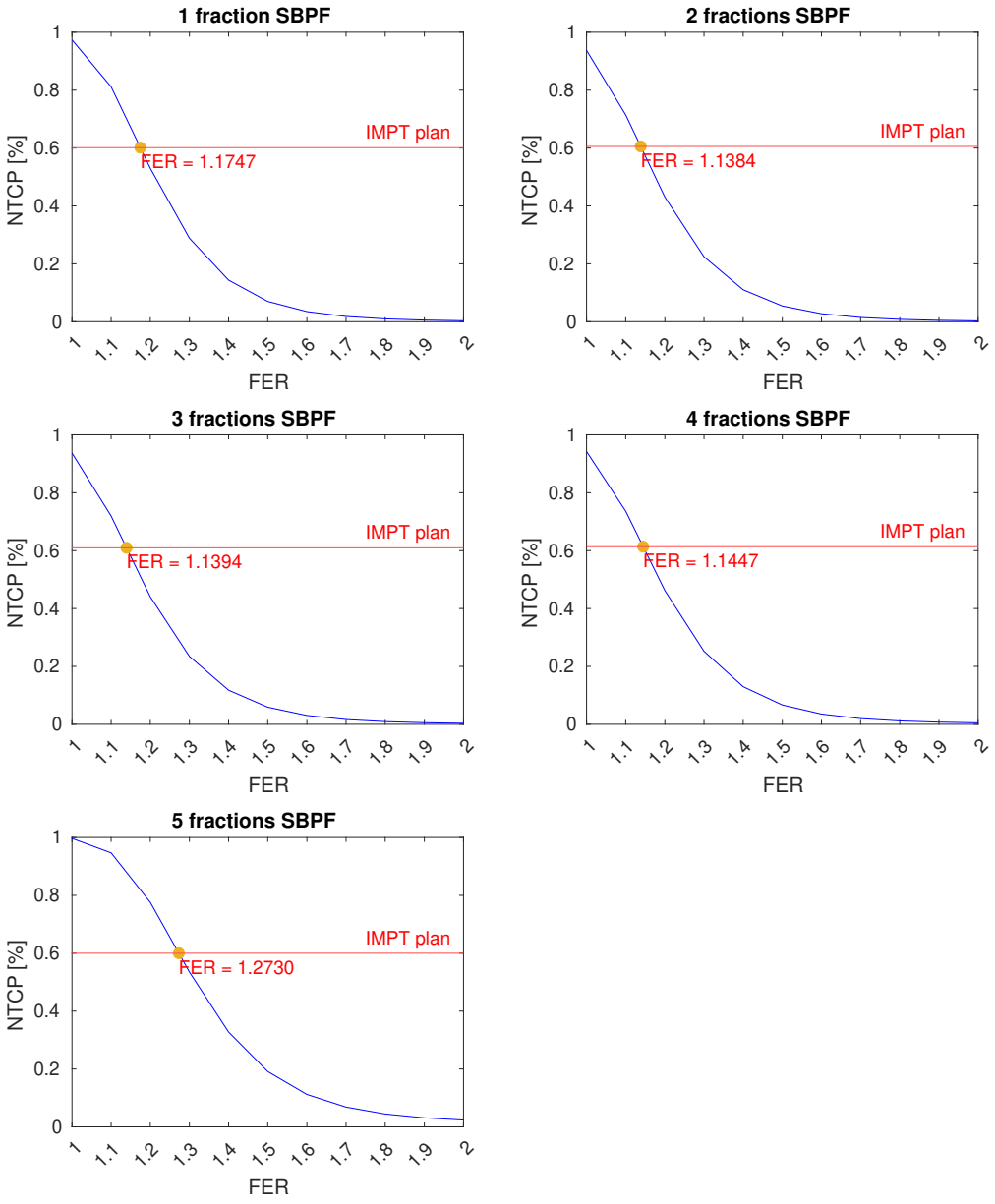

Figure 3.10: Normal tissue control probability of developing fibrosis for five ridge filter plans for different magnitudes of the FER. The red line represents the NTCP of the IMPT plans, which can be found in table 3.8

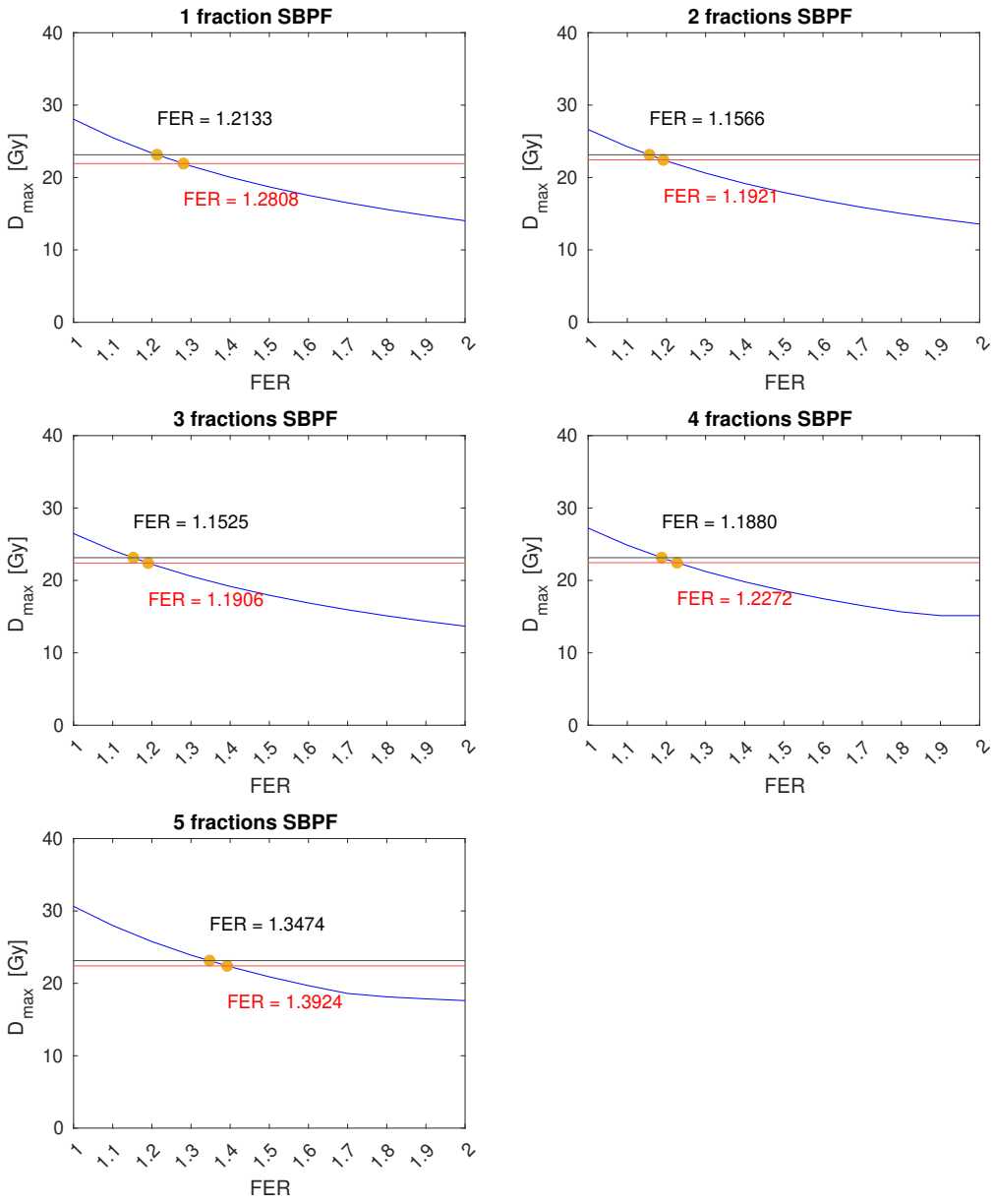

Figure 3.11: Maximal dose in healthy breast tissue for five ridge filter plans for different magnitudes of the FER. The black line represents the recommendation of 23.14 Gy and the red line represents the maximal dose of the IMPT plans, which can be found in table 3.9

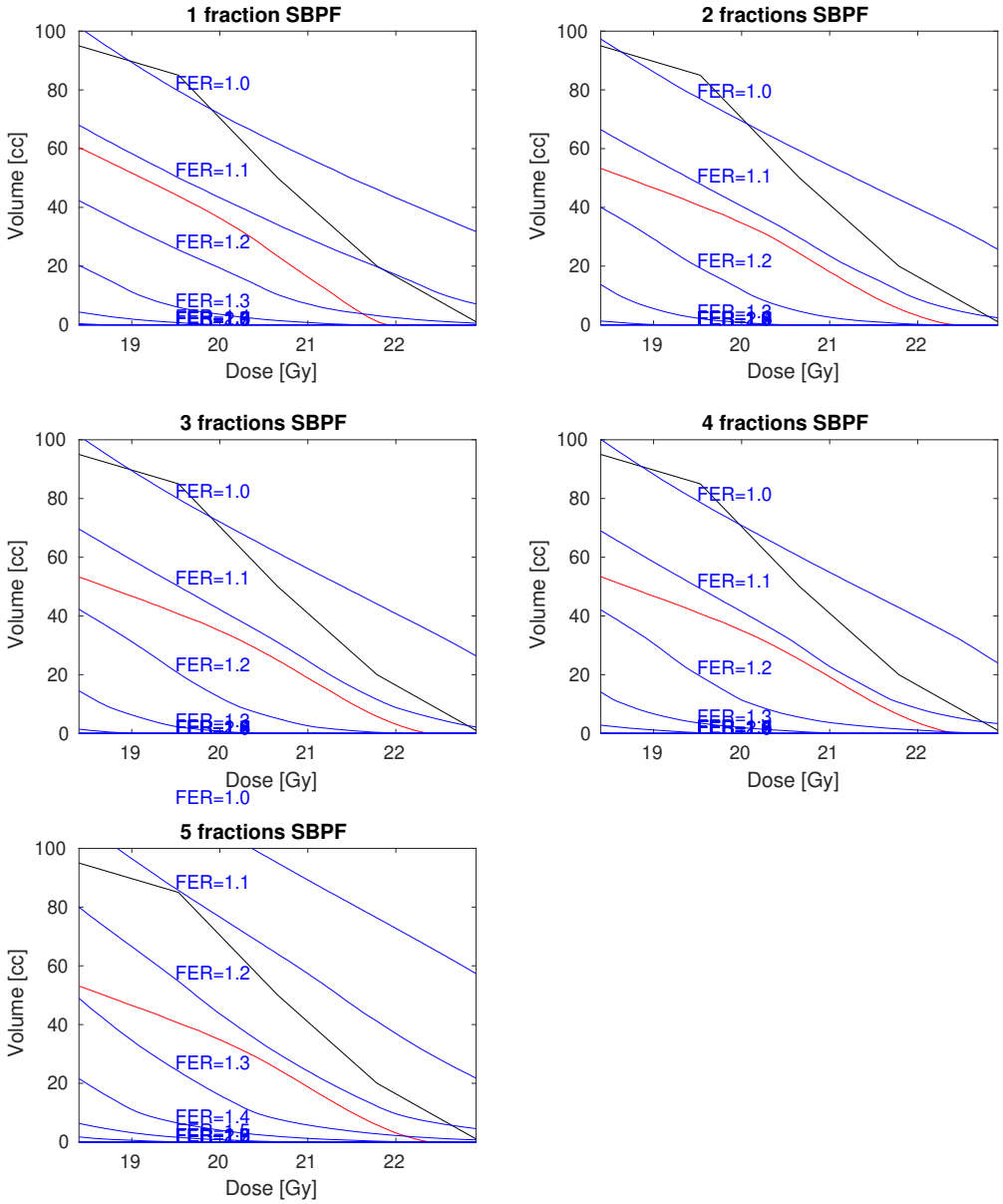

Figure 3.12: Dose-volume curves for the healthy breast tissue for the dose range 18.94 - 22.92 Gy. The dose-volume curve is drawn for every value of FER. The black line represents the constraints from Rahimi et al. [48] and the red line shows the dose-volume curves from the IMPT plans.

3.4.5. FLASH effect

Table 3.10 shows a summary of the results for all metrics. The last column states the value of FER for which the ridge filter treatment plan outperforms the IMPT treatment plan on all metrics: uniformity by the homogeneity index, coverage by the conformity index, risk of fibrosis by the NTCP, and risk of fat necrosis by the maximal dose.

Table 3.10: Overview of the results of the evaluation of the five different IMPT and ridge filter treatment plans. The required FER for a ridge filter treatment plan to benefit the equivalent IMPT plan is stated in the last column.

	Number of fractions	**Beam Angles (°)**	**HI**	**CI**	**NTCP**	D_{max} **(Gy)**	**Required FER**
IMPT	1	30	1.0066	1.0374	0.6013	21.9236	-
Ridge filter	1	30	1.1755	1.5756	0.9738	28.0527	1.2808
IMPT	1	25, 45	1.0337	1.0117	0.6056	22.4361	-
Ridge filter	2	25, 45	1.1474	1.5208	0.9374	26.6298	1.1921
IMPT	1	25, 30, 45	1.0320	1.0151	0.6098	22.4008	-
Ridge filter	3	25, 30, 45	1.1364	1.5605	0.9372	26.4761	1.1906
IMPT	1	25, 30, 40, 45	1.0307	1.0158	0.6137	22.4488	-
Ridge filter	4	25, 30, 40, 45	1.1375	1.5460	0.9425	27.2319	1.2272
IMPT	1	20, 25, 30, 40, 45	1.0268	1.0138	0.6089	22.4163	-
Ridge filter	5	20, 25, 30, 40, 45	1.1081	2.0576	0.9968	30.6319	1.3924

4

Discussion

This chapter will discuss the findings and methodology of the study. First, the results of chapter 3 will be discussed. Next, section 4.2 elaborates on the general treatment planning method and the clinical acceptability of the generated IMPT treatment plans. The ridge filter treatment planning method, including the SOBP database and the implementation in iCycle, is discussed in section 4.3. This is followed by a discussion of the implementation and theory of the FLASH effect in section 4.4. Section 4.5 evaluates the toxicity-model endpoints. Finally, recommendations for future work are given.

4.1. Results

The main finding in this study is that for a FLASH effect of 20-40% it could be feasible to generate a ridge filter treatment plan that is as clinically acceptable compared to a conventional IMPT treatment plan. However, this conclusion comes with certain assumptions and limitations that will be discussed further in this chapter. In this section, the results of the optimized dose distributions and the results of the optimizations themselves will be discussed for both the IMPT and the ridge filter treatment plans. Moreover, the results for the FLASH enhancement ratios are reviewed.

4.1.1. IMPT treatment plans

The iCycle wishlist, appendix B, functioned successfully in generating clinically acceptable IMPT treatment plans. In table 3.6, it can be seen that the uniformity of the IMPT treatment plans all satisfy the ICRU constraint of 1.07 and improve for an increase in the number of beam angles, with a HI of 1.0337 for 2 fractions to 1.0268 for 5 fractions. Surprisingly, the HI of the IMPT treatment plan with 1 fraction was found to be most favorable with a homogeneity index of 1.0066. The conformality indices also show a substantial improvement by an increase in the number of beam angles. This is expected as IMPT (with multiple fields) in general improves the coverage of the target volume compared to a single field. As a perfectly conform treatment plan has a CI of 1.0, the results for the IMPT plans 1.0117 - 1.0374 are clinically acceptable. The HI and CI results match the dose distribution in fig. 3.1, showing a conform and homogeneous dose in the PTV with a slight overdose near the proximal edge of the PTV.

The metrics for the toxicities can be found in section 3.4.3 and section 3.4.4. No specific correlation can be seen in table 3.8 between the NTCP of developing fibrosis and the number of beam angles of the IMPT treatment plan. The risk of developing fibrosis is approximately 60% for an IMPT treatment plan with a single fraction of 21 Gy. The maximum dose and the dose-volume curves (in the dose range of 18.94 - 22.92 Gy) of healthy breast tissue are assessed to evaluate the risk of developing fat necrosis. Both metrics outperformed the recommendations of Rahimi et al. [48] for all beam angles. This is well shown in fig. 3.11 and fig. 3.12 since all of the red lines (indicating the IMPT treatment plans) are positioned below the black lines, which indicate the maximum constraints imposed by the recommendations. The results imply that no painful fat necrosis will develop from the dose of the IMPT treatment plans. No significant discrepancies can be seen between treatment plans with different beam angles in the metrics for fat necrosis.

The optimization results are summarized in table 3.2. It can be seen that the optimization times increase significantly for an increasing number of beam angles. This is expected as IMPT is a multi-field optimization (MFO) where both the dose contribution from each individual beam and the dose distribution of all beams are optimized. The number of energy layers shows a slightly declining increase for an increasing number of beam angles. This indicates that an additional beam angle adds new energy layers but also removes redundant energy layers. In the last column of table 3.2 it can be seen that the number of lateral positions increases substantially from one fraction to two fractions and increases with small numbers between two and five fractions.

Dose distributions of the selected energy layers for the single fraction IMPT treatment plan are presented in fig. 3.2. The figures indicate a depth range of approximately 6.5 - 15.0 cm in water. Fat tissue has a slightly lower density than water, so it is expected that the proton beams will end up slightly deeper in the patient. Including the range shifter of 57 mm, the range in the patient will be just above 0.8 - 9.3 cm. As the PTV of this patient is located at a depth of approximately 3.3 - 9.5 cm, the selected energy layers cover the position of the target.

4.1.2. Ridge filter treatment plans

The results for the homogeneity and conformality indices and the metrics for toxicities of the ridge filter treatment plans without an applied FER can be found in table 3.10. It can be seen that the results score significantly worse than the IMPT treatment plans. This is expected since the ridge filter treatment plans are restricted in pencil beam selection by the SOBP beams, which will be further discussed in section 4.3.1. However, it can be seen that the HIs of the ridge filter treatment plans improve by increasing the number of fractions (and thereby also the beam angles), from 1.1755 for 1 fraction to 1.1081 for 5 fractions. No significant correlation can be seen between the dose coverage and the number of fractions. The CIs in the range of 1.5208 - 2.0576 indicate that relatively much dose is given to the healthy tissue surrounding the PTV. The values for HI and CI can be verified in fig. 3.3, where the dose distribution for a ridge filter treatment plan with three fractions is shown. It can be seen that the dose within the PTV includes relatively more shades of red than the IMPT dose distribution in table 3.2 (indicating relatively more inhomogeneity) and that there is much overdosage in the tissue surrounding the PTV, given a less conform dose.

The overdosage in the tissue surrounding the PTV is in agreement with the high NTCP and D_{max} values. The results for D_{max} are 26.47 - 30.63 Gy, where the recommendation is to stay below 23.14 Gy (recalculated to the number of fractions). Moreover, the NTCP of developing fibrosis of the ridge filter treatment plans is 93.42%-99.68%. In the dose-volume curves in fig. 3.12 it can be seen that the ridge filter treatment plans without an applied FLASH effect (FER = 1.0) mainly deviate from the recommendations in the volumes receiving relatively high doses. No clear correlation can be seen between the number of beam angles and the metrics; NTCP, D_{max}, and the dose-volume constraints.

The optimization results of the individual SBPF dose distributions for five fractions are listed in table 3.3. It took an average of 2:22h to optimize a single fraction ridge filter treatment plan. The number of energy layers remained relatively constant with either 8 or 9 energy layers. The same applies to the number of lateral positions in a range of 65 - 77, shown in the last column. This indicates that the target volume has a relatively bigger surface from 25° compared to the 40° beam angle. The optimization itself and the implementation of SOBP in iCycle are elaborated in section 4.3.2.

The dose distribution of the selected energy layers for a single fraction ridge filter treatment plan with a beam angle of 30° is shown in fig. 3.6. The figures show a depth in water in a range of approximately 7.5 - 17.0 cm. This range is decreased to 1.8 - 11.3 cm due to the 57 mm range shifter and slightly increased due to the density of the fat tissue through which the proton beam propagates. The chosen energy layers cover the positions of the tumor, as the PTV of this patient is located in a range of approximately 3.3 - 9.5 cm. The range of the selected energy layers is even larger, which is probably needed to cover the distal edge of the tumor with the SOBPs.

4.1.3. FER

The FLASH effect is applied to the ridge filter treatment plans by decreasing the dose in the healthy tissue with the FER. Eleven FER values in steps of 0.1 between 1.0 - 2.0 are applied to all breast tissue voxels outside the CTV. Subsequently, the HI, CI, and metrics for toxicities are calculated to determine

to which value of FER, the ridge filter treatment plans can benefit the IMPT treatment plans. In the last column of table 3.10, these FERs are stated for every fractionated treatment plan. The resulting FERs are between 1.1906 - 1.3924 and mainly depend on the maximum dose in the healthy breast tissue, D_{max}.

4.1.4. Patient 2

The section above discussed the results of patient 1, which are stated in chapter 3. Unfortunately, the results of the second patient (appendix C) are significantly less beneficial. Even though the homogeneity indices of the individual SBPF ridge filter treatment plans are similar to those of patient 1, the dose distribution shows a substantial overdose. The recalculation of these ridge filter treatment plans to equivalent single dose fractions, as shown in fig. C.3, shows poor dose coverage. The poor dose coverage leads to significant overdoses in the healthy tissue which is also indicated by the toxicity-model endpoints. Three of the five generated ridge filter treatment plans require a FER between 1.8944 - 1.9998 and two treatment plans require a FER $>$ 2.0 to benefit the IMPT treatment plans. As with patient 1, the FERs in patient 1 mainly depend on the D_{max}.

The cause of the poor dose coverage and difference in results has not been indicated. No significant correlation was found for the number of lateral positions or energy layers. An important difference between the two patients is the volume of the target volume. The main part of the optimization is performed on the planning target volume, which for patient 2 is 50% as large as the PTV of patient 1. Due to the time limitations for this thesis, it was not possible to further investigate the cause of the significant differences between the two patients. Future research should definitely investigate the cause of the poor dose coverage and focus on the patients' inclusion requirements for this optimization method.

4.2. Treatment planning

This section will review the used methodology for generating the treatment plans.

CT data

The treatment plans in this study are planned on patient CT data without actual tumor tissue. Even though the CT data's anatomy is different from the anatomy of primary radiotherapy, the geometry is similar and therefore suitable to use for the purpose of this thesis. If patient data with tumor tissue would be used, no difference is expected for the results of the magnitude of the FLASH effect. However, the proton beams will then have a smaller range in the patient, since tumor tissue has a higher density compared to breast (fat) tissue. This might enable the used SOBP database to be suitable for tumors positioned closer to the skin than the exclusion in this study of 2.5 cm.

Wishlist

The final wishlist (appendix B) has been developed in an iterative process of testing the optimizer and is shown to be effective in achieving the required constraints and objectives for IMPT treatment plans. The constraints are also met in the ridge filter treatment plans but the objectives are sometimes not achieved. The maximum dose in the GTV and PTV are often higher than the set maximum, which indicates an inhomogeneous dose in the PTV. Moreover, the dose given to the breast tissue outside the PTV is often higher than the maximizing objectives in the wishlist.

With conventional IMPT, overdosage in the area surrounding the PTV is often tackled by introducing multiple rings surrounding the PTV. The dose fall-off can be controlled by reducing the maximum allowed dose in every ring farther away from the PTV. However, with SOBP beams it is impossible to restrict the optimizer in the dose of the tissue surrounding the PTV. In order to give a sufficient dose to the PTV, it is unavoidable that there will be pristine Bragg peaks at the top or tail of the SOBP beams positioned outside the PTV. This is especially due to the fixed width of the SOBP, which will be further discussed in section 4.3.1.

It could be argued that the wish list mainly strives for achieving a uniform dose and is less strict on conformality. This is because sufficient homogeneity is required for tumor control and the loss of conformality is expected to be compensated by the FLASH effect. It is assumed that the wishlist achieves the best optimization results possible for the implementation of ridge filter generated SOBP beams in this study.

Robust optimization
In this study, only one planning scenario is included while the standard of care in clinical IMPT is treatment planning with robust optimization. Robust optimization is a way of treatment planning which includes uncertainties affecting the final position of the Bragg peaks. Besides the nominal scenario, also patient shifts and uncertainties such as undershooting and overshooting are taken into account. Basic robust optimization includes 9 scenarios, resulting in the determination of a certain treatment plan taking nine times as long. In the majority of proton therapy, even 27 scenarios are used, also including changes in the surrounding area of the target. Nevertheless, the purpose of the IMPT treatment plans generated in this study is not to be used in the clinic but mainly to compare them with the results of ridge filter plans. The clinical implementation of the FLASH-compatible ridge filter plans is not expected in the near future and moreover, it is time-consuming to generate multiple scenarios. It is therefore sufficient to only include one nominal scenario and use the metrics for dose uniformity and dose coverage to assess the treatment plans on clinical acceptability.

An alternative method to include position uncertainties with ridge filter generated beams is a beam-specific PTV [45, 49]. The beam-specific PTV concept applies distal and proximal margins for range uncertainty for each beam direction. Moreover, lateral margins are determined relative to the beam directions and misalignment is accounted for by adding margins from density correction.

4.2.1. SBPF

The ridge filter treatment plans are designed with SBPF delivery, with the assumption that in each fraction a uniform dose (SFUD) from one beam angle should be delivered to the target to ensure tumor control. In table 3.4, the homogeneity index of the single fraction treatment plans is listed for the case of a final ridge filter treatment plan with five fractions. ICRU [26] recommends a homogeneity index of 1.07 for a uniform dose distribution. In clinical practice, maximum doses up to 1.12 are accepted. It was expected that the ridge filter treatment plans will not give an ideal homogeneous distribution because of the limited freedom in spot selection. As can be seen, none of the SFUD treatment plans satisfy the 1.07 constraint.

Table 3.4 shows significant differences in uniformity between beam angles for which no explanation has been found. No correlation can be seen between the HIs and the number of energy layers or the number of lateral positions. Furthermore, no divergent tissue has been found in the CT data which suggests that there should not be major differences in the tissue the proton beams propagate. Because of the yet undefined differences in uniformity of the treatment plans, the results should be interpreted with caution.

The single fraction doses with the best homogeneity indices are selected for the multiple fractionation schedules and are expected to improve uniformity for multiple beam angles. Table 3.10 supports this assumption, as the homogeneity index of the ridge filter treatment plans improves for an increasing number of beam angles. So, it can be concluded that SBPF dose delivery with single fractions as homogeneous as possible is a feasible approach for ridge filter treatment planning.

Even though the single fraction ridge filter doses are not uniform doses individually, the SBPF dose delivery with multiple beam angles improved tumor control for the ridge filter treatment plans. A drawback of the ridge filter treatment plans with multiple fractions is that relatively more dose is deposited in the healthy tissue. This drawback is supported by the increased conformality indices for the ridge filter treatment plans with multiple fractions (and thereby beam angles) in table 3.10.

However, the theory behind the SBPF delivery is that the FLASH effect outweighs the loss of fractionation. As with breast tumor tissue, there is no biological fractionation benefit, the fractionation loss is mainly the loss of dose coverage. The effect of FLASH on the dose coverage can be seen in comparing fig. 3.3 and fig. 3.7a. In fig. 3.3, the ridge filter treatment plan is shown without an applied FER and in fig. 3.7a the ridge filter treatment plan with a FER of 1.2 is shown. The significant improvement in the dose coverage of the target volume due to the FLASH effect is clearly visible and supported by the steep curves in fig. 3.9. The next section will elaborate further on the FLASH effect in this study.

4.3. Ridge filter treatment plans

The ridge filter treatment plans are generated by using the SOBP database from the simulation and implementation of Meijer [39]. The ridge filter itself and the SOBP implementation have some limitations that will be covered in this section.

4.3.1. SOBP database

In fig. 2.4 it can be seen that the SOBP is quite inhomogeneous. This could have several reasons. It could be due to the limitations of the ridge filter that is used. The ridge filter in this study is optimized to give an SOBP of 3 cm for a proton beam energy of 154 MeV. It could therefore be expected that for energy far below or above the 154 MeV, the SOBP will not be as smooth. However, in fig. 2.4 the SOBP of 154 MeV is shown and this SOBP is not homogeneous itself.

Another possible reason could be the limitations of the method to rewrite the simulated SOBP energy spectra as a weighted sum of pristine Bragg peaks. The non-negative linear least squares method is performed for 19 energy levels: every 10 MeV from 70 to 250 MeV. For all energy levels in between, the results are interpolated by shifting the energies of the pristine Bragg peaks of the nearest energy level (1 of the 19). The interpolated results are therefore not accurately retrieved. Moreover, the non-negative linear least squares optimization was restricted to the minimal distance between energy levels of 3 MeV. This energy discretization could be reduced to improve the homogeneity of the SOBP.

Ridge filter

A limitation of the used ridge filter is the fixed width. In fig. 3.5(b) the position of the pristine Bragg peaks of the SOBP beams in a ridge filter plan is shown. It can be seen that at the widest part of the PTV (approximately 4 cm), the SOBPs are alternately positioned at the distal and proximal edges. This is probably due to the restriction of one SOBP per lateral position. The SOBP now has the same width for every energy level. This means that the optimizer can only fill the target with an SOBP beam of 3 cm long. In the case of small tumor sizes, this results in an overdose in the surrounding tissue while for tumor size > 3 cm this can lead to an underdose in the target since only one lateral position per energy can be selected.

To fully cover the tumor, it would be best to have SOBP beams of various widths available during treatment. However, this requires multiple ridge filters or modulation of the ridge filter during treatment which might be too time-consuming for FLASH treatment times. An alternative is to investigate for every tumor size the optimal width of SOBP beams and use a ridge filter that generates SOBP with that fixed width.

In future investigations, it might be interesting to implement a curved ridge filter. As most of the tumors have a rounded shape, a generic curved ridge filter might give an improved dose distribution of the SOBP beams. Moreover, the benefit of a patient-specific ridge filter over a generic ridge filter could be investigated.

Patient exclusion

The available energies of the used SOBP database between 110 - 240 MeV limit the range of the SOBP beams and thereby the suitable tumors. It was found that the set-up, with the current SOBP database and a range shifter of 57 mm, is only sufficient for a range of 2.5 - 30 cm in the patient. Unfortunately, this range limited the number of patients feasible for this study. The CT data of 12 patients were available and only 2 patients had tumors in the range of 2.5 - 30 cm. The tumors of the other 10 patients were positioned relatively closer to the skin.

Besides tumor position, the tumor size is also a relevant parameter for the in- and exclusion of suitable patients. Patients with tumors $\leq$ 2.5 cm (GTV) are used in this study. Treatment plans are planned to give a homogeneous dose to the PTV. The GTVs in this study are expanded by 5.5 cm and 5.0 cm to the PTV for respectively patient 1 and patient 2. The fixed SOBP width of 3 cm enabled to generate relatively good ridge filter treatment plans for the tumors in this study. However, it might be interesting to investigate if the dose distribution can be improved by optimizing the fixed SOBP width for a specific tumor size.

4.3.2. Implementation in iCycle

The SOBP beams in iCycle are well implemented. The optimization selects the suitable distal and lateral positions, replaces the pristine pencil beams with SOBPs, and results in a dose distribution with SOBP beams. However, since it is an adjustment of an existing pristine Bragg peak optimization, there are still some things that could be improved.

The pencil beam selection method with a regular grid is an eligible solution for the lateral positions of SOBP beams. Nevertheless, the distal position of the pencil beams could be improved. Now, the initial candidate pencil beams include the energy layers with relative energy spacing of one pristine Bragg peak width in the range of the tumor's position. However, the final dose distribution includes only energy layers for every lateral position so the relative spacing between pristine energy layers is not relevant. But, energy spacing is still required since including all energy layers positioned in the range of the tumor will make the optimization too time-consuming. Future research could look into the impact of absolute energy layer spacing or optimize the relative energy spacing factor. This could be implemented in the optimization specification of the wishlist.

One of the final steps of the optimization is to ensure only one SOBP is chosen for every lateral position. This is done after the optimization itself is done, by finding double lateral positions and removing the lateral positions with the lowest weights. This might not lead to the optimal distribution of lateral positions. Setting criteria for the initial energy selection could improve the final dose distribution. Additionally, the removal itself could be improved. An iterative process of optimization could be used as an alternative to remove the double lateral positions with the lowest weight.

Moreover, it was found that the optimization of the ridge filter treatment plans requires a substantial amount of memory, roughly 500 GB for individual treatment plans. Even though the average optimization time was about 2:22h, treatment plans with a relatively high number of voxels in the target volumes were killed if there was not enough memory available for the optimizer. This could be solved by reducing the number of voxels of the target volume used in the dose calculation. However, using fewer voxels can lead to an inaccurate dose distribution. The extensive memory use compared to conventional IMPT could be explained by the correlated weights of the SOBP. To enable an accurate dose optimization for relatively large target volumes, the optimization could be split into different batches to limit peak consumption. A suggestion would be to take e.g. 50 spots per batch, optimize the weights, add these to the previous batch and continue with the next batch. Further research into the source of memory use is recommended.

4.4. FLASH effect

In this study, the feasibility of the FLASH effect is investigated in a PBS set-up with a ridge filter. The proposed method is assumed to achieve FLASH compatible dose-rates and the differential impact on the damage observed between healthy and tumor tissue is applied by the FER. The implementation of the FLASH effect will be discussed in this section.

4.4.1. Dose-rates

The ridge filter set-up presumes that the maximum dose-rate is achieved with the maximum initial beam energy of 244 MeV and minimal intervention of the proton beam. In this study, it is assumed that the set-up with ridge filter and range compensator fulfills the FLASH dose rate constraint of $\geq$ 40 Gy/s. However, no measurements of the dose-rate have been executed or simulated to confirm if the set-up is able to achieve FLASH-compatible dose-rates. Until now, FLASH has been observed in dose rates up to 124 Gy/s [53]. However, not much is known about the magnitude of the FLASH effect by a varying dose-rate. Multiple studies are investigating the impact of the dose rate on the FLASH effect [18, 19, 34] including among other simultaneous dose and dose rate optimization (SDDRO). Further research should be undertaken to investigate the impact on the dose-rates within the proposed method.

4.4.2. FER

In this study, the fraction dose in each healthy tissue voxel is decreased by the FER while the fraction dose in the voxels of the CTV remains unchanged. It could be argued that the biological effect of FLASH might not be as binary as the current application of the FER. However, a model with more parameters also entails complexity and more uncertainties.

As mentioned in section 1.1, the level of oxygen depletion is expected to play a role in the differential effect. However, recent studies [8, 28] suggest that the FLASH effect may not be fully explained by the role of oxygen depletion. Even though the exact mechanism behind the differential effect remains unspecified, the biological difference between healthy and tumor tissue has been observed. Multiple in vivo animal studies found a reduction in healthy tissue toxicity with FLASH radiotherapy while

maintaining equivalent tumor control, indicating a differential effect between healthy and tumor tissue. Therefore the FER, the ratio of damage in healthy tissue with conventional versus FLASH dose-rates, is a sufficient tool to apply the FLASH effect in treatment planning.

Furthermore, the implementation of FLASH in this study includes a threshold of 7 Gy. The threshold model suggests that healthy tissues start to respond similarly to FLASH dose rates as to conventional dose-rates but from a certain threshold, develop in a second 'phase' where radioresistance is induced. In that phase, an increased dose is needed to damage the healthy tissue. This finding is supported by various reports studying the biological effect of FLASH in animals [17, 42, 50]. The threshold dose is not known accurately and is expected to depend on the oxygen level in healthy tissues. However, it is estimated to be in the range of 3.5 - 7 Gy [37]. Further research is needed on the biological mechanisms behind FLASH and especially on the possible variation between tissues to determine an exact threshold dose.

This study found a FER of 20 - 40% to generate clinically acceptable ridge filter plans. Experimental data in prior studies show a FER greater than 1.8 [16]. A FER of 1.8 in this study would enable a reduction in the risk of fibrosis by 97.36% compared to IMPT treatment plans and a significant reduction in risk of fat necrosis, as can be seen in fig. 3.12.

4.5. Toxicity-model endpoints

Fibrosis and fat necrosis are the two main radiation side-effects seen in breast cancer patients receiving hypofractionated radiotherapy. Therefore, metrics for these toxicities are taken into account to research the feasibility of the generated ridge filter treatment plans.

4.5.1. Fibrosis

The risk of developing breast fibrosis is assessed by the NTCP model of Avanzo et al. [2]. This NTCP model includes the generalized average of the dose in the healthy breast tissue. Breast tissue is characterized as a serial organ at risk, so a complication occurs if a small volume of the breast receives too much dose. Therefore, the maximum dose is weighed more in the NTCP model, eq. (2.7), as the volume effect is close to zero (n = 0.66). Since there is at least one night between each fraction in this study, it is assumed that the healthy tissue cells repair completely (h = 0) in between every fraction. The report of Avanzo et al. [2] investigated the dose schedules of patients in literature that developed fibrosis and stated that for a BEUD of 107.2 Gy there is a 50% risk of developing fibrosis. Moreover, they determined the slope (m) of the NTCP model based on this literature.

In this study, a single 21 Gy fraction in an IMPT treatment plan carries a 60% risk of developing fibrosis, as can be seen in table 3.8. The NTCPs for ridge filter treatment plans are even higher than the single fraction IMPT treatment plans, above 90%. However, the FLASH effect is expected to outweigh the loss of healthy tissue sparing compared to the generated IMPT plans. In fig. 3.10 the NTCP values for every value of FER are shown. It can be seen that the NTCP decreases substantially if the magnitude of FER is increased. For a FER of 1.2730, all ridge filter treatment plans benefit the IMPT treatment plans in the risk of developing painful fibrosis.

Comparison of these NTCPs with those of clinical fractionation schedules confirms that fibrosis is an important side-effect of hypofractionated radiotherapy. In clinical practice, partial breast patients are treated with 5 fractions of 5.2 Gy, giving an NTCP for the risk of developing fibrosis of 0.83%. The increased dose level is required for the definitive radiotherapy purpose but compared to the current standard of care, the increase in the risk of developing fibrosis is significant. A FER of 1.8 - 1.9 is required for the ridge filter treatment plans to get an NTCP $\leq$ 0.83%.

4.5.2. Fat necrosis

To assess the risk of developing fat necrosis, recommendations on dose constraints from the paper of Rahimi et al. [48] are used. These constraints are based on a clinical phase I trial including 75 patients. The dosimetric constraints from Rahimi et al. [48] are recalculated in this study to the iso-effective dose level of a single fraction treatment instead of five fractions. It is assumed that treatment plans that adhere to the dose constraints will not result in painful fat necrosis. However, as the study of Rahimi et al. [48] includes a limited number of patients and dose-fractionated schedules, caution must

be applied, as the findings might not be an exact measure of the risk of fat necrosis.

All IMPT treatment plans in this study fulfill the established maximum dose and dose-volume constraints. In table 3.9 and fig. 3.11, it can be seen that the D_{max} range from 21.92 - 22.45 Gy and satisfy the limit of 23.14 Gy. Moreover, fig. 3.12 shows that the IMPT treatment plans (red lines) stay below the constraints line (visualized in black). The values found for the ridge filter treatment plans are substantially higher than the IMPT treatment plans. As discussed in section 4.1.3, the FER for which the ridge filter treatment plans benefit the IMPT treatment plans mainly depends on the maximum dose in the healthy tissue. It is expected that the maximum dose of the ridge filter treatment plans is higher than with IMPT treatment plans due to the reduced conformality index, caused by the limited spot-selection. For a FER of 1.3924, all ridge filter treatment plans outperform the IMPT treatment plans in the dose constraints for developing painful fat necrosis.

A comparison with the maximum dose and dose-volume curves for the current partial breast irradiation fractionation schedules confirms that fat necrosis is a significant side-effect of hypofractionated radiation. With 5 Gy delivered each fraction, the dose level is not even close to the single fraction dose levels between 18.94 - 22.92 Gy. This indicates that there is a minimal risk of developing fat necrosis with the current standard of care. Therefore, it is crucial that further study is conducted on fat necrosis with hypofractionated radiation and the associated dose limitations to reduce this toxicity. An NTCP model for the risk of developing fat necrosis would be useful.

A note of caution in the metrics used for developing fat necrosis is the volume of the PTV and the breast. Rahimi et al. [48] found that fat necrosis barely developed in patients with breast volumes $\leq$ 1000 cc and therefore the constraints were developed for patients with breast volumes $\geq$ 1000 cc. The patient used in this study all met this requirement. Although the PTV is not found to be a predictive measure for the development of fat necrosis, Rahimi et al. [48] included a recommendation of PTV $\leq$ 100 cc since it is intimately related to the achievable dose recommendations. Patient 1 complied with this but the PTV of patient 2 is larger than 100 cc. This is confirmed by fig. C.12 in the appendix as for patient 2 the dose-volume curves of the IMPT and ridge filter treatment plans are positioned closer to the recommendation line.

4.6. Future work

This chapter elaborated on some limitations of this study and proposed suggestions for improvement. In this section, several suggestions for future research are listed.

- Investigate if there is an optimal SOBP width for every tumor size.
- Study the possibilities and results for a curved ridge filter, potentially patient-specific.
- Improve the iCycle optimization by including an iterative process for selecting one SOBP energy for every lateral position.
- Optimize the discretization of energy layers in the initial energy selection.
- Investigate and potentially decrease the extended memory use of the SOBP treatment planning optimizer.
- Investigate the dose-rates that can be achieved with the proposed ridge-filter set-up.
- Include more patients.
- Research the development of fibrosis due to surgery in the current standard of care.
- Develop an NTCP model for fat necrosis and potentially other toxicities in hypofractionated radiotherapy.
- Research on the biological mechanisms behind FLASH and the dose and dose-rate thresholds of FLASH.
- Investigate the impact of fractionated FLASH treatments.
- Test the feasibility of beam-specific PTVs for ridge filter treatment plans.

5

Conclusion

This study set out to investigate the feasibility of FLASH proton therapy with ridge filtered beam for definitive treatment of early-breast cancer patients. Definitive radiotherapy requires an increased biological effect of dose-fractionation schedules compared to postoperative radiotherapy since the number and density of tumor cells are significantly higher. Moreover, conventional fractionation is not beneficial because of the relatively low α/β ratio of breast tumor tissue which requires giving hypofractionated treatment ($>$ 2 Gy per fraction). The dose escalation of hypofractionated treatment schedules causes an increase in the risk of developing toxicities in surrounding healthy tissue. FLASH could be a good solution to decrease these toxicities and spare healthy tissue.

We proposed a pencil beam scanning set-up with a ridge filter and a compensator to maximize the dose-rate while being able to make use of the sharp distal dose fall-off of proton therapy. The compensator provides robustness and enables to enforce the dose fall-off at the distal edge while the ridge filter generates SOBP beams that avoid the time-consuming process of switching the beam energy during treatment. However, the generated SOBP beams limit the spot selection in ridge filter plans and therefore give less favorable dose distributions compared to IMPT.

Our results indicate that with a FLASH effect of 20 - 40%, it is feasible to generate ridge filter treatment plans that outperform iso-effective IMPT treatment plans in dose uniformity, dose coverage, and risks of developing fibrosis and fat necrosis.

Compared to the current standard of care in postoperative partial breast irradiation with proton therapy, the definitive FLASH ridge filter treatment plans increase the risk of developing toxicities significantly. However, the standard of care includes surgery, which is also a cause of developing fibrosis [4]. More research on the development of fibrosis after both surgery and radiotherapy is needed to determine if the FLASH ridge filter treatment plans are clinically acceptable. Moreover, it is important to bear in mind that the intended group of patients is now not eligible for surgery due to medical reasons. So although it is desired to minimize the toxicities of radiotherapy, for these patients the trade-off between treating the tumor and developing side effects is different from that of the average patient.

In this thesis, the differential effect of FLASH in damage to healthy tissue is assumed due to ultra-high dose rates compared to conventional dose rates. However, future work is needed to verify if FLASH-compatible dose-rates can be achieved with this set-up. The method proposes the maximum dose-rate by the maximal beam energy of 244 MeV but the interaction with the ridge filter and the compensator is expected to decrease the initial dose rate of the 244 MeV beam. Furthermore, there is still limited knowledge about the FLASH effect so biological investigations are needed on the mechanisms behind FLASH. Before it can be implemented in the clinic it must be assured for which specifications of the fraction dose and dose-rate the healthy tissue experiences less damage than with conventional IMPT.

The study's findings indicate that it is feasible to generate ridge filter treatment plans that benefit IMPT treatment plans. However, the dosimetric feasibility is limited by tumor characteristics (size and location), has shown significant differences between patients and so requires further investigation. More understanding of the optimal ridge filter, SOBP beam optimization, and the FLASH effect is required before clinically acceptable FLASH-compatible ridge filter treatment plans can be developed.

References

[1] Akulinichev, S. V., Kokontsev, D. A., and Yakovlev, I. A. Possible improvement of proton energy filter for radiotherapy. *Nucl. Instrum. Methods Phys. Res. Sect. A-Accel. Spectrom. Dect. Assoc. Equip.*, 977, 2020.

[2] Avanzo, M., Stancanello, J., Trovò, M., Jena, R., Roncadin, M., Trovò, M. G., and Capra, E. Complication probability model for subcutaneous fibrosis based on published data of partial and whole breast irradiation. *Physica Medica*, 28(4):296–306, 2012.

[3] Barry, A. and Fyles, A. Establishing the role of stereotactic ablative body radiotherapy in early-stage breast cancer. *International Journal of Breast Cancer*, 2018, 2018.

[4] Bartelink, H., Maingon, P., Poortmans, P., Weltens, C., Fourquet, A., Jager, J., Schinagl, D., Oei, B., Rodenhuis, C., Horiot, J.-C., et al. Whole-breast irradiation with or without a boost for patients treated with breast-conserving surgery for early breast cancer: 20-year follow-up of a randomised phase 3 trial. *The lancet oncology*, 16(1):47–56, 2015.

[5] Beyreuther, E., Brand, M., Hans, S., Hideghéty, K., Karsch, L., Leßmann, E., Schürer, M., Szabó, E. R., and Pawelke, J. Feasibility of proton flash effect tested by zebrafish embryo irradiation. *Radiother Oncol*, 139:46–50, 2019.

[6] Bourhis, J., Sozzi, W. J., Jorge, P. G., Gaide, O., Bailat, C., Duclos, F., Patin, D., Ozsahin, M., Bochud, F., Germond, J.-F., et al. Treatment of a first patient with flash-radiotherapy. *Radiotherapy and oncology*, 139:18–22, 2019.

[7] Breedveld, S., Storchi, P. R., Voet, P. W., and Heijmen, B. J. icycle: Integrated, multicriterial beam angle, and profile optimization for generation of coplanar and noncoplanar imrt plans. *Medical physics*, 39(2):951–963, 2012.

[8] Cao, X., Zhang, R., Esipova, T. V., Allu, S. R., Ashraf, R., Rahman, M., Gunn, J. R., Bruza, P., Gladstone, D. J., Williams, B. B., et al. Quantification of oxygen depletion during flash irradiation in vitro and in vivo. *International Journal of Radiation Oncology* Biology* Physics*, 111(1):240–248, 2021.

[9] Charaghvandi, R., Van Asselen, B., Philippens, M., Verkooijen, H., Van Gils, C., Van Diest, P., Pijnappel, R., Hobbelink, M., Witkamp, A., van Dalen, T., et al. Redefining radiotherapy for early-stage breast cancer with single dose ablative treatment: a study protocol. *BMC cancer*, 17(1):1–9, 2017.

[10] Correa, C., Harris, E. E., Leonardi, M. C., Smith, B. D., Taghian, A. G., Thompson, A. M., White, J., and Harris, J. R. Accelerated partial breast irradiation: executive summary for the update of an astro evidence-based consensus statement. *Practical radiation oncology*, 7(2):73–79, 2017.

[11] Cox, J. D. Toxicity criteria of the radiation therapy oncology group (rtog) and the european organization for research and treatment of cancer (eortc). *Int J Radiat Oncol Biol Phys*, 31:1341–1346, 1995.

[12] Cunningham, S., McCauley, S., Vairamani, K., Speth, J., Girdhani, S., Abel, E., Sharma, R. A., Perentesis, J. P., Wells, S. I., Mascia, A., and Sertorio, M. Flash proton pencil beam scanning irradiation minimizes radiation-induced leg contracture and skin toxicity in mice. *Cancers*, 13(5): 1–15, 2021.

[13] Diffenderfer, E. S., Verginadis, I. I., Kim, M. M., Shoniyozov, K., Velalopoulou, A., Goia, D., Putt, M., Hagan, S., Avery, S., Teo, K., Zou, W., Lin, A., Swisher-McClure, S., Koch, C., Kennedy, A. R., Minn, A., Maity, A., Busch, T. M., Dong, L., Koumenis, C., Metz, J., and Cengel, K. A. Design,

implementation, and in vivo validation of a novel proton flash radiation therapy system. *Int J Radiat Oncol Biol Phys*, 106(2):440–448, 2020.

[14] Diffenderfer, E. S., Sørensen, B. S., Mazal, A., and Carlson, D. J. The current status of preclinical proton flash radiation and future directions. *Medical Physics*, 49(3):2039–2054, 2022.

[15] Dokic, I., Meister, S., Bojcevski, J., Tessonnier, T., Walsh, D., Knoll, M., Mein, S., Tang, Z., Vogelbacher, L., Rittmueller, C., Moustafa, M., Krunic, D., Brons, S., Haberer, T., Debus, J., Mairani, A., and Abdollahi, A. Neuroprotective effects of ultra-high dose rate flash bragg peak proton irradiation. *Int J Radiat Oncol Biol Phys*, 2022.

[16] Favaudon, V., Caplier, L., Monceau, V., Pouzoulet, F., Sayarath, M., Fouillade, C., Poupon, M.-F., Brito, I., Hupé, P., and Bourhis, J. Ultrahigh dose-rate flash irradiation increases the differential response between normal and tumor tissue in mice. *Science translational medicine*, 6(245), 2014.

[17] Field, S. and Bewley, D. Effects of dose-rate on the radiation response of rat skin. *International Journal of Radiation Biology and Related Studies in Physics, Chemistry and Medicine*, 26(3):259–267, 1974.

[18] Gao, H., Lin, B., Lin, Y., Fu, S., Langen, K., Liu, T., and Bradley, J. Simultaneous dose and dose rate optimization (sddro) for flash proton therapy. *Med Phys*, 47(12):6388–6395, 2020.

[19] Gao, H., Liu, J., Lin, Y., Gan, G. N., Pratx, G., Wang, F., Langen, K., Bradley, J. D., Rotondo, R. L., Li, H. H., and Chen, R. C. Simultaneous dose and dose rate optimization (sddro) of the flash effect for pencil-beam-scanning proton therapy. *Med Phys*, 49(3):2014–2025, 2022.

[20] Group, E. B. C. T. C. et al. Effects of radiotherapy and of differences in the extent of surgery for early breast cancer on local recurrence and 15-year survival: an overview of the randomised trials. *The Lancet*, 366(9503):2087–2106, 2005.

[21] Habraken, S., Breedveld, S., Groen, J., Nuyttens, J., and Hoogeman, M. Trade-off in healthy tissue sparing of flash and fractionation in stereotactic proton therapy of lung lesions with transmission beams. *Radiotherapy and Oncology*, 2022.

[22] Hickey, B. E., Lehman, M., Francis, D. P., and See, A. M. Partial breast irradiation for early breast cancer. *Cochrane Database of Systematic Reviews*, 2016.

[23] Hoekstra, N. High-precision adjuvant radiotherapy for early-stage breast cancer patients to reduce toxicity and improve survival, 2022. URL https://repub.eur.nl/pub/137088.

[24] Horton, J. K., Blitzblau, R. C., Yoo, S., Geradts, J., Chang, Z., Baker, J. A., Georgiade, G. S., Chen, W., Siamakpour-Reihani, S., Wang, C., et al. Preoperative single-fraction partial breast radiation therapy: A novel phase 1, dose-escalation protocol with radiation response biomarkers. *International Journal of Radiation Oncology* Biology* Physics*, 92(4):846–855, 2015.

[25] Ibrahimi, A. Characterization of the proton beam line in the experimental room of hollandptc, 2020. URL http://resolver.tudelft.nl/uuid:34e200d1-f744-4685-b4d0-2cfa2efce158.

[26] ICRU. International commission on radiation units and measurements: Prescribing, recording and reporting proton-beam therapy, 2007.

[27] ICRU. International commission on radiation units and measurements: Prescribing, recording, and reporting photon-beam intensity-modulated radiation therapy (imrt), 2010.

[28] Jansen, J., Knoll, J., Beyreuther, E., Pawelke, J., Skuza, R., Hanley, R., Brons, S., Pagliari, F., and Seco, J. Does flash deplete oxygen? experimental evaluation for photons, protons, and carbon ions. *Medical physics*, 48(7):3982–3990, 2021.

[29] Kaiser, A., Eley, J., Onyeuku, N., Rice, S., Wright, C., McGovern, N., Sank, M., Zhu, M., Vujaskovic, Z., Simone, C., and Hussain, A. Proton therapy delivery and its clinical application in select solid tumor malignancies. *Journal of Visualized Experiments*, 02 2019.

[30] Kim, M. M., Verginadis, I. I., Goia, D., Haertter, A., Shoniyozov, K., Zou, W., Maity, A., Busch, T. M., Metz, J. M., Cengel, K. A., Dong, L., Koumenis, C., and Diffenderfer, E. S. Comparison of flash proton entrance and the spread-out bragg peak dose regions in the sparing of mouse intestinal crypts and in a pancreatic tumor model. *Cancers*, 13(16), 2021.

[31] König, L., Hörner-Rieber, J., Forsthoefel, M., Haering, P., Meixner, E., Eichkorn, T., Krämer, A., Mielke, T., Tonndorf-Martini, E., Haefner, M. F., et al. Secondary malignancy risk following proton vs. x-ray radiotherapy of thymic epithelial tumors: A comparative modeling study of thoracic organ-specific cancer risk. *Cancers*, 14(10):2409, 2022.

[32] Krämer, M. and Durante, M. Ion beam transport calculations and treatment plans in particle therapy. *The European Physical Journal D*, 60(1):195–202, 2010.

[33] KWF. Behandeling van kanker, 2022. URL https://www.kwf.nl/kanker/wat-is-kanker/behandeling-van-kanker.

[34] Lin, Y., Lin, B., Fu, S., Folkerts, M. M., Abel, E., Bradley, J., and Gao, H. Sddro-joint: simultaneous dose and dose rate optimization with the joint use of transmission beams and bragg peaks for flash proton therapy. *Physics in Medicine & Biology*, 2021.

[35] Lischalk, J. W., Chen, H., Repka, M. C., Campbell, L. D., Obayomi-Davies, O., Kataria, S., Kole, T. P., Rudra, S., and Collins, B. T. Definitive hypofractionated radiation therapy for early stage breast cancer: Dosimetric feasibility of stereotactic ablative radiotherapy and proton beam therapy for intact breast tumors. *Advances in Radiation Oncology*, 3(3):447–457, 2018.

[36] Lyman, J. T. Complication probability as assessed from dose-volume histograms. *Radiation Research*, 104(2s):S13–S19, 1985.

[37] MacKay, R., Burnet, N., Lowe, M., Rothwell, B., Kirkby, N., Kirkby, K., and Hendry, J. Flash radiotherapy: Considerations for multibeam and hypofractionation dose delivery. *Radiotherapy and Oncology*, 164:122–127, 2021.

[38] Martin, A., Daniel, M., Drinkwater, D., and Clarys, J. Adipose tissue density, estimated adipose lipid fraction and whole body adiposity in male cadavers. *International journal of obesity and related metabolic disorders: journal of the International Association for the Study of Obesity*, 18 (2):79–83, 1994.

[39] Meijer, A. Back to the future: Towards ridge filters in clinical flash proton therapy treatment planning for neuro-oncological targets, 2021. URL https://repository.tudelft.nl/islandora/object/uuid%3A6b8e90ad-ff14-4ae3-915b-b2a26a310d6b?collection=education.

[40] Mohamed, N., Lee, A., and Lee, N. Y. Proton beam radiation therapy treatment for head and neck cancer. *Precision Radiation Oncology*, 6(1):59–68, 2022.

[41] Mulliez, T., Miedema, G., Van Parijs, H., Hottat, N., Vassilieff, M., Gillet, E., Baeyens, L., Voordeckers, M., Coelmont, J., Besse-Hammer, T., et al. Pre-operative accelerated radiotherapy for early stage breast cancer patients (popart): A feasibility study. *Radiotherapy and Oncology*, 170: 118–121, 2022.

[42] Nias, A., Swallow, A., Keene, J., and Hodgson, B. Effects of pulses of radiation on the survival of mammalian cells. *The British Journal of Radiology*, 42(499):553–553, 1969.

[43] Paganetti, H. *Proton Therapy Physics*. CRC Press, 2012.

[44] Palta, M., Yoo, S., Adamson, J. D., Prosnitz, L. R., and Horton, J. K. Preoperative single fraction partial breast radiotherapy for early-stage breast cancer. *International Journal of Radiation Oncology* Biology* Physics*, 82(1):37–42, 2012.

[45] Park, P. C., Zhu, X. R., Lee, A. K., Sahoo, N., Melancon, A. D., Zhang, L., and Dong, L. A beam-specific planning target volume (ptv) design for proton therapy to account for setup and range uncertainties. *International Journal of Radiation Oncology* Biology* Physics*, 82(2):e329–e336, 2012.

[46] Patriarca, A., Fouillade, C., Auger, M., Martin, F., Pouzoulet, F., Nauraye, C., Heinrich, S., Favaudon, V., Meyroneinc, S., Dendale, R., Mazal, A., Poortmans, P., Verrelle, P., and De Marzi, L. Experimental set-up for flash proton irradiation of small animals using a clinical system. *Int J Radiat Oncol Biol Phys*, 102(3):619–626, 2018.

[47] Qi, X. S., White, J., and Li, X. A. Is α/β for breast cancer really low? *Radiotherapy and Oncology*, 100(2):282–288, 2011.

[48] Rahimi, A., Zhang, Y., Kim, D. W., Morgan, H., Hossain, F., Leitch, M., Wooldridge, R., Seiler, S., Goudreau, S., Haley, B., et al. Risk factors for fat necrosis after stereotactic partial breast irradiation for early-stage breast cancer in a phase 1 clinical trial. *International Journal of Radiation Oncology* Biology* Physics*, 108(3):697–706, 2020.

[49] Rietzel, E. and Bert, C. Respiratory motion management in particle therapy. *Medical physics*, 37 (2):449–460, 2010.

[50] Rothwell, B. C., Kirkby, N., Merchant, M. J., Chadwick, A., Lowe, M., Mackay, R. I., Hendry, J. H., and Kirkby, K. J. Determining the parameter space for effective oxygen depletion for flash radiation therapy. *Physics in Medicine & Biology*, 66(5):055020, 2021.

[51] Sørensen, B. S., Sitarz, M. K., Ankjærgaard, C., Johansen, J., Andersen, C. E., Kanouta, E., Overgaard, C., Grau, C., and Poulsen, P. In vivo validation and tissue sparing factor for acute damage of pencil beam scanning proton flash. *Radiother Oncol*, 161:S447–S448, 2021.

[52] Trialists' Group, T. S. The uk standardisation of breast radiotherapy (start) trial b of radiotherapy hypofractionation for treatment of early breast cancer: a randomised trial. *The Lancet*, 371(9618): 1098–1107, 2008.

[53] Velalopoulou, A., Karagounis, I. V., Cramer, G. M., Kim, M. M., Skoufos, G., Goia, D., Hagan, S., Verginadis, I. I., Shoniyozov, K., Chiango, J., Cerullo, M., Varner, K., Yao, L., Qin, L., Hatzigeorgiou, A. G., Minn, A. J., Putt, M., Lanza, M., Assenmacher, C. A., Radaelli, E., Huck, J., Diffenderfer, E., Dong, L., Metz, J., Koumenis, C., Cengel, K. A., Maity, A., and Busch, T. M. Flash proton radiotherapy spares normal epithelial and mesenchymal tissues while preserving sarcoma response. *Cancer Res*, 81(18):4808–4821, 2021.

[54] Veluvolu, M., Patel, M., Narayanasamy, G., and Kim, T. Definitive single fraction stereotactic ablative radiotherapy for inoperable early-stage breast cancer: A case report. *Reports of Practical Oncology and Radiotherapy*, 25(5):760–764, 2020.

[55] Veronesi, U., Orecchia, R., Luini, A., Galimberti, V., Gatti, G., Intra, M., Veronesi, P., Leonardi, M. C., Ciocca, M., Lazzari, R., et al. Full-dose intraoperative radiotherapy with electrons during breast-conserving surgery: experience with 590 cases. *Annals of surgery*, 242(1):101, 2005.

[56] Vicini, F. A., Chen, P., Wallace, M., Mitchell, C., Hasan, Y., Grills, I., Kestin, L., Schell, S., Goldstein, N. S., Kunzman, J., et al. Interim cosmetic results and toxicity using 3d conformal external beam radiotherapy to deliver accelerated partial breast irradiation in patients with early-stage breast cancer treated with breast-conserving therapy. *International Journal of Radiation Oncology* Biology* Physics*, 69(4):1124–1130, 2007.

[57] Vozenin, M.-C., Hendry, J. H., and Limoli, C. Biological benefits of ultra-high dose rate flash radiotherapy: sleeping beauty awoken. *Clinical oncology*, 31(7):407–415, 2019.

[58] Water van de, S., Safai, S., Schippers, J. M., Weber, D. C., and Lomax, A. J. Towards flash proton therapy: the impact of treatment planning and machine characteristics on achievable dose rates. *Acta Oncol*, 58(10):1463–1469, 2019.

[59] Water van de, S., Kraan, A., Breedveld, S., Schillemans, W., Teguh, D., Kooy, H., Madden, T., Heijmen, B., and Hoogeman, M. Improved efficiency of multi-criteria impt treatment planning using iterative resampling of randomly placed pencil beams. *Physics in Medicine & Biology*, 58 (19):6969, 2013.

[60] Whelan, T. J., Kim, D.-H., and Sussman, J. Clinical experience using hypofractionated radiation schedules in breast cancer. *Seminars in radiation oncology*, 18(4):257–264, 2008.

[61] World Health Organization. Cancer, 2018. URL https://www.who.int/health-topics/cancer#tab=tab_1.

[62] Zerella, M. A., Zaffaroni, M., Ronci, G., Dicuonzo, S., Rojas, D. P., Morra, A., Fodor, C., Rondi, E., Vigorito, S., Botta, F., et al. Single fraction ablative preoperative radiation treatment for early-stage breast cancer: the crystal study–a phase i/ii clinical trial protocol. *BMC cancer*, 22(1):1–12, 2022.

[63] Zhang, G., Wang, J., Wang, Y., and Peng, H. Proton flash: passive scattering or pencil beam scanning? *Phys Med Biol*, 66(3):03NT01, 2021.

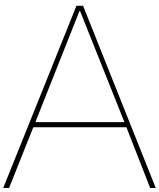

Literature Review

FLASH Proton Therapy to the Clinic

Abstract. FLASH therapy shows promising healthy tissue sparing effects in pre-clinical studies. The high potential of FLASH in proton therapy is attracting research on the biological, technological and clinical aspects. In vivo studies investigating the biological FLASH effect with proton beams are discussed of which the majority confirms the healthy tissue sparing. Importantly, the technological possibilities and challenges that come with treatment delivery and treatment planning are outlined. While the first studies have focused on passive scattering, the more advanced pencil beam scanning technique has shown beneficial effects to achieve ultra-high dose-rates. A substantial difference in proton therapy could be made by using ridge filters to obtain FLASH compatible spread-out Bragg peak beams. Such treatment planning could be beneficial for complex tumor sites, of which breast cancer would be a suitable first treatment site to investigate clinically. Besides, transmission beams could be a solution for specific treatment sites in heterogeneous tissues such as lung tumors. This review shows the high potential of bringing FLASH proton therapy to the clinic.

1 Introduction

The trade-off between irradiating tumor tissue and sparing healthy tissue is a major incentive for research in radiotherapy. Radiation-induced toxicity to adjacent healthy tissue is still a crucial limiting factor for the deliverable dose to the tumor in clinical applications. Recently, dose delivery with ultra-high dose-rates (UHDR) has shown a differential effect in damage observed in healthy tissue. This FLASH effect has shown promising results in saving healthy tissue while maintaining tumor control. To achieve the FLASH effect, the treatment dose is delivered in a much shorter time and thereby at a dose-rate a thousand times higher than with conventional radiotherapy. Even though dose-rate dependence of radio-sensitivity has been known since the late 1960s [2, 11], FLASH as a differential effect was first discovered by Favaudon et al. [8]. This study investigated the effect of electron beam with dose-rates > 40 Gy/s (UHDR) on lung tumors in mice. It was shown that UHDR irradiation was less fibrogenic than conventional irradiation while being comparable in efficiency for the tumor tissue. The promising result attracted scientific interest and the number of studies related to FLASH radiotherapy has increased since. Besides electrons, research has expanded to introduce FLASH in other radiation modalities such as photon and proton therapy. Especially the latter, proton therapy, has been highlighted in recent studies due to its high potential. The superior physical properties of protons makes proton therapy well-suited for deep-seated targets and also more precise, compared to photons. Introducing FLASH in proton treatments could result in a major improvement in saving healthy tissue while preserving tumor control.

However, before implementation in clinical proton therapy, more understanding of the biological FLASH effect and UHDR parameters is needed. Studies have focused on the verification of the proton FLASH effect in pre-clinical animal studies, the underlying biological mechanisms, the technological challenges to realize ultra-high dose-rates and the physical parameters required to achieve a FLASH effect. This literature review aims to provide an overview of the current status of literature of clinical FLASH proton therapy. Thereby focusing on pre-clinical studies investigating the proton FLASH effect and reports studying possible treatment delivery methods and planning systems. The objective of this review is to provide context for a master thesis project on the implementation of FLASH in proton therapy treatment planning.

2 Methodology

Search strategy

A systematic literature search was conducted in the digital databases of Embase, Medline and the

Web of Science. The search was performed with the purpose to identify all articles that contribute to the research of the feasibility of FLASH in proton therapy. FLASH has been studied in multiple modalities; electron, photon and proton radiotherapy. To include relevant results from FLASH studies with non-proton beams, the search term focused on FLASH particle therapy. Details of the databases and the used search terms can be found in Appendix A.

Selection process

The literature search of the databases yielded 561 records. After duplicates were removed, the title and abstract of 324 records were screened and 227 records were excluded. Inclusion criteria focused on (pre-)clinical treatment planning systems of FLASH proton therapy with transmission and/or Bragg peak beams. The majority of records were removed because there was no medical application or the study was not related to radiotherapy. Besides, records were excluded if they were not relevant for FLASH proton therapy or not applicable for transmission beams or Bragg peak beams. Finally, articles on beamline and dosimetric characterization and in-depth biological studies were not included since these records were too specific for this review. The full text of 28 reports was not available or not accessible by Erasmus MC or Delft University of Technology subscriptions. This resulted in a total number of 69 reports to be assessed on their eligibility for the scope of this review. Conference abstracts, reviews and non-relevant records were excluded at this point, which resulted in a total number of 24 studies. A schematic overview of the identification and selection of literature is shown in fig. 1.

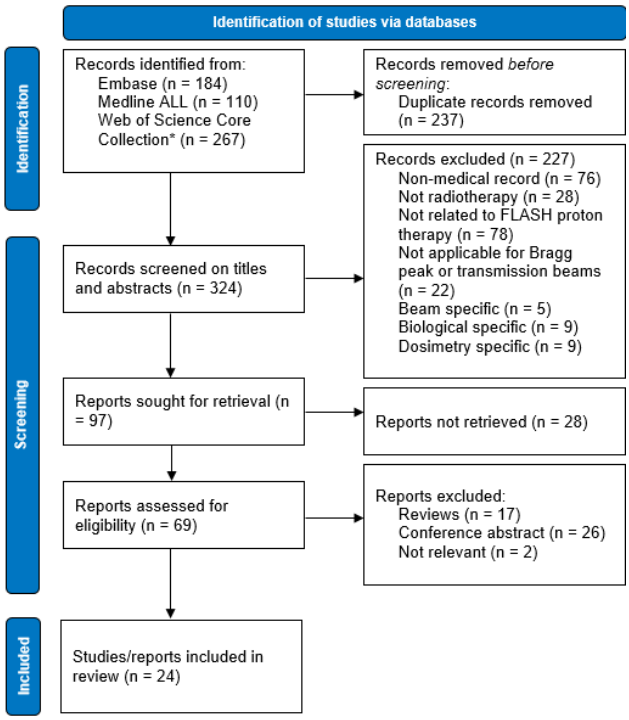

Figure 1: PRISMA 2020 Flow diagram of the literature search and selection process of this review [21].

3 Results

Biological effect

To verify the biological effect of FLASH in proton therapy, multiple in vivo small animal experiments have been conducted. A relative simple way of measuring the biological FLASH effect is reported in the study of Zhang et al. [35]. Abdomen tumors were irradiated in mice with either conventional or ultra-high dose-rates (108 Gy/s) and measured the weight loss and survival rate. From the results, they concluded that UHDR proton beams are less harmful to the normal gastrointestinal tract than conventional proton beams.

A different approach to study the biological FLASH effect is by measuring DNA synthesis, this was done by both Diffenderfer et al. [6] and Kim et al. [14]. After irradiating mice with conventional (1 Gy/s) and UHDR beams (78 Gy/s [6] and 108 Gy/s [14]), all mice were injected with a certain biochemical that enables to monitor DNA synthesis. The results of the study of Diffenderfer et al. showed that UHDR irradiated mice had reduced acute and chronic gastrointestinal damage with no additional impact on the tumor control. Similarly, the UHDR irradiated mice in the study of Kim et al. exhibited healthy tissue sparing and similar tumor growth control compared to conventional irradiated mice.

The report of Cunningham et al. [5] measured skin damage to investigate the acute radiation effect of FLASH. After irradiating leg tumors in mice with dose-rates of 57 and 115 Gy/s, the plasma and skin levels, skin toxicity and leg contracture were all significantly decreased compared to the mice irradiated with conventional dose-rates (1 Gy/s). Besides, tumor growth was measured after irradiation and no difference was observed between the conventional and FLASH compatible dose-rates. Thereby showing a healthy tissue sparing effect while maintaining equivalent tumor growth control. Another in vivo experiment with leg tumors in mice was performed by Sørensen et al. [24]. They scored the skin damage and calculated a dose modification factor, the ratio between the dose to produce skin damage in 50% of mice with conventional dose-rates and the equivalent dose for FLASH. Results showed that a 44-58% higher dose was required with UHDR to obtain the same level of skin damage, thereby showing a healthy tissue sparing effect. Velalopoulou et al. [29] studied the FLASH effect on skin damage as well and besides, the damage to muscle and bone tissue. They found that compared with conventional proton therapy, the FLASH effect can reduce skin damage and stem cell depletion and that UHDR has similar anti-tumor efficacy.

Instead of DNA synthesis, Dokic et al. [7] studied the biological FLASH effect by measuring the DNA damage with a double-strand break (DSB) surrogate marker. Compared to conventional irradiated mice, mice irradiated with UHDR showed a sparing effect of the healthy tissue in the brain.

To this end, most reports study the FLASH effect in mice. Beyreuther et al. [3], on the contrary, irradiated zebrafish with a UHDR proton beam. To measure the biological effect this study looked at the embryonic survival and the development of abnormalities with dose-rate of 100 Gy/s. In contrast to the above studies, the results of this study showed no significant evidence of the FLASH effect. Compared to conventional dose-rates, no influence of the proton dose-rate was found on the embryonic survival or development of abnormalities. However, at one dose point, a significant difference for pericardial edema[1] was found in the benefit of UHDR.

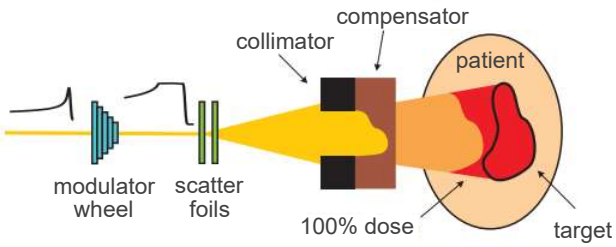

Figure 2: Schematic representation of passive scattering with a modulator, collimator and compensator [32].

Technological challenges

Realizing FLASH compatible dose-rates with existing proton therapy systems comes with technological challenges. Reports investigating the FLASH effect in proton therapy have focused among others on the choice of proton beam delivery and the treatment planning method. The majority of those reports describe proton beam delivery with either passive scattering (PS) or pencil beam scanning (PBS). This section will highlight both methods, including the underlying differences, advantages and challenges of introducing UHDR. Besides, different methods of treatment planning; transmission beams, Bragg peak beams and spread-out Bragg peak beams (SOBP) will be addressed.

Treatment delivery

Passive scattering & FLASH

Passive scattering (PS) uses scattering in a thin plate to broaden the size of the incident generated beam, see fig. 2. The lateral edge of the scattered beam is set by e.g. an aperture, a multi-leaf collimator or a range compensator, which enable to determine the position patient specific. A range modulator is placed before the scatterers to slow down protons for the required distal position. Since this method does not require intermediate processes, the beam irradiation times are relatively low.

[1] Acute radiation effect where watery fluid accumulates in the pericardial sac of the heart

A drawback of passive scattering however, is that the maximum dose ends up in the healthy tissue in front of the proximal boundary of the target [1]. This reduces the quality and conformity of the irradiation and can possibly lead to complications of surrounding healthy organs. Moreover, the use of scattering causes energy losses. Due to inelastic Coulomb interaction between the protons and the scatter material a broader beam will be produced. The same energy is released but over a larger volume, pulling down the dose-rate. Additionally, energy selection will filter out a large number of protons to narrow the beams in energy spread and lateral size. Resulting in the intensity of the beam not being large enough to irradiate the target with FLASH compatible dose-rates.

Nevertheless, multiple studies on FLASH proton therapy used passive scattering as treatment delivery due to the relatively simple set-up. To tackle the non-homogeneous dose distribution of conventional passive scattering, Beyreuther et al. placed a second scatterer with minimum reduction in proton fluence in the passive scattering beam set-up. With this set-up, they were able to reach a UHDR of over 100 Gy/s with a homogeneous dose distribution of a sample area of 6.5 mm in diameter. A similar double-scattered beam set-up was applied in the study of Diffenderfer et al.. After comparing UHDR with conventional dose-rates in this set-up, the authors concluded that the main limitation of UHDR in passive scattering will be the maximum field size that can be achieved. A dose-rate of 100 Gy/s requires a beam current of approximately 600 nA to treat a 5 cm x 5 cm field. Zhang et al. [35] also studied the FLASH effect with double scattered protons. To compensate for potential dose drop-off caused by scattering, an additional plastic absorber is placed in front of the target against the aperture. This set-up was able to achieve a dose-rate up to 138 Gy/s with a relatively small homogeneous radiation field of 12 x 16 mm. A method to achieve a high level of conformity of irradiation, is the placement of a ridge filter in the beam set-up, proposed in the studies of Akulinichev et al. [1], Kim et al. [14], Kourkafas et al. [15], Patriarca et al. [22] and Zhang et al. [34]. A ridge filter creates a poly-energetic proton beam with varying ranges and Bragg peaks from an incident mono-energetic proton beam. Usually, these are optimized 3D printed filters as shown in fig. 3. The combination of the different Bragg peak beams will together give a larger, fixed spread out Bragg peak (SOBP). Which will be further elaborated in section Spread-out Bragg peak beams. Use of a ridge filter enables to achieve variable dose-rates for a fixed proton beam energy. Thereby allowing a seamless transition between ultra-high and conventional dose-rates. Nevertheless, with a standard ridge filter healthy tissue surrounding the tumor can still receive maximum doses of irradiation. Therefore, Akulinichev et al. introduced a combined energy filter, a filter consisting of both a standard ridge filter and a shielding screen. The shielding screen is arranged such that it covers the strips of the ridge filter. In that way, the energy spectrum of the transmitted protons can be changed locally to control the maximum dose given to the target. Results of Monte-Carlo calculations showed a high level of conformity of irradiation with the use of this combined energy filter.

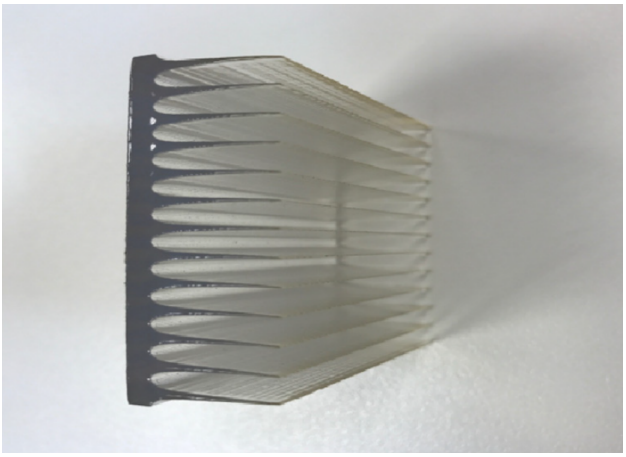

Figure 3: Example of 3D printed ridge filter [22].

Pencil beam scanning & FLASH

Pencil beam scanning (PBS) is a technologically more advanced delivery technique compared to passive scattering. It is often more precise and is used by the majority of proton therapy centers. The proton beams are created by delivering a sequence of pristine Bragg beams spot by spot, see fig. 4. To address an entire 3D target volume,

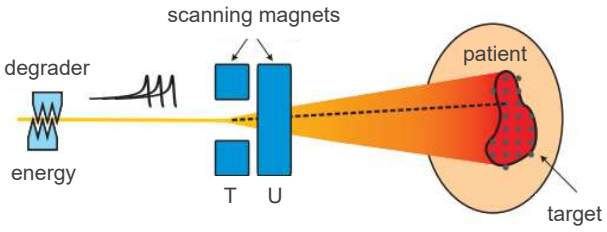

Figure 4: Schematic representation of pencil beam scanning with a energy degrader [32].

the pencil beam is steered by dipole magnets and covers the lateral position layer by layer. The distal position of the proton beam is determined by varying the energy of the beam, with for example an energy degrader.

The precise dose delivery of PBS combined with the dose sparing effect of FLASH on healthy tissue could be a promising combination. Besides, PBS can provide a high local dose-rate to the point of the pencil beam. Thereby expanding the possible treatment field size compared to PS.

However, the challenge of PBS and FLASH lies within the time and distances between pencil beam spots. PBS requires switching of the beam energy during treatment, this beam energy switching time is usually 0.1-1.0 s [1, 13] due to the mechanical displacement moderator material. With UHDR treatment times of <0.1 s, PBS spot scanning speed must be in the order of ms to stay within this time constraint. Where the spot scanning speed determines the dose-rate, the spot size is an important factor determining the rapidity of the transverse dose-rate falloff for a given spot [12]. Next to time constraints, energy switching of the proton beam also influences plan quality. Using multiple proton energies can increase the total number of proton spots which results in smaller spot weights and thereby the optimization will push the minimum MU constraint [9]. Another challenge of PBS are the energy degraders that are used to reduce the incident proton energy. Just as with scatter materials (section Passive scattering & FLASH), inelastic Coulomb interactions between the protons and energy degrader causes energy loss. The resulting proton beam is not able to reach a sufficient beam current to achieve the FLASH compatible dose-rates. For example, a 70 MeV proton beam going through an energy degrader loses up to 99% of dose-rate [14].

A possible solution to do reach UHDR with PBS is the introduction of a ridge filter [13]. This solution explained at section Passive scattering & FLASH works for both PS as PBS energy challenges. With the use of a stationary ridge filter, variable dose-rates can be achieved for one proton beam energy. Thereby, also saving the beam energy switching time of 0.1-1.0 s with conventional PBS. Literature examples, introducing e.g. a ridge filter, a compensator and a collimator to achieve a SOBP with PBS are stated in section Spread-out Bragg peak beams.

Treatment planning

Transmission beams

The maximum dose-rate is achieved by the maximum beam energy, approximately $230-250$ MeV for current proton therapy systems [30]. Proton beams with these energies have a range of $35-38$ cm in water [20] and therefore shoot through the patient [31]. The 'shoot-through' beams, often referred to as transmission beams, can be realized by multiple treatment delivery methods, including passive scattering and pencil beam scanning.

Maar als ik nu ga schrijven zegt die helemaal niks.

Advantageous of transmission beams in combination with FLASH is that no beam energy will get lost and ultra-high dose-rates can be achieved relatively easily. When multiple fields are chosen, transmission beams can achieve comparable conformity as Bragg-peak based plans. Moreover, there are dosimetric advantages. Range uncertainties are minimized [12], there is no additional dose in the organs-at-risk (OARs) and there is sharp lateral penumbra at all depths [23].

Since transmission beams 'shoot-through' the patient, healthy tissue in the beam path before and after the target will also be irradiated. Thereby deducting the healthy tissue saving aspect of proton therapy. Moreover, since the Bragg peak lies behind the patient, the transmission beam does not have the sharp distal dose fall-off after exiting the target that can be

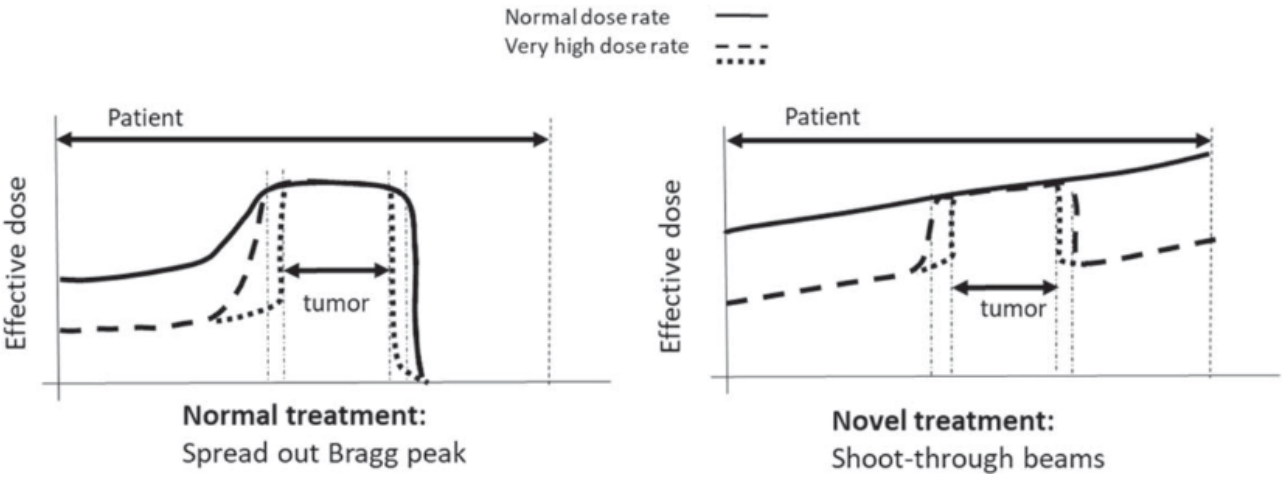

Figure 5: Schematic overview of spread-out Bragg peak (SOBP) beams and transmission ('shoot-through') beams [30].

achieved with conventional Bragg peak beams. This requires more beam angles to ensure the target dose conformity and uniformity [9].

Transmission beams are often used in literature to demonstrate the FLASH proton therapy effect. The choice for transmission beams is pragmatic, besides the dosimetric advantages it is simply the easiest method to achieve high dose-rates. The 'shoot-through' set-ups described in the reports of Diffenderfer et al. [6], Kang et al. [13], Schwarz et al. [23], Sørensen et al. [24], van de Water et al. [25], van Marlen et al. [26] and [30] all achieved a dose-rate of > 40 Gy/s. These studies investigated varying treatment sites, in vivo studies have focused on abdomen Diffenderfer et al. and leg tumors in mice [24]. Whereas silico studies have focused on multiple sites e.g. lung, liver, prostate, pancreas, head-and-neck and brain tumors.

Spread-out Bragg peak beams

A spread-out Bragg peak (SOBP) requires energy modulation of the proton beam, for example by a ridge filter. By modulation of the energy, a mono-energetic proton beam is translated to a poly-energetic proton beam with varying ranges and Bragg peaks. The combination of the different Bragg peak beams will together give a larger, fixed SOBP. Based on the succession of layer of beam spots, SOBP beams allow precise dose delivery to the tumor volume [5]. In fig. 5 a simplified overview of the dose distributions with SOBP and transmission beams are shown.

The drawback of SOBP beams is that energy modulation is required, which comes with inefficiency of the beam transmission and thereby makes it difficult to achieve sufficiently high enough FLASH compatible dose-rates. Moreover, to date there is limited in vivo data for FLASH irradiation from PBS systems using SOBP treatment planning.

To achieve a SOBP with UHDR, the study of Kourkafas et al. proposed a range modulator wheel. First, the beam passes a single scatterer, acting as a range shifter and removing two-thirds of the proton's kinetic energy. Followed by the 3D printed modulator wheel, designed with 48 periods of 8 steps, which produces a flat depth-dose distributed SOBP. Even though a substantial part of the kinetic energy of the protons is lost in this set-up, a dose-rate of 75 Gy/s could be reached. A non-rotating range modulator is applied by Schwarz et al.. In addition, the 3D range modulator of this study is coupled to a field-specific range shifter. This enables all fields, regardless the distal position of the target, to achieve the highest beam energy available and thereby the highest beam current possible, resulting in dose-rates over 100 Gy/s. Another method, mentioned before, is the use of a ridge filter to obtain a SOBP. Compared to the conventional energy modulation methods, a ridge filter allows

a time saving of a factor 5-10 [22]. Therefore, Patriarca et al. [22] was the first to propose and design a 3D printed plastic ridge filter to study the FLASH effect on small animals. A dose-rate of 40 Gy/s was achieved with their proposed set-up. Zhang et al. [34] proposed a similar set-up, combining the ridge filter with a range shifter (range modulator) to compare the FLASH effect in passive scattering and pencil beam scanning treatment plans.

4 Discussion

Biological aspects

The biological effect of FLASH proton therapy has been confirmed in multiple in vivo animal studies [5–7, 14, 24, 29, 34]. However, these studies do differ in method; dose-rate, dose delivery, measurements, the choice of beam, etc. For example the dose-rate; the first electron therapy FLASH studies [8] have set the UHDR threshold on $>$ 40 Gy/s. The dose-rates used in the studies that investigate the biological effect differ from 40 Gy/s up to 120 Gy/s [7]. Thereby, it is challenging to compare the studies directly. Also, the experimental data is still scarce and the biological mechanisms of the FLASH effect is not globally agreed on. Nevertheless, the first human trial with UHDR electron beam has been conducted [4] and the first proton trial has started [28]. Results of Bourhis et al. [4] showed positive results in the long-term biological responses of the healthy tissue with FLASH.

Not all experiments show the beneficial aspect of FLASH over conventional proton therapy [3]. Nonetheless, the most studies do show similar tumor control and sparing of the healthy tissue. Although a lot of research is still needed, it can be stated that the biological FLASH effect is confirmed for proton therapy.

Technological aspects

The feasibility of UHDR has been investigated with different treatment modalities and planning methods.

Passive scattering is a relatively easy method to deliver proton beams. However, the conventional set-up with scatter foils reduces the initial beam energy which makes it difficult to achieve FLASH compatible dose-rates. Yet, the first studies in FLASH proton therapy used scattering for beam delivering [3, 6, 14, 15, 22, 29, 30, 35]. This choice is because it is relatively simple to radiate the target area with a homogeneous dose. Nevertheless, PBS has a better position in taking care of precise delivery. Therefore a trend can be seen where more studies research the feasibility of UHDR with conventional PBS systems [5, 7, 9, 10, 12, 13, 16, 17, 23–27, 31, 34]. The disadvantage of PBS is that more factors need to be accounted for dose-rate quantification. Such as the time it costs to change the energy per spot, this is way to slow for FLASH treatment. To overcome this, studies have showed that FLASH compatible dose-rates can be achieved with high proton energy and placing a compensator, possibly a collimator and a ridge filter. Still, the different factors such as inter-spot switch time, dose threshold, spot dose weighting effect etc. [22] could have implications on the FLASH effect that needs to be evaluated further.

Several treatment planning studies have looked into the factors that affect the feasibility of FLASH. Next to dose-rates, these studies focused on the dose uniformity in the target and the dose delivered to healthy tissue. The majority of the treatment planning studies include either transmission plans or SOBP plans.
The choice for single-energy proton beam transmission plans is primarily pragmatic, since it is a relatively easy method to achieve high dose-rates. Besides, transmission beams can be beneficial for certain treatment sites since there is no range uncertainty and there is a sharp lateral penumbra at all depths [23]. The studies in this literature review conducting transmission beams [9, 13, 23–26, 30] show that it can achieve high dose-rate coverage in healthy tissue and good target uniformity [31]. However, transmission plans under perform in sparing healthy tissue distal to the target. Therefore, these plans are not suitable for certain treatment sites and patients as OARs could be in the beam path, affecting the overall plan quality. A more advanced method of treatment planning is by realizing a spread-out Bragg peak beam which gives better dose conformity around targets and increased healthy tis-

sue sparing compared to transmission beams. To achieve such a beam, a range modulator wheel [15, 23] and a ridge filter [1, 13, 14, 22, 34] are proposed. The set-ups with range modulator wheels achieved dose-rates over 100 Gy/s. However, if dose-rates are increased, the range modulator might not be able to keep up with the rotating frequency of the wheel [15]. This might complicate the FLASH effect, whereas a ridge filter has a more fine periodic structure. Therefore, the ridge filter is more delicate solution. Even though the use of SOBP seems promising in target conformity and healthy tissue sparing at UHDR, there is limited in vivo data available. Nevertheless, the study of Kim et al. that is available shows evidence of improving tumor control while reducing toxicity of healthy tissue using SOBP beams.

Despite the choice of treatment modality and planning method, the studies used in this literature review vary their approach in dose-rate determination. Some papers mention the use of metrics to calculate the dose-rate. Popular used metrics are dose-averaged dose-rate (DADR) [9, 10, 12, 13, 16, 23, 25–27, 31], average dose-rate (ADR) [12, 31] and dose-threshold dose-rate (DTDR) [12, 31]. Where DADR gives the highest dose-rate, not considering a time or dose-threshold and has the better dose-rate uniformity [12]. Since not all studies use the same calculation method, it is complex to compare different studies on the dose-rates.

Similar to dose-rate calculation; dose and dose-rate optimization is a subject that appears in numerous studies. The FLASH effect comes with the planning trade-off of minimizing the dose received by healthy tissue while also meeting the minimum dose threshold of $3.5 - 7$ Gy [19] to the target. Gao et al. [9] for example proposed a simultaneous dose and dose-rate optimization (SDDRO) to optimize both the dose distribution as the tissue-receiving dose-rate distribution. This treatment optimization method has been further studied by both Gao et al. [10] and Lin et al. [17]. Where Lin et al. included both transmission and Bragg peak beams in the optimization.

An interesting subject in the field of (FLASH) treatment planning is hypofractionation [12, 23, 25]. With a hypofractionated treatment schedule, the total dose of radiation is divided into large doses over a small number of fractions (1-5) [20]. This allows for escalation of the biologically effective dose and potentially improves tumor control. Combined with FLASH, hypofractionation can increase the dose-rate coverage for sparing healthy tissue and may further improve the FLASH effect [9, 17]. This statement is verified by the study of van de Water et al., who showed that hypofractionation resulted in higher dose-rates, especially for transmission beams. Moreover Krieger et al. [16] compared a variety of PBS treatment scenarios and found a positive clinical benefit for hypofractionated transmission beam plans. However, increasing the dose makes accurate delivery of every fraction more critical and requires improved methods for the prediction of the biological effect.

Taking into account the technological aspects mentioned above, a variety of possibilities to achieve FLASH compatible dose-rates has been investigated. Discussing treatment delivery methods shows an advantage of pencil beam scanning over passive scattering to achieve a homogeneous dose distribution with FLASH dose-rates. Although, realizing UHDR with PBS does require high proton energy beams with a set-up including a compensator, potentially a collimator and a ridge filter. The use of a stationary ridge filter is an elegant approach to achieve a SOBP. As of limited in vivo data is available on the FLASH effect with SOBP beams, further research is needed. On the other hand, pencil beam scanning with transmission beams could be beneficial on certain treatment sites where it possible to irradiate with a 'shoot-through' beam without delivering too much dose to organs-at-risk.

Clinical aspects

As of the number of pre-clinical studies in FLASH therapy is increasing, the evidence is gathering that the FLASH effect exists. The results show perspective to further investigate FLASH experiments in the clinic. Nevertheless, the question remains on how to implement FLASH therapy clinically. It could be stated that proton therapy has specific advantages over other radiotherapy modalities. Where electron beams are restricted to superficial tumors, current photon therapy systems are not capable of achieving UHDR. Proton

therapy enables precise and accurate delivery of high dose thereby allowing the treatment of deep-seated tumors.

Besides the limited field size and dose-rate limitation of passive scattering, it is important to note is that the majority of proton therapy centers use pencil beam scanning for treatment delivery. Next to the advantages of PBS over PS, it is therefore convenient to use existing PBS systems to implement FLASH in the clinic.

The highest dose-rate with a cyclotron can be achieved with the maximum beam energy. With beam energies of 230 - 250 MeV this results in transmission beams that lack the characteristic sharp dose fall-off for the tissue behind the tumor compared to conventional proton treatment planning. However, these 'shoot-through' beams minimize range uncertainties in heterogeneous tissues which makes them well-suited for treatment sites as lung and head-and-neck. Yet, FLASH proton therapy could benefit other treatment sites by using the Bragg peak characteristics. The use of a ridge filter enables to achieve a SOBP dose-distribution which is suitable for more complex tumors surrounded by vital organs. In the first clinical studies, breast cancer would be a proper treatment site to start investigate proton FLASH. With regard to current breast cancer treated patients, there is room to decrease the level of toxicity and besides it is a relevant site to spare organs-at-risk such as the heart [18, 33].

Limitations

There are some limitations to this review. First of all, it is possible that some relevant studies are missing because the search strategy was not complete enough. Besides, since the field of FLASH radiotherapy is a rapid growing research community, it might be that recent papers are missing. Second, this review mainly focuses on passive scattering, pencil beam scanning, transmission beams and spread-out Bragg peak beams while there might be other treatment delivery or planning methods that could benefit FLASH proton therapy.

5 Conclusions

Clinical research on FLASH in proton therapy is promising. Multiple in vivo studies confirm the biological FLASH effect, showing similar tumor control and improved healthy tissue sparing. However, there is still a lot unknown on the biological mechanisms behind FLASH that needs to be further investigated. Also, there is no consensus yet on the boundary conditions under which the FLASH effect occurs. A variety of metrics has been proposed to compare dose-rates of which recent studies mainly used the same dose-averaged dose-rate (DADR) metric.

Moreover, currently available proton beam systems are able to achieve FLASH compatible ultra-high dose-rates. While passive scattering is a relatively simple method to realize a proton beam, pencil beam scanning has a high potential to combine precise delivery and high dose-rates to maximize the FLASH effect. Both transmission beams and spread-out Bragg peak beams are suitable for FLASH proton therapy. While transmission beams are more suitable for targets in heterogeneous tissues surrounded by a relatively low number of critical organs, SOBP beams could be a promising solution in saving healthy tissue both proximal and distal to the target at more complex treatment sites. To fully adapt and develop existing proton therapy technology to meet the challenges of FLASH, more research is required to understand the impact of delivery conditions and establish the required treatment parameters.

Even though research is needed on the biological, technological and clinical aspects, FLASH proton therapy has high potential to bring benefit and is definitely worth to further investigate clinically.

Acknowledgements

The author wishes to thank Dr. Maarten (M.F.M.) Engel from the Erasmus MC Medical Library for developing and updating the search strategies.

References

1. Akulinichev, S. V., Kokontsev, D. A., and Yakovlev, I. A. Possible improvement of proton energy filter for radiotherapy. *Nucl. Instrum. Methods Phys. Res. Sect. A-Accel. Spectrom. Dect. Assoc. Equip.*, 977, 2020.

2. Berry, R. J., Hall, E. J., Forster, D. W., Storr, T. H., and Goodman, M. J. Survival of mammalian cells exposed to x rays at ultra-high dose-rates. *The British Journal of Radiology*, 42(494):102–107, 1969.

3. Beyreuther, E., Brand, M., Hans, S., Hideghéty, K., Karsch, L., Leßmann, E., Schürer, M., Szabó, E. R., and Pawelke, J. Feasibility of proton flash effect tested by zebrafish embryo irradiation. *Radiother Oncol*, 139:46–50, 2019.

4. Bourhis, J., Sozzi, W. J., Jorge, P. G., Gaide, O., Bailat, C., Duclos, F., Patin, D., Ozsahin, M., Bochud, F., Germond, J. F., Moeckli, R., and Vozenin, M. C. Treatment of a first patient with flash-radiotherapy. *Radiother Oncol*, 139:18–22, 2019.

5. Cunningham, S., McCauley, S., Vairamani, K., Speth, J., Girdhani, S., Abel, E., Sharma, R. A., Perentesis, J. P., Wells, S. I., Mascia, A., and Sertorio, M. Flash proton pencil beam scanning irradiation minimizes radiation-induced leg contracture and skin toxicity in mice. *Cancers*, 13(5): 1–15, 2021.

6. Diffenderfer, E. S., Verginadis, I. I., Kim, M. M., Shoniyozov, K., Velalopoulou, A., Goia, D., Putt, M., Hagan, S., Avery, S., Teo, K., Zou, W., Lin, A., Swisher-McClure, S., Koch, C., Kennedy, A. R., Minn, A., Maity, A., Busch, T. M., Dong, L., Koumenis, C., Metz, J., and Cengel, K. A. Design, implementation, and in vivo validation of a novel proton flash radiation therapy system. *Int J Radiat Oncol Biol Phys*, 106(2):440–448, 2020.

7. Dokic, I., Meister, S., Bojcevski, J., Tessonnier, T., Walsh, D., Knoll, M., Mein, S., Tang, Z., Vogelbacher, L., Rittmueller, C., Moustafa, M., Krunic, D., Brons, S., Haberer, T., Debus, J., Mairani, A., and Abdollahi, A. Neuroprotective effects of ultra-high dose rate flash bragg peak proton irradiation. *Int J Radiat Oncol Biol Phys*, 2022.

8. Favaudon, V., Caplier, L., Monceau, V., Pouzoulet, F., Sayarath, M., Fouillade, C., Poupon, M.-F., Brito, I., Hupé, P., and Bourhis, J. Ultrahigh dose-rate flash irradiation increases the differential response between normal and tumor tissue in mice. *Science translational medicine*, 6 (245), 2014.

9. Gao, H., Lin, B., Lin, Y., Fu, S., Langen, K., Liu, T., and Bradley, J. Simultaneous dose and dose rate optimization (sddro) for flash proton therapy. *Med Phys*, 47(12):6388–6395, 2020.

10. Gao, H., Liu, J., Lin, Y., Gan, G. N., Pratx, G., Wang, F., Langen, K., Bradley, J. D., Rotondo, R. L., Li, H. H., and Chen, R. C. Simultaneous dose and dose rate optimization (sddro) of the flash effect for pencil-beam-scanning proton therapy. *Med Phys*, 49(3):2014–2025, 2022.

11. Hornsey, S. and Alper, T. Unexpected dose-rate effect in the killing of mice by radiation. *Nature*, 210(5032):212–213, 1966.

12. Kang, M., Wei, S., Isabelle Choi, J., Simone, C. B., and Lin, H. Quantitative assessment of 3d dose rate for proton pencil beam scanning flash radiotherapy and its application for lung hypofractionation treatment planning. *Cancers*, 13(14), 2021.

13. Kang, M., Wei, S., Choi, J. I., Lin, H., and Simone, C. B. A universal range shifter and range compensator can enable proton pencil beam scanning single-energy bragg peak flash-rt treatment using current commercially available proton systems. *Int J Radiat Oncol Biol Phys*, 2022.

14. Kim, M. M., Verginadis, I. I., Goia, D., Haertter, A., Shoniyozov, K., Zou, W., Maity, A., Busch, T. M., Metz, J. M., Cengel, K. A., Dong, L., Koumenis, C., and Diffenderfer, E. S. Comparison of flash proton entrance and the spread-out bragg peak dose regions in the sparing of mouse intestinal crypts and in a pancreatic tumor model. *Cancers*, 13(16), 2021.

15. Kourkafas, G., Bundesmann, J., Fanselow, T., Denker, A., Ehrhardt, V. H., Gollrad, J., Budach, V., Weber, A., Kociok, N., Joussen, A. M., and Heufelder, J. Flash proton irradiation setup with a modulator wheel for a single mouse eye. *Med Phys*, 48(4):1839–1845, 2021.

16. Krieger, M., van de Water, S., Folkerts, M. M., Mazal, A., Fabiano, S., Bizzocchi, N., Weber, D. C., Safai, S., and Lomax, A. J. A quantitative flash effectiveness model to reveal potentials and pitfalls of high dose rate proton therapy. *Med Phys*, 49(3):2026–2038, 2022.

17. Lin, Y., Lin, B., Fu, S., Folkerts, M. M., Abel, E., Bradley, J., and Gao, H. Sddro-joint: simultaneous dose and dose rate optimization with the joint use of transmission beams and bragg peaks for flash proton therapy. *Physics in Medicine & Biology*, 2021.

18. Lischalk, J., Chen, H., Repka, M., Campbell, L., Obayomi-Davies, O., Kataria, S., Kole, T., Rudra, S., and Collins, B. Definitive hypofractionated radiation therapy for early stage breast cancer: Dosimetric feasibility of stereotactic ablative radiotherapy and proton beam therapy for intact breast tumors. *Advances in Radiation Oncology*, 3(3):447–457, 2018.

19. MacKay, R., Burnet, N., Lowe, M., Rothwell, B., Kirkby, N., Kirkby, K., and Hendry, J. Flash radiotherapy: Considerations for multibeam and hypofractionation dose delivery. *Radiotherapy and Oncology*, 164:122–127, 2021.

20. Paganetti, H. *Proton Therapy Physics*. CRC Press, 2012. ISBN 978-1-4398-3645-3.

21. Page, M. J., McKenzie, J. E., Bossuyt, P. M., Boutron, I., Hoffmann, T. C., Mulrow, C. D., Shamseer, L., Tetzlaff, J., Akl, E., and Brennan, S. The prisma 2020 statement: An updated guideline for reporting systematic reviews. *International Journal of Surgery*, 88, 2021.

22. Patriarca, A., Fouillade, C., Auger, M., Martin, F., Pouzoulet, F., Nauraye, C., Heinrich, S., Favaudon, V., Meyroneinc, S., Dendale, R., Mazal, A., Poortmans, P., Verrelle, P., and De Marzi, L. Experimental set-up for flash proton irradiation of small animals using a clinical system. *Int J Radiat Oncol Biol Phys*, 102(3):619–626, 2018.

23. Schwarz, M., Traneus, E., Safai, S., Kolano, A., and van de Water, S. Treatment planning for flash radiotherapy: General aspects and applications to proton beams. *Med Phys*, 2022.

24. Sørensen, B. S., Sitarz, M. K., Ankjærgaard, C., Johansen, J., Andersen, C. E., Kanouta, E., Overgaard, C., Grau, C., and Poulsen, P. In vivo validation and tissue sparing factor for acute damage of pencil beam scanning proton flash. *Radiother Oncol*, 161:S447–S448, 2021.

25. van de Water, S., Safai, S., Schippers, J. M., Weber, D. C., and Lomax, A. J. Towards flash proton therapy: the impact of treatment planning and machine characteristics on achievable dose rates. *Acta Oncol*, 58(10):1463–1469, 2019.

26. van Marlen, P., Dahele, M., Folkerts, M., Abel, E., Slotman, B. J., and Verbakel, W. Bringing flash to the clinic: Treatment planning considerations for ultrahigh dose-rate proton beams. *Int J Radiat Oncol Biol Phys*, 106(3):621–629, 2020.

27. van Marlen, P., Dahele, M., Folkerts, M., Abel, E., Slotman, B. J., and Verbakel, W. Ultra-high dose rate transmission beam proton therapy for conventionally fractionated head and neck cancer: Treatment planning and dose rate distributions. *Cancers*, 13(8), 2021.

28. Varian Medical Systems. Varian and the cincinnati children's/uc health proton therapy center complete enrollment of fast-01, first human clinical trial of flash therapy for cancer, Oct 2021. URL `https://www.varian.com/about-varian/newsroom/press-releases/varian-and-cincinnati-childrensuc-health-proton-therapy-0`.

29. Velalopoulou, A., Karagounis, I. V., Cramer, G. M., Kim, M. M., Skoufos, G., Goia, D., Hagan, S., Verginadis, I. I., Shoniyozov, K., Chiango, J., Cerullo, M., Varner, K., Yao, L., Qin, L., Hatzigeorgiou, A. G., Minn, A. J., Putt, M., Lanza, M., Assenmacher, C. A., Radaelli, E., Huck, J., Diffenderfer, E., Dong, L., Metz, J., Koumenis, C., Cengel, K. A., Maity, A., and Busch, T. M. Flash proton radiotherapy spares normal epithelial and mesenchymal tissues while preserving sarcoma response. *Cancer Res*, 81(18):4808–4821, 2021.

30. Verhaegen, F., Wanders, R. G., Wolfs, C., and Eekers, D. Considerations for shoot-through flash proton therapy. *Phys Med Biol*, 66(6):06NT01, 2021.

31. Wei, S., Lin, H., Choi, J. I., Simone, C. B., and Kang, M. A novel proton pencil beam scanning flash rt delivery method enables optimal oar sparing and ultra-high dose rate delivery: A comprehensive dosimetry study for lung tumors. *Cancers*, 13(22), 2021.

32. Zenklusen, S. M. *Exploring the potential of advanced pencil beam scanning for treating moving targets with the new Gantry 2 at the Paul Scherrer Institut*. PhD thesis, ETH Zurich, 2010.

33. Zerella, M. A., Zaffaroni, M., Ronci, G., Dicuonzo, S., Rojas, D. P., Morra, A., Fodor, C., Rondi, E., Vigorito, S., Botta, F., et al. Single fraction ablative preoperative radiation treatment for early-stage breast cancer: the crystal study–a phase i/ii clinical trial protocol. *BMC cancer*, 22 (1):1–12, 2022.

34. Zhang, G., Wang, J., Wang, Y., and Peng, H. Proton flash: passive scattering or pencil beam scanning? *Phys Med Biol*, 66(3):03NT01, 2021.

35. Zhang, Q., Cascio, E., Li, C., Yang, Q., Gerweck, L. E., Huang, P., Gottschalk, B., Flanz, J., and Schuemann, J. Flash investigations using protons: Design of delivery system, preclinical setup and confirmation of flash effect with protons in animal systems. *Radiat Res*, 194(6):656–664, 2020.

Appendix A Search Terms

Embase

((('proton therapy'/de OR 'particle therapy'/de OR 'proton therapy system'/de) AND ('megadose'/de OR 'high dose radiotherapy'/de OR 'drug megadose'/mj)) OR (((FLASH OR ultra-high-dose* OR high-dose-rate*) NEAR/9 (proton* OR particl*) NEAR/3 (therap* OR radio* OR radiat* OR irradiat* OR deliver* OR effect* OR beam* OR treatment*)) OR ((FLASH OR ultra-high-dose* OR high-dose-rate*) NEAR/3 (PT))):ab,ti,kw)

Medline

((((FLASH OR ultra-high-dose* OR high-dose-rate*) ADJ9 (proton* OR particl*) ADJ3 (therap* OR radio* OR radiat* OR irradiat* OR deliver* OR effect* OR beam* OR treatment*)) OR ((FLASH OR ultra-high-dose* OR high-dose-rate*) ADJ3 (PT))).ab,ti,kf.)

Web of Science

TS=(((((FLASH OR ultra-high-dose* OR high-dose-rate*) NEAR/9 (proton* OR particl*) NEAR/2 (therap* OR radio* OR radiat* OR irradiat* OR deliver* OR effect* OR beam* OR treatment*)) OR ((FLASH OR ultra-high-dose* OR high-dose-rate*) NEAR/2 (PT)))))

Appendix B Search Details

Table 1: Overview of the databases used for this literature review. The databases were accessed on 04-04-2022.

Database searched	Platform	Years of coverage
Embase	Embase.com	1971 - Present
Medline ALL	Ovid	1946 - Present
Web of Science Core Collection*	Web of Knowledge	1975 - Present

*Science Citation Index Expanded (1975-present) ; Social Sciences Citation Index (1975-present) ; Arts & Humanities Citation Index (1975-present) ; Conference Proceedings Citation Index- Science (1990-present) ; Conference Proceedings Citation Index- Social Science & Humanities (1990-present) ; Emerging Sources Citation Index (2005-present)

B

Wishlists

Table B.1: Wishlist used for generating treatment plans for early-stage breast cancer patients, with D_{pr} the prescribed dose.

Structure		Min/Max	Type	Goal	Priority
1	GTV	Maximize (minimum)	Linear	D_{pr}	Constraint
2	PTV without GTV	Maximize (minimum)	Linear	$0.98 \cdot D_{pr}$	Constraint
3	PTV without GTV	Minimize (maximum)	Linear	$1.12 \cdot D_{pr}$	1
4	GTV	Minimize (maximum)	Linear	$1.14 \cdot D_{pr}$	2
5	Mamma Ipsilateraal without PTV	Minimize (maximum)	Linear	$0.32 \cdot D_{pr}$	3
6	Region Outside PTV	Minimize (maximum)	Linear	$0.62 \cdot D_{pr}$	4
7	Region Outside PTV	Minimize (maximum)	Mean	0	5

C

Results second patient

C.1. IMPT treatment plans

An example of a generated IMPT treatment plan is shown in fig. C.1. The treatment plan prescribed a dose of 21 Gy to the PTV (delineated in red). The yellow delineation represents the GTV. The uniformity of this plan is expressed in the HI = 0.9768 and the coverage of the PTV is 1.0175.

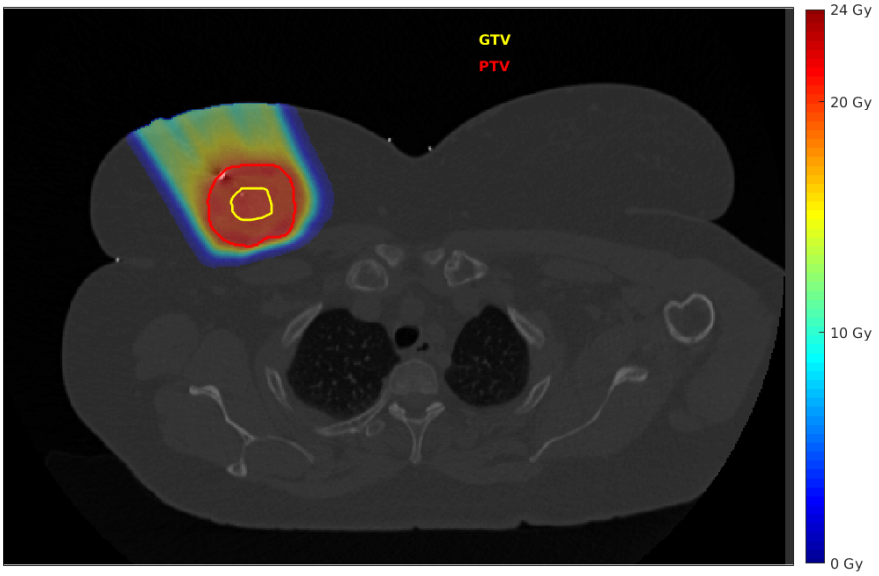

Figure C.1: Dose distribution of a single fraction IMPT plan with a prescribed dose of 21 Gy and three beam angles, 20°, 25°, 35°.

The results of the optimization of IMPT treatment plans are presented in table C.1, including the treatment planning times and the number of energy layers and lateral positions in the final plan. In fig. C.2, the dose distributions of the selected energy layers for the single fraction IMPT treatment plan are shown.

Table C.1: Optimization results of the treatment planning times, number of selected energy layers, and the number of lateral positions for the IMPT treatment plans.

Treatments plans	Beam angles (°)	Treatment planning time (HH:MM)	Number of energy layers	Number of lateral positions
1 fraction	20	2:01	14	391
2 fractions	15, 35	6:27	26	467
3 fractions	20, 25, 35	12:36	37	484
4 fractions	15, 20, 30, 35	22:12	47	490
5 fractions	15, 20, 25, 30, 35	35:44	55	483

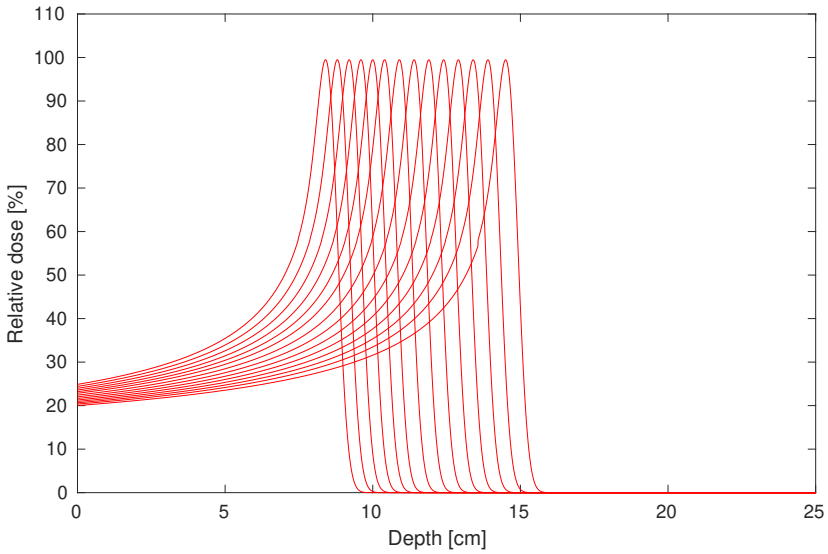

Figure C.2: Relative dose distribution in water of the selected energy layers for a single fraction IMPT treatment plan with a beam angle of 30°.

C.2. Ridge filter treatment plans

An example of a generated ridge filter treatment plan is shown in fig. C.3. This treatment plan is the iso-effective single-fraction dose distribution of three separate SFUD plans. In fig. C.4 the dose distribution of the individual plans is given. These treatment plans are prescribed on 11.55 Gy such that the three fractions together have an iso-effective single-fraction dose of 21 Gy, comparable to the IMPT treatment plan in fig. C.1. The HI of the individual fraction doses are 1.1482, 1.2069, and 1.0640 for respectively the beam angles 20°, 25°, and 35°. The conformality index of the overall ridge filter plan is 2.5533, indicating an significant overdose.

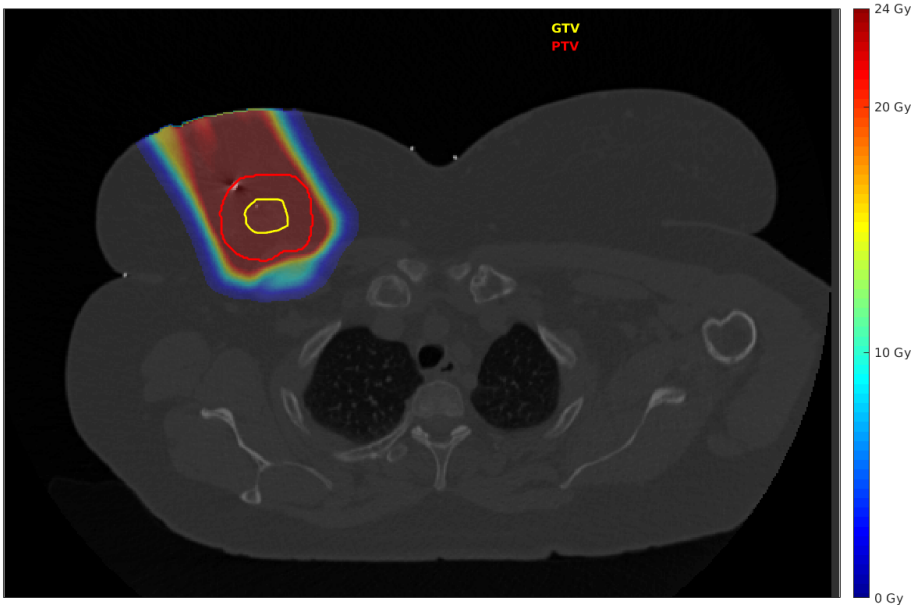

Figure C.3: Dose distribution of a ridge filter plan consisting of three single-field uniform dose fractions with three different angles, 20°, 25°, 35°, and each fraction a prescribed dose of 11.55 Gy.

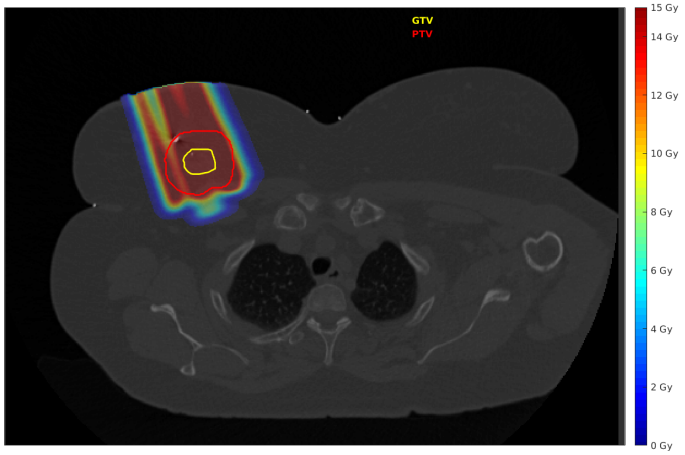

(a) Beam angle 20°.

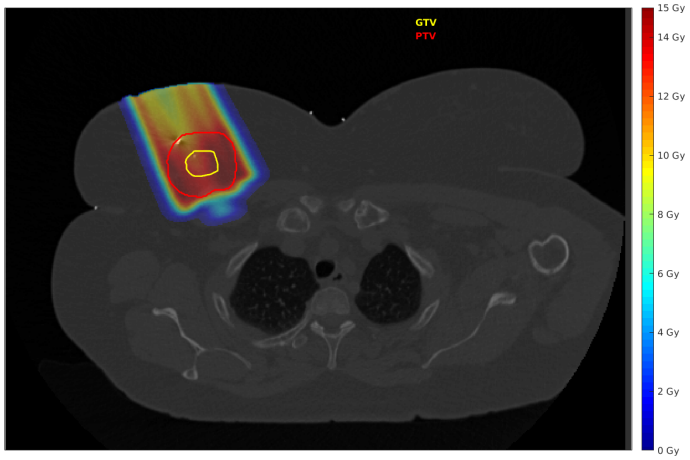

(b) Beam angle 25°.

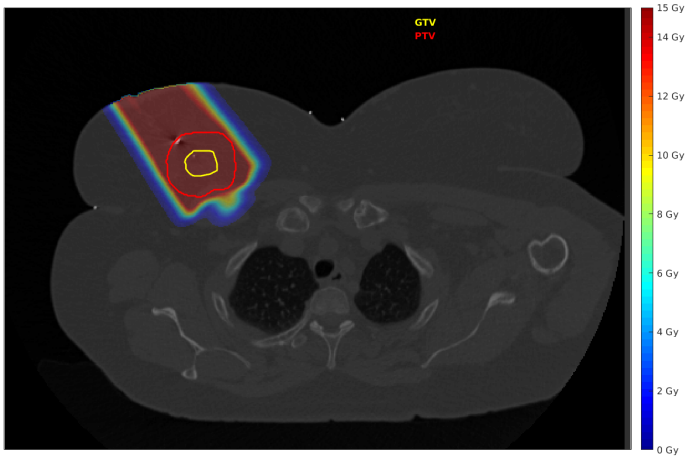

(c) Beam angle 35°.

Figure C.4: Dose distribution of three SFUD fractions, each having a prescribed dose of 11.55 Gy.

C.2.1. Implementation in iCycle

The main difference between the IMPT and ridge filter treatment plans is the freedom of spot selection. Where IMPT has the freedom to position pristine Bragg peaks across the entire target volume, ridge filter treatment plans require the pristine Bragg peaks belonging to one SOBP to be positioned at the same lateral position. Besides, only one SOBP can be selected for every lateral position. Figure C.5 shows this difference in positioning of the pristine Bragg peaks for generated treatment plans of both IMPT and ridge filter. It can be seen that the Bragg peak spots of the ridge filter plans are all positioned in series on a specified regular grid.

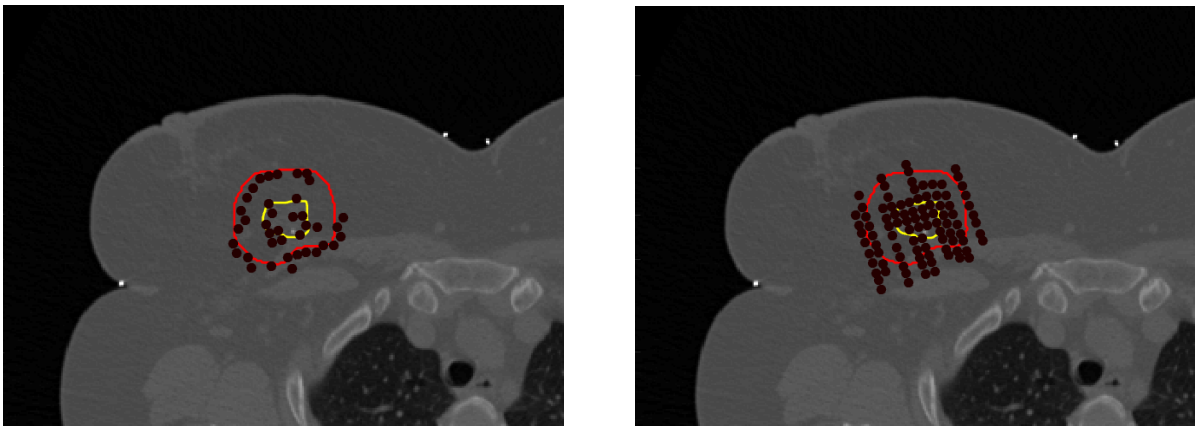

(a) (b)

Figure C.5: Example of the pristine Bragg peak locations (black dots) in an IMPT (a) and ridge filter (b) treatment plan with single beam angle 20°. The yellow and red circles are delineations of respectively the GTV and PTV.

The optimization times from the optimization of the ridge filter treatment plans are stated in table C.2. In fig. C.6 the depth range for one treatment plan is shown, by plotting the SOBP beams belonging to the selected energy layers.

Table C.2: Optimization results of the treatment planning times, number of selected energy layers, and the number of lateral positions for the beam angles of the five fractions ridge filter treatment plan.

Beam angle (°)	Treatment planning time (HH:MM)	Number of energy layers	Number of lateral positions
15	2:25	8	115
20	2:08	7	127
25	2:18	7	119
30	2:04	7	117
35	3:32	9	123

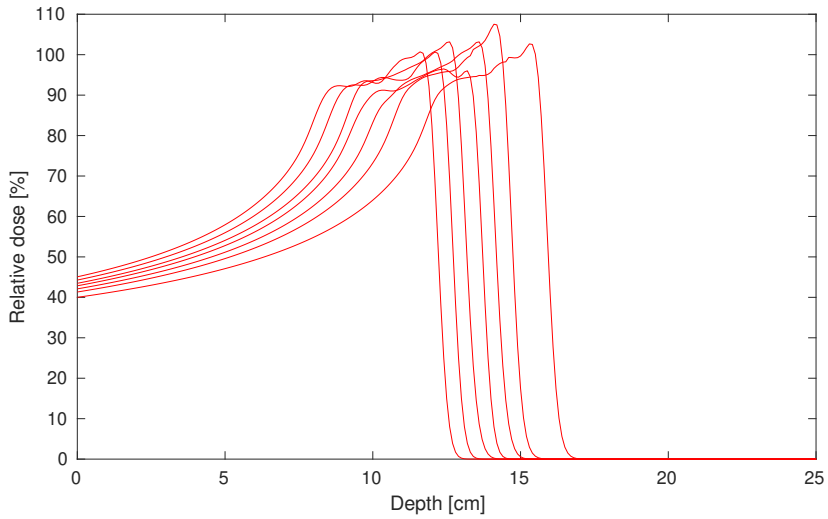

Figure C.6: Relative dose distribution in water of the SOBP beams of the selected energy layers for a single fraction ridge filter treatment plan with a beam angle of 30°.

C.2.2. SBPF

The ridge filter treatment plans are generated as single beam per fraction delivery, where each fraction a uniform dose is delivered. In table C.3 the homogeneity indices for ridge filter plans with a prescribed dose of 8.65 Gy (five fraction schedule) are given. The final SBPF ridge filter treatment plans are generated with the five beam angles with favorable homogeneity indices (closest to 1.07), varying between 15 and 50 degrees for each patient. This is repeated for the treatment plans with 1, 2, 3, and 4 beam angles. For this patient, this resulted in the beam angles listed in table C.4.

Table C.3: HI for different beam angles for SFUD ridge filter treatment plans with single fraction doses of 8.65 Gy.

Beam angle (°)	Homogeneity index
15	1.1844
20	1.2301
25	1.2063
30	1.4817
35	1.0986
40	1.5498
45	1.6550
50	3.1520

Table C.4: Selected beam angles for the SBPF fractionated ridge filter plans

Number of fractions	Selected beam angles (°)
1	20°
2	15°, 35°
3	20°, 25°, 35°
4	15°, 20°, 30°, 35°
5	15°, 20°, 25°, 30°, 35°

C.2.3. FLASH effect

The FLASH effect is applied by reducing the dose in the healthy breast tissue by the FLASH enhancement ratio. The dose distribution with applied FLASH effect by increasing FER is shown in fig. C.7. It can be seen that the dose in the voxels outside the CTV is reduced while the dose in the CTV remains the same. Moreover, the dose of voxels below the threshold of 7 Gy is not changed.

C.3. Analysis

The generated IMPT and ridge filter plans are all assessed on the homogeneity and conformity index for clinical acceptability. Moreover, the risk of developing fibrosis and fat necrosis is calculated. This section will show the evaluation results for five different treatment plans varying the number of beam angles: 1, 2, 3, 4, and 5. To conclude the analysis, the results of the IMPT and ridge filter treatment plans are summarized and the FERs for which the ridge filter treatment plans outperform the IMPT plans are listed.

C.3.1. Uniformity

Figure C.8 gives the results of the homogeneity indices of the five generated ridge filter treatment plans, which are compared to the results for the IMPT treatment plans, table C.5. It can be seen that the HI curves decrease with an increase in FER. The HI indicates the ratio of the near minimum dose in the PTV and the prescribed dose in the PTV. As the FER is applied to all voxels except for the CTV cells, within the PTV the FER is only applied to the voxels laying in a ring around the CTV. The near-minimum dose of the PTV is expected at the edge of the PTV, probably most likely outside the CTV. It is therefore expected that the near-minimum dose and thereby the HI follows the linear regression of the FER. With a FER of 1.1789, all treatment plans satisfy the clinical recommendation for the homogeneity index and from a FER of 1.2716, the ridge filter treatment plans benefit the IMPT plans in uniformity. The ridge filter treatment plan with 5 fractions shows the most homogeneous treatment plan.

Table C.5: Homogeneity indices for the five IMPT treatment plans with single fraction doses of 21 Gy.

Number of beam angles	Homogeneity index
1	0.9781
2	0.9813
3	0.9768
4	0.9842
5	0.9942

C.3.2. Coverage

Figure C.9 gives the results of the conformity indices of the five generated ridge filter treatment plans, which are compared to the results for the IMPT treatment plans, table 3.7. It can be seen that the CI reaches a certain threshold of approximately CI = 0.6. This limitation is the volume ratio of the CTV and PTV. For a certain FER, there are no voxels outside the PTV receiving a dose level $\geq$ 95% of the prescribed dose. The dose level of the voxels in the CTV does not change so the conformality index will just be the volume of the CTV divided by the PTV. With a FER of 1.6409, all treatment plans benefit the IMPT plans in conformity. The ridge filter treatment plan with 2 fractions shows the highest coverage in the dose distribution.

Table C.6: Conformity indices for the five IMPT treatment plans with single fraction doses of 21 Gy.

Number of beam angles	Conformity index
1	1.0052
2	0.9995
3	1.0175
4	1.0020
5	1.0012

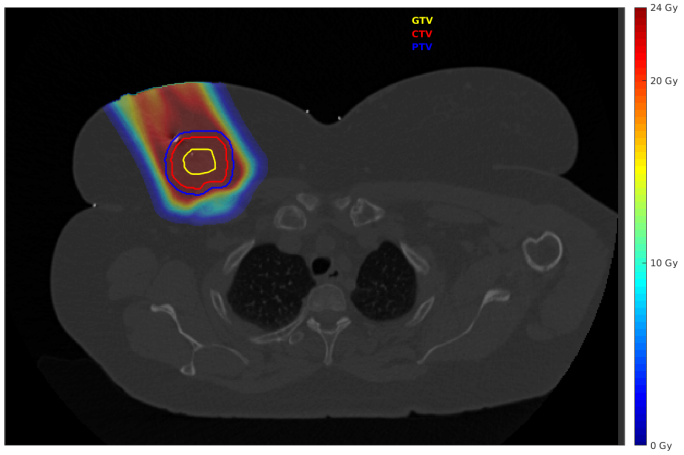

(a) FER=1.2.

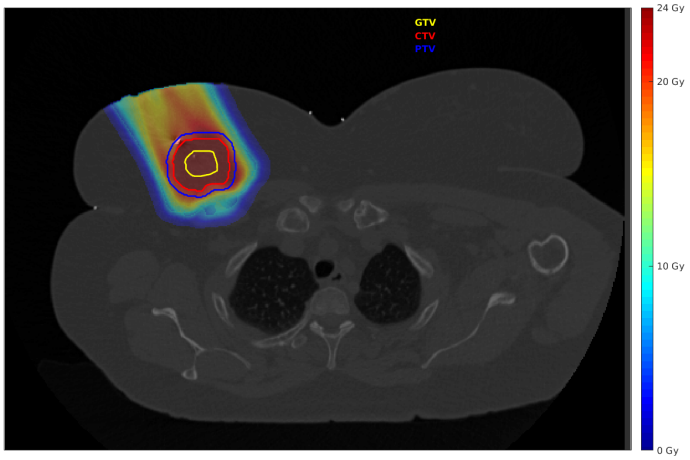

(b) FER=1.5.

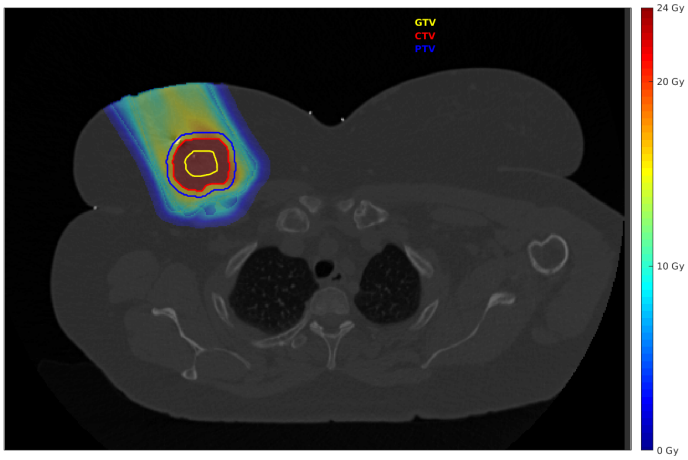

(c) FER=2.0.

Figure C.7: Dose distribution of ridge filter treatment plan from fig. C.3 for different values for FER applied to the healthy tissue.

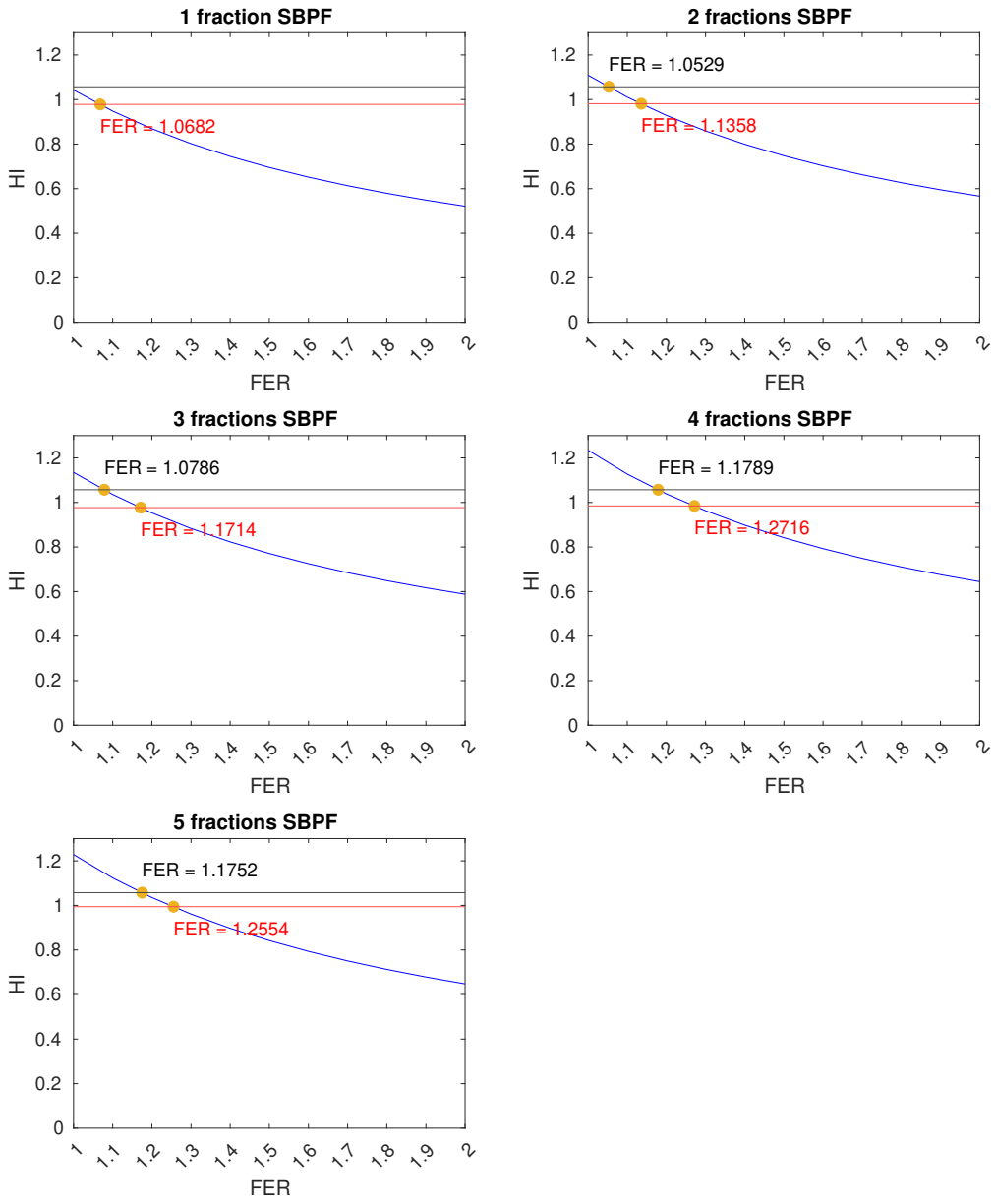

Figure C.8: Homogeneity indices of the five ridge filter treatment plans for different magnitudes of the FLASH enhancement ratio. The black line represents the clinical recommendation of HI = 1.07 and the red line represents the HI of the IMPT plans, which can be found in table C.5

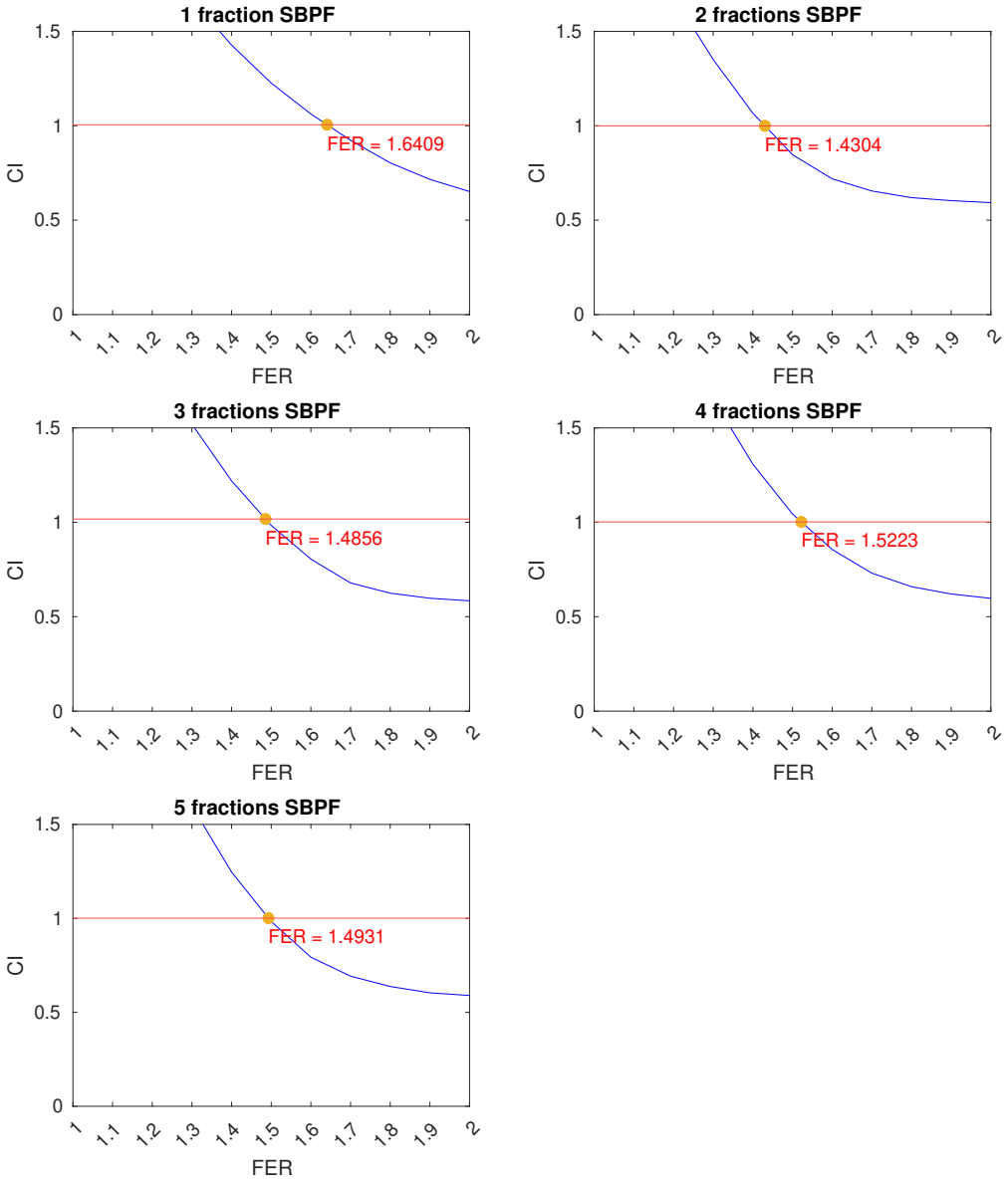

Figure C.9: Conformality indices of five ridge filter treatment plans for different magnitudes of the FER. The red line represents the CI of the IMPT plans, which can be found in table C.6

C.3.3. Fibrosis

The risk of fibrosis is expressed through the normal tissue control probability and the results are shown in fig. C.10. It can be seen that the FER has a substantial impact on the risk of fibrosis. With a FER of 1.8605, all treatment plans benefit the IMPT plans in the risk of developing painful fibrosis. The ridge filter treatment plan with 3 fractions shows the most favorable values for NTCP.

Table C.7: Normal tissue control probabilities for the five IMPT treatment plans with single fraction doses of 21 Gy.

Number of beam angles	NTCP
1	0.5818
2	0.5976
3	0.5766
4	0.5918
5	0.5929

C.3.4. Fat necrosis

The first metric on fat necrosis is the maximum dose in the healthy tissue, results can be found in fig. C.11. The results for the 2 - 5 fractions are relatively high but the maximal dose of the 5 fractions treatment plan is significantly higher, requiring a FER > 2. With a FER of 1.9187, the treatment plans for 2 - 5 fractions satisfy the recommendations from Rahimi et al. [48]. The ridge filter treatment plan with 3 fractions shows the lowest maximal dose curve.

Table C.8: Maximal dose for the five IMPT treatment plans with single fraction doses of 21 Gy.

Number of beam angles	D_{max}
1	21.5919
2	22.2069
3	22.7476
4	22.1242
5	22.1420

The other recommendations of Rahimi et al. [48] prescribe limitations on the volumes receiving 18.94, 19.56, 20.66, 21.79, and 22.92 Gy. In fig. C.12, the dose-volume curves for the healthy breast tissue are shown. It can be seen that a FER > 2 is required for all ridge filter treatment plans to benefit the IMPT treatment plans. Moreover, it can be seen that the smallest discrepancy between the ridge filter plan curves and the constraint curves is often near the maximum dose.

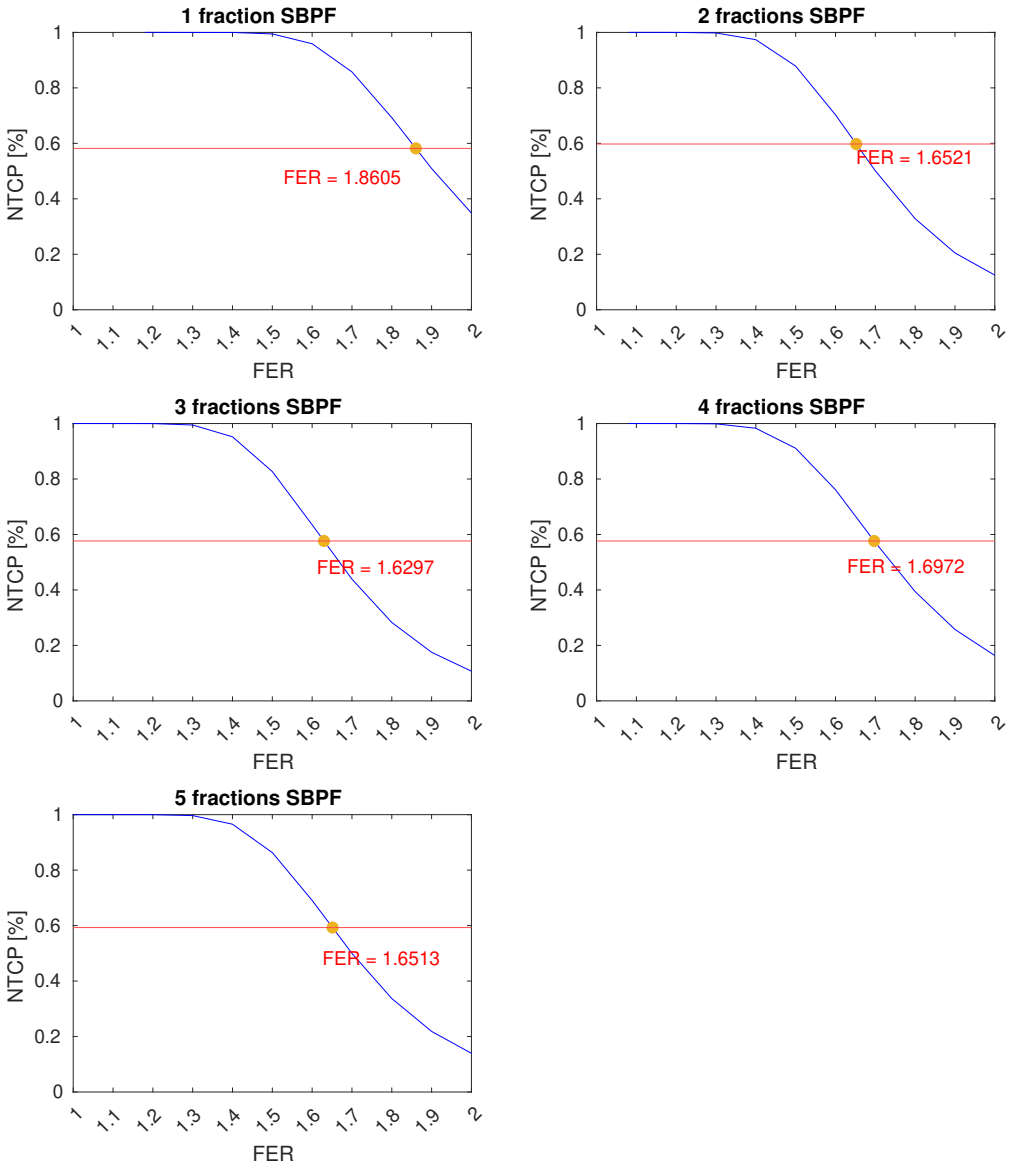

Figure C.10: Normal tissue control probability of developing fibrosis for five ridge filter plans for different magnitudes of the FER. The red line represents the NTCP of the IMPT plans, which can be found in table C.7

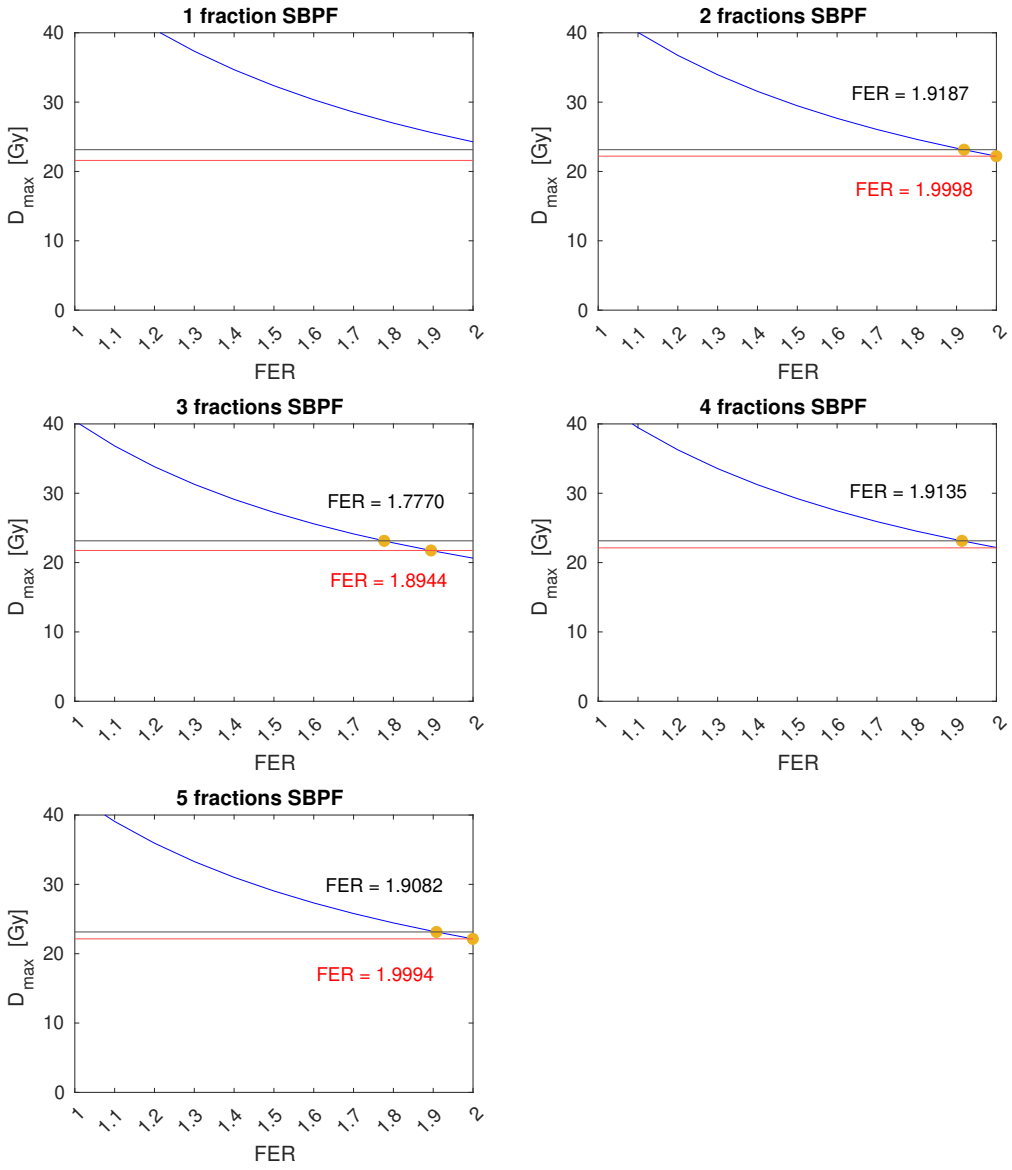

Figure C.11: Maximal dose in healthy breast tissue for five ridge filter plans for different magnitudes of the FER. The black line represents the recommendation of 23.14 Gy and the red line represents the maximal dose of the IMPT plans, which can be found in table C.8

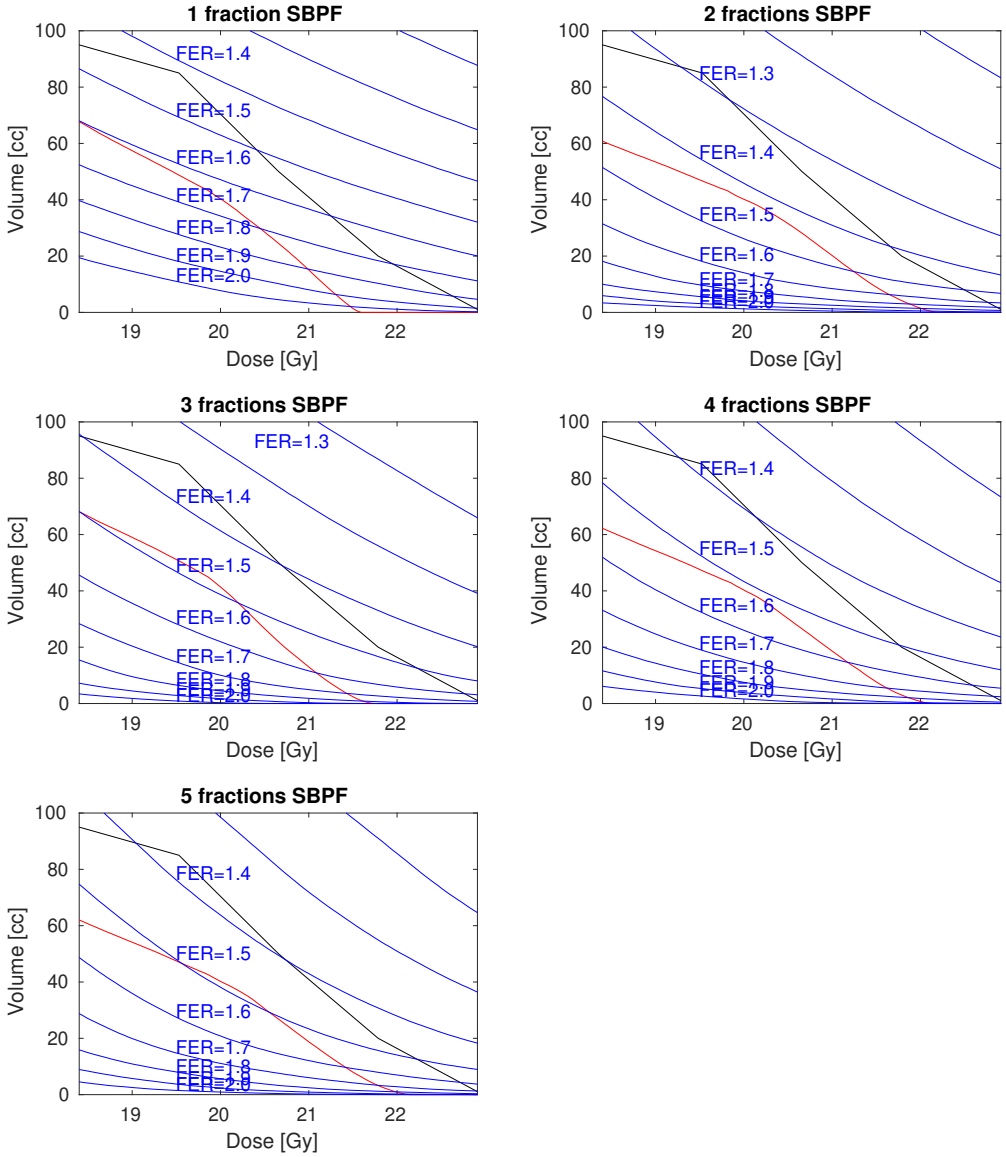

Figure C.12: Dose-volume curves for the healthy breast tissue for the dose range 18.94 - 22.92 Gy. The dose-volume curve is drawn for every value of FER. The black line represents the constraints from Rahimi et al. [48] and the red line shows the dose-volume curves from the IMPT plans.

C.3.5. FLASH effect

Table C.9 shows a summary of the results for all metrics. The last column states the value of FER for which the ridge filter treatment plan outperforms the IMPT treatment plan on all metrics: uniformity by the homogeneity index, coverage by the conformity index, risk of fibrosis by the NTCP, and risk of fat necrosis by the maximal dose.

Table C.9: Overview of the results of the evaluation of the five different IMPT and ridge filter treatment plans. The required FER for a ridge filter treatment plan to benefit the equivalent IMPT plan is stated in the last column.

	Number of fractions	**Beam Angles (°)**	**HI**	**CI**	**NTCP**	D_{max} **(Gy)**	**Required FER**
IMPT	1	20	0.9781	1.0052	0.5818	21.5919	-
Ridge filter	1	20	1.0427	2.5620	1.0000	48.5440	> 2.0
IMPT	1	15, 35	0.9813	0.9995	0.5976	22.2069	-
Ridge filter	2	15, 35	1.1092	2.4242	1.0000	44.0124	1.9998
IMPT	1	20, 25, 35	0.9768	1.0175	0.5766	22.7476	-
Ridge filter	3	20, 25, 35	1.1350	2.5533	1.0000	40.4108	1.8944
IMPT	1	15, 20, 30, 35	0.9842	1.0020	0.5918	22.1242	-
Ridge filter	4	15, 20, 30, 35	1.2343	2.6475	1.0000	43.2928	> 2.0
IMPT	1	15, 20, 25, 30, 35	0.9942	1.0012	0.5929	22.1420	-
Ridge filter	5	15, 20, 25, 30, 35	1.2281	2.6212	1.0000	42.8287	1.9994